Mass Transfer in Multi-Phase Single Particle Systems

by

Jonathan Tsu-Wei Su

Department of Mechanical Engineering and Materials Science
Duke University

Date:_____

Approved:

_____
David Needham, Supervisor

_____
David Katz

_____
Adrian Bejan

_____
Stefan Zauscher

Dissertation submitted in partial fulfillment of
the requirements for the degree of Doctor of Philosophy in Department of Mechanical Engineering and Materials Science in the Graduate School
of Duke University

2011

ABSTRACT

Mass Transfer in Multi-Phase Single Particle Systems

by

Jonathan Tsu-Wei Su

Department of Mechanical Engineering and Materials Science
Duke University

Date:_____

Approved:

_____
David Needham, Supervisor

_____
David Katz

_____
Adrian Bejan

_____
Stefan Zauscher

An abstract of a dissertation submitted in partial
fulfillment of the requirements for the degree
of Doctor of Philosophy in the Department of
Department of Mechanical Engineering and Materials Science in the Graduate School
of Duke University

2011

Abstract

This thesis addresses mass transfer in multi-phase single particle systems. By using a novel technique based upon the micropipette, the dissolution of liquid and gas droplets in a liquid medium can be observed. Three classes of experimental systems are observed: pure liquid droplet dissolution in a pure liquid environment, miscible mixture liquid droplet dissolution in a pure liquid environment, and solute-containing liquid droplet dissolution in a pure liquid environment. Experiments on the dissolution of pure droplets of water in n-alcohols and n-alkanes showed that water droplets dissolved ten times faster in the alcohols as compared to in the alkanes. When solubility was taken into account, however, and diffusion coefficients calculated using the Epstein-Plesset equation, diffusion constants for alkanes were twenty five times higher in alkanes than for the corresponding alcohol (for example 12.5 vs 0.5 x 10-8 cm^2/s for pentane and pentanol). This difference in rates of diffusion of the single molecules reflects the effect of hydrogen bonding on small solute diffusion, which is expounded upon in Chapter 2.

A model for the dissolution of a droplet containing a mixture, each component of which is soluble in the surrounding liquid medium is presented in Chapter 3. The model is based upon a reduced surface area approximation and the assumption of ideal homogenous mixing : Mass flux $\frac{dm_i}{dt} = Afrac_i D_i (c_i - c_s)\left\{\frac{1}{R} + \frac{1}{\sqrt{\pi D_i t}}\right\}$, where $Afrac_i$ is the

area fraction of component i, c_i and c_s are the initial and saturation concentrations of the droplet material in the surrounding medium, respectively, R is the radius of the droplet, t is time, and D_i is the coefficient of diffusion of component i in the surrounding medium. This model was tested for the dissolution of ethyl acetate and butyl acetate in water and the dissolution of butyl acetate and amyl acetate in water, and was found to provide a good fit. In Chapter 4, a partial differential equation, $\frac{R^2}{D}\frac{\partial c}{\partial t}\Big|_{\eta} = \frac{\propto\eta}{D}\frac{\partial c}{\partial \eta} + \frac{\partial^2 c}{\partial \eta^2} + \frac{2}{\eta}\frac{\partial c}{\partial \eta}$, is presented for the dissolution of a solute containing droplet in a liquid medium, and shell or bead formation is predicted. In Chapter 5, an application of the solute containing droplet dissolution is presented in which suspensions of glassified protein microspehres are used to improve the injectability of protein based pharmaceuticals. Injectability is related to viscosity, and the viscosity of a suspension may be predicted to follow the Krieger Dougherty equation: $\frac{\eta(\Phi)}{\eta_0} = \left(1 - \frac{\Phi}{\Phi_m}\right)^{-2.5\Phi_m}$, where Φ is the volume fraction of the suspensate, η is the viscosity of the overall suspension, η_0 is the viscosity of the suspending fluid, and Φm is the maximum possible volume fraction. Finally, in Chapter 6, various experimental methods used to generate droplets are addressed.

Dedication

To my parents and grandparents, who made all this possible.

Contents

List of Tables

List of Figures

1. Overview of Thesis

1.1 Overall Goal and Specific Aims

The focus of this thesis is the dissolution of liquid droplets in a surrounding liquid solvent. The micropipette is central to the ability to form and observe these droplets. The micropipette is a single tapered glass capillary which can be made to have an outlet diameter ranging from 4-10 microns, allowing the careful manipulation of small (10 – 200 micron diameter) droplet. Since the micropipette is mounted on a microscope, the dissolution of these droplets can be observed and recorded. Single droplet studies were used to characterize the dissolution of liquid droplets in a surrounding solvent. Gas in liquid droplets have been studied previously by Duncan and Needham[1], who also began the work on liquid in liquid systems[2] and solution in liquid systems, showing that these systems could be modeled using the Epstein-Plesset equation[2, 3]. This thesis builds upon this previous work and extends it to study three different types systems: pure liquid droplet dissolution in a pure liquid environment, liquid mixture droplet dissolution in a pure liquid environment, and liquid solution droplet dissolution in a pure liquid environment (as illustrated in Figure 1.) The Epstein-Plesset equation was applied to the dissolution of pure droplets in order to obtain diffusion coefficients, and new models for the dissolution of droplet mixtures and solution droplets were developed in this work.

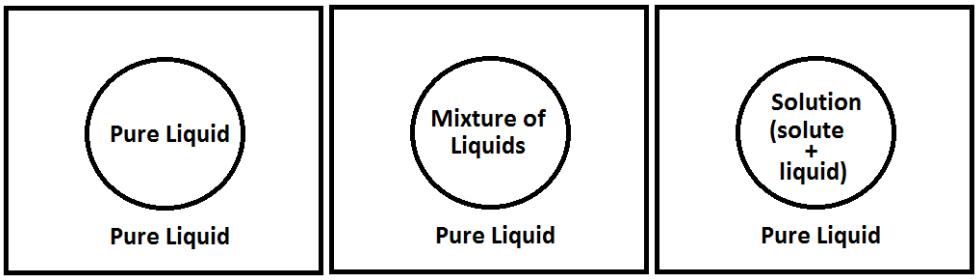

Figure 1. Systems of study: Pure liquid droplet dissolution in a pure liquid, Droplets of a liquid mixture dissolving in a pure liquid, and solution droplets dissolving in a pure liquid.

Specific Aim 1: The aim of the research in Chapter 2 was to measure the diffusion coefficients of water in various *n*-alkanes and *n*-alcohols in order to determine the effect of hydrogen bonding on water diffusion. These diffusion coefficients were plotted and compared to the Stokes-Einstein prediction, and α values determined. SA1 evaluated two hypotheses:

Specific Hypothesis 1a: The Epstein-Plesset equation: $\frac{dR}{dt} = -\frac{Dc_s(1-f)}{\rho}\left\{\frac{1}{R} + \frac{1}{\sqrt{\pi Dt}}\right\}$ can be fit to droplet dissolution data (droplet size vs time) to obtain diffusion coefficients of the droplet material in its surroundings. This hypothesis was tested for water in *n*-butanol and water in *n*-hexane, and was found to be correct.

Specific Hypothesis 1b: The diffusion of a small solute such as water will follow the fractional viscosity power law $D \sim \eta^{\alpha}$. Diffusion of water in the *n*-alcohols will be slower than diffusion in the *n*-alkanes, not due to cluster diffusion but because of increased residence times at the –OH group. These hypotheses were found to be correct.

Specific Aim 2: The aim of the proposed research in Chapter 3 was to measure and model the dissolution of a droplet consisting of a mixture of two liquids where one component has a higher rate of mass transfer into the surrounding medium than the other due to its higher solubility or faster diffusion. The systems chosen were ethyl acetate/butyl acetate and butyl acetate/amyl acetate in water. Mass loss during formation of a pure liquid droplet is relatively unimportant, as the concentration of a pure liquid is always constant. Once a droplet is a mixture, or contains a solute, however, mass loss must be tracked during the droplet formation (i.e., including the initial "blowing out'). Mass lost during this process was determined by applying the Epstein Plesset equation to droplet dimensions measured during the 'blowing out' process. SA2 evaluated two hypotheses:

Specific Hypothesis 2a: Mass transfer of one component of a mixture in a droplet will occur according to a <u>reduced surface area modification</u> to the Epstein-Plesset equation $\frac{dm_i}{dt} = Afrac_i D_i (c_i - c_s)\left\{\frac{1}{R} + \frac{1}{\sqrt{\pi D_i t}}\right\}$. This hypothesis was found to be valid for the systems studied.

Specific Hypothesis 2b: Mass loss in a droplet during droplet formation on a micropipette can be accurately approximated from its first emergence by application of the Epstein Plesset equation $\frac{dm}{dt} = D(c_i - c_s)\left\{\frac{1}{R} + \frac{1}{\sqrt{\pi D t}}\right\}$ and measurement of droplet dimensions and final concentration. This hypothesis was found to be partially true,

depending on the system studied. To minimize any error due to mass loss during droplet formation, droplets should be 'blown out' as quickly as possible.

Specific Aim 3: The aim of the proposed research in Chapter 4 was to develop and test a model for dissolution of a two component solution microdroplet, dissolving in a second phase, where time evolution of concentration gradients are modeled giving rise to either a homogenous bead or insoluble shell.. The expectation was that a homogenous bead will form if the solute diffuses at a comparable speed to the diffusive processes responsible for droplet shrinkage. Conversely, shell formation was promoted if the solute has much slower diffusion and equilibration within the droplet than the rate at which solvent was lost. SA3 evaluated two hypothesis:

Specific Hypothesis 3: The equation $\frac{R^2}{D}\frac{\partial c}{\partial t}\Big|_{\eta} = \frac{\propto\eta}{D}\frac{\partial c}{\partial \eta} + \frac{\partial^2 c}{\partial \eta^2} + \frac{2}{\eta}\frac{\partial c}{\partial \eta}$, with boundary conditions: $\frac{\partial c}{\partial \eta} = 0\ at\ \eta = 0$, and $\frac{D}{R}\frac{\partial c}{\partial \eta} + c\frac{dR}{dt} = 0\ at\ \eta = 1$ accurately reflects the solute concentration profile of small fast diffusing (salt and small proteins), and large slow diffusing (large proteins, polymers, and low solubility surfactants) within a droplet and can be used to predict structure formation in a desolvating droplet. This hypothesis was found to be qualitatively true.

Specific Aim 4: Delivery of protein therapeutics is limited by the high viscosity and therefore reduced injectability of highly concentrated protein solutions. The

objective of Chapter 5 is to determine if and to what extent suspensions of glassified protein microspheres can be used to improve the injectability of high concentration protein therapeutics. The viscosity of suspensions of glass beads were evaluated using a syringe based method. SA4 will evaluate the hypothesis:

Specific Hypothesis 4: Suspensions of glass beads will have a lower viscosity than a solution of comparable or lower concentration, as predicted by both the Einstein $\left(\eta = \eta_0\left(1 + \frac{5}{2}\varphi\right)\right)$ and Krieger-Dougherty $\left(\eta(\varphi) = \eta_0\left(1 - \frac{\varphi}{\varphi_m}\right)^{-2.5\varphi_m}\right)$ relations. Further work is required to validate this hypothesis, but the foundation for its validity was established.

1.2 Chapter 2: Dissolution of Pure Liquid Droplets

Since the dissolution of a pure liquid micro-droplet into a surrounding liquid is governed purely by solubility and diffusion, knowledge of the solubility of the droplet material in its surrounding allows the measurement of the diffusion coefficient of that material in its surroundings. The diffusion coefficients of water in n-alcohols (*n*-butanol to *n*-octanol) and *n*-alkanes (*n*-pentane to *n*-tetradecane) were measured using a two chamber modification to the micropipette technique of Duncan and Needham[2]. Despite the fact that water droplets in *n*-alcohol dissolve much more quickly than water droplets in *n*-alkanes, the measured diffusion coefficients for water in the *n*-alkanes were twenty five times higher than for the corresponding alcohol (for example 12.5 vs 0.5 x 10-8 cm^2/s for pentane and pentanol). This is attributed to hydrogen bonding. A

diffusion coefficient-viscosity relation of $D = 4x10^{-5}\eta^{-.782}$ for water diffusing through the *n*-alkanes, and $D = 1x10^{-5}\eta^{-.761}$ for water diffusing in the *n*-alcohols (where D is diffusion coefficient, and η is viscosity of the solvent) was obtained. The Macedo-Litovitz and Chung [4] activation energy modifications to the Cohen and Turnbull free volume theory[5] state that the free volume theory prediction for diffusion must be modified $D_{01} = D_0 e^{(-\frac{E}{RT})}$, where D_0 is the Cohen and Turnbull prediction, and E is the activation energy necessary to break free from the neighboring molecules. The ratio of the two diffusion coefficient-viscosity relationships obtained experimentally reveals a difference in activation energy for escaping neighboring molecules to be approximately 1.39RT higher for water in the *n*-alcohols. As 1.39RT (3.5 kJ/mol) is quite low in comparison with the strength of a moderate hydrogen bond (4-15 kJ/mol), the most likely explanation is that water forms, on average, fewer than one hydrogen bond in every diffusion step.

A modification to the Epstein Plesset equation was also introduced to model dissolution of a spherical droplet where part of the sphere's surface area is obscured, such as in the case of a sphere on the end of a pipette filled with a saturated 'plug' (made necessary by development of a two chamber method for micropipette experiments, discussed in Chapter 2.)

1.3 Chapter 3: Droplet Mixtures

If a pure droplet is blown into a solvent, the concentration of the droplet is at all times constant. This is not the case for a droplet which contains a solute, or a mixture. Mass is lost during the 'blowing out' process, and, depending on the system, this mass loss can be significant. It is possible to estimate the amount of mass lost during this process based on measurements of the droplet diameter during this process and the assumptions of the Epstein Plesset equation. This correction is presented in Chapter 3, along with modifications to the technique which are required to maintain careful control over the concentration of the droplets (to reiterate -- measures that are unnecessary for pure droplets, as pure droplets are always at constant concentration.)

The Epstein Plesset equation has been tested for the dissolution of a pure liquid droplet in a liquid, but must be modified to apply to droplet mixtures. A modification to the Epstein Plesset equation was created by assuming perfect mixing, that mass transfer of each component is proportional to surface area at the droplet interface, and keeping track of the proportions of each component that remain in the droplet. Experimentally, this modification was evaluated by using droplets of mixtures of ethyl and butyl acetate and butyl and amyl acetate, both blown into water.

1.4 Chapter 4: Shell and Bead Formation in a Solute-Containing Dissolving Droplet

A previous student, Duncan, began the study of the dissolution of droplets of water containing NaCl (or common table salt) into dehydrating solvents[6]. As the

droplets shrank, a salt crystal formed. Because the droplets may be assumed to be spherical, the concentration of salt within the droplet just prior to supersaturated homogenous crystallization could be measured and was found to be approximately 10 M. Duncan also observed the dissolution of protein containing droplets in a number of solvents, obtaining glassified protein beads. In some instances, for example if a droplet of albumin solution is blown into pentanol, a bead forms. If, however, bovine catalase solution is blown into pentanol, the result is a shell. This may be attributed to how quickly protein diffuses inside the dehydrating droplet as compared to how quickly the droplet itself dehydrates; as the droplet dehydrates, the concentration of protein rises at the boundary of the droplet. This rise in concentration drives diffusion towards the center of the droplet. Once the concentration of protein in solution rises above the critical supersaturation value, solute precipitation occurs. If the concentration of protein within the droplet is fairly uniform, a bead will form. If the concentration of protein at the edge of the droplet reaches critical supersaturation before the center of the droplet reaches supersaturation, however, a shell will form. Fick's second law and the Epstein Plesset equation were combined to form a partial differential equation for the concentration inside a shrinking droplet. This equation was solved numerically.

1.6 Chapter 5: Application: Analysis of Injectable Suspensions

Beads of amorphous protein 'glass' are one invention which resulted from the dehydration of protein solution in a number of solvents. Protein pharmaceuticals are

useful because they possess greater specificity and selectivity than any non-biological small molecule drug[7]. Proteins have been used as pharmaceuticals since 1922, when insulin was first identified[7-10]. Protein is, however, rather fragile -- even when protein is kept in a cool, dark, sterile, aqueous environment, it will degrade after a few weeks [7]. Due to poor absorption through other routes, most protein and peptide pharmaceuticals must be injected, either intravenously (for example Rituxan® and Herceptin®) or subcutaneously.

High concentrations of protein solution are commonly very viscous, and therefore difficult to inject. Dilute solutions, while injectable, may have a large volume which renders them difficult or slow to deliver[11]. Suspensions of microglassified protein beads, however, may offer low viscosity (and hence greater injectability) while also having a high overall concentration. This would permit the easy injection of large amounts of protein therapeutics. A syringe based method for measurement of viscosity, based upon the time to fill a vertical 1 mL syringe, was tested in Chapter 5. While this method proved to be a good measure of liquid viscosity, the measurement of suspension viscosity was hindered by settling of the glass beads used. While dilute suspensions of glass beads did have a viscosity roughly in line with the predictions given in by the Kreiger Dougerty equation, higher concentrations showed a deviation which was most likely the result of changing concentrations due to rapid settling, despite stirring.

1.7 Chapter 6: Microdroplet Size Control

As the glassified protein microspheres are a result of dehydration of the initial emulsion droplet suspension, simple vortexing of the water in oil emulsion or homogenizing with bench top homogenizers routinely creates a wide distribution of microglassified bead sizes (from sub-micron to tens of microns). For several applications envisioned for this new technology (such as the formation of polymer microspheres) the formation of highly monodisperse populations of protein solution droplets is a desireable first step.

Microdroplet creation methods can be divided into two categories: bulk methods and capillary based methods[12-14]. Bulk based methods generally involve two immiscible phases being placed into contact with one another. Agitation is then used to disperse one phase into the other. Common examples of bulk droplet generation methods are stirring, shaking, homogenization, and ultrasonication. Bulk droplet creation methods have the advantage of allowing for the rapid creation of large numbers of droplets. The drawback of bulk droplet creation methods is, however, that since these methods are generally locally inhomogenous, these methods produce polydisperse populations of droplets.

Capillary based methods are methods such as microfluidics, and generally involve the stretching of a fluid thread to make use of the Rayleigh instability. Methods for generating droplets using microfluidics can range from simple syringe needle and

tubing setups to precise channels created through lithography. While capable of creating large numbers of monodisperse microdroplets, capillary methods generally possess the drawback of having a low throughput.

A number of methods of generating dispersions were attempted. Both bulk based methods (including stirring, vortexing, and shaking), and syringe needle based capillary methods were attempted, with no success. Equipment limitations made capillary methods difficult, as the available syringe pump was incapable of generating the necessary flow rates. Nonetheless, a syringe needle and tubing method was identified as the most promising of the methods to generate a monodisperse population of droplets.

2. Dissolution of a Pure Liquid Droplets – The effect of hydrogen bonding on the diffusion of water

2.1 Introduction

Very specifically, this chapter is about the measurement of the diffusion coefficients of water through n-alkanes and n-alcohols and what those diffusion coefficients say about how hydrogen bonding affects diffusion. Diffusion coefficients of water in n-alcohols and n-alkanes have been measured by watching droplets dissolve and fitting the Epstein Plesset equation to the dissolution. These diffusion coefficients contain information about the effect of hydrogen bonding on the diffusion of a small solute, water, as it moves through a solvent of larger molecules, since water can hydrogen bond with alcohols, but cannot hydrogen bond with alkanes. What does that mean? Well, diffusion is the process of mass transfer because of the random thermal motion of molecules. Water will interact differently with alkanes than it will with alcohols, and so, water molecules will move differently through the two materials. To really understand these results, it's important to understand what an atom or molecule is, how atoms and molecules can interact, how diffusion occurs on the molecular length scale, and how these interactions can change this motion.

Portions of this chapter, and some figures, have been reprinted with permission from Su, J.T., et al., *The effect of hydrogen bonding on the diffusion of water in n-alkanes and n-alcohols measured with a novel single microdroplet method.* Journal of Chemical Physics, 2010. 132(4): p. -.Copyright 2010, American Institute of Physics. This article was written

primarily by Jonathan Su, but was edited by David Needham. Other authors helped to develop the techniques which were presented in the paper, but all of the data was taken by Su.

2.1 Atoms and Molecules

To really understand the forces between atoms the composition and structure of the atom must be understood. This section will deal with what atoms are and what they are made of, and sets up the next section, which will deal with the forces between the atoms, including different kinds of bonding (ionic, covalent) and intermolecular forces such as van der Waals.

To begin with, everything – all matter -- is made out of atoms: air, water, buildings, and people. The so called 'atomic hypothesis' has been around since ancient Greece, but it really wasn't absolutely proven that atoms were not a mere mathematical construction until 1905, when a young Swiss patent clerk named Albert Einstein derived equations for Brownian motion based on the motion of atoms[15]. These atoms are always moving around, and how quickly they move around (their kinetic energy) is related to the temperature of the system; at absolute zero, the atoms don't move, and as temperature increases, atoms move more quickly. In fact, according to Chapman and Cowling's seminal work on the Mathematical Theory of Non-Uniform Gases[16], the temperature of a gas in a uniform steady state may be defined according to the equation:

$$\frac{1}{2}m\overline{C^2} = \frac{3}{2}kT, \qquad \textbf{(1)}$$

where T is the temperature, k is Boltzmann's constant (1.3806504 J/K), $\overline{C^2}$ is the square of the average velocity of the molecules, and m is the mass of the molecules. Now atoms themselves are made of three types of subatomic particles: positively charged protons, neutral neutrons, and negatively charged electrons. One of the first models of how these were all arranged was the 1904 Thompson, or 'plum pudding' model of the atom, which essentially assumed that the negatively charged electrons floated around in a positively charged 'pudding'. [17] In 1909, though, Lord Rutherford bombarded gold foil with alpha particles and found that some of the alpha particles were deflected much more than would be expected. He concluded that this was because most of the mass of the atom was in a central nucleus, which the electrons orbited, much like the planets orbit the Sun[18]. The modern view of the atom is that it consists of a dense nucleus, which contains the protons and the neutrons, and that this nucleus is surrounded by electrons, which tend to fall into certain electron orbitals, which describe the most likely location of electrons. These orbitals are described by Schrodinger's equation[19], which is analytically solvable for the hydrogen atom, but becomes extremely difficult to solve analytically for anything more complicated than that[17]. Schrodinger's equation for the hydrogen atom has been used to predict the shape of the electron orbitals for the other atoms[17]. Now that the composition of the atom has been discussed, the next section will deal with the forces between their atoms: their interactions, which arise from the electrostatic forces between these subatomic particles.

2.1.4 Intermolecular and Interatomic Interactions

As the previous section said, all matter is made out of atoms, which are always moving around because of thermal vibrations. Not only are these atoms moving around, but when they get close enough to one another, they will start to exert appreciable forces on each other. Short ranged molecular interactions result from electrostatic interactions between atoms and molecules. There are many general 'types' of force which are important and will be examined in this section, including covalent bonds, ionic bonds, van der Waals forces, and the hydrogen bond, which will be discussed separately and in more depth in the next section, since those bonds occupy a central role in the chapter.

A common type of atomic interaction is the covalent bond, found for example in the hydrogen molecule (H_2), or between the atoms of petane (C_5H_{12}.) Covalent bonds minimize the potential energy of two atoms[20], and are formed when two atoms approach closely enough to 'share' electrons, changing the electron distribution about the atoms. In larger atoms, the inner orbitals remain relatively unaffected as compared to the original atoms, while the outer orbitals change configurations. In the hydrogen molecule, the bond between the two hydrogen atoms is covalent. Each hydrogen atom has a positively charged proton and a negatively charged electron. Electrostatic interactions cause the electron to be attracted to the proton. If two hydrogen atoms are brought more closely together, additional forces occur – each hydrogen atom's electron

will also be attracted to the other hydrogen atom's proton, and the electrons will be repelled from one another, as will the protons. At some distance (the bond distance of H_2: 0.74 A), the energy of the system is minimized – closer, and the proton-proton repulsion becomes quite strong, too far, and the attractive proton-electron forces draw the molecules closer. In a pure covalent bond, electrons are shared equally between the atoms[20].

Another kind of atomic interaction is the ionic bond. In the covalent bond, electrons are shared, but in a purely ionic bond, electrons are transferred completely from one atom to another. There is likely no purely ionic bonded diatomic molecule[20]. For example, in the case of NaCl, sodium has a small ionization energy (~5 eV) and an even smaller electron affinity (~0.5 eV), while chlorine has an ionization energy of more than 10 eV and a large electron affinity (~4 eV). Hence, sodium loses an electron easily to become Na^+, while chlorine accepts the electron to be Cl^- [20]. Thus, ionic bonding occurs.

Molecules may have dipole moments, either permanent or induced. A permanent dipole exists even in an isolated molecule; for example, in water, which has an oxygen atom bound to two hydrogen atoms. The oxygen atom tends to draw the hydrogen's electrons towards itself, which results in a molecule in which charge is not evenly distributed. This results in a dipole moment – the dipole moment of water is 1.85 D[21].

Van der Waals interactions are a combination of short range repulsion between electrons in filled orbitals of atoms on neighboring atoms, and attraction due to induced dipoles which result from repulsions between electrons in neighboring atoms. This occurs in even nonpolar atoms, as even an atom which is overall nonpolar can be, at any instant, due to the position of its large, positively charged protons versus the small mobile electrons, have an instantaneous dipole[21].

Most atoms and molecules are generally attracted to each other. Should atoms approach too closely, they repel because the electrons surrounding the atoms cannot fill the same space (the Pauli Exclusion principle)[22]. The distance at which an atom can be considered a non-interpenetrable hard sphere is known as the van der Waals radius. This section has discussed a number of inter-atomic and inter-molecular interactions. In the next section, a special kind of molecule-molecule interaction known as the hydrogen bond will be discussed.

2.1.5 Hydrogen Bonds

Because of the central importance of the hydrogen bond to this chapter, it will be examined in greater detail in this section. The hydrogen bond was first proposed by Linus Pauling, who wrote in his 1939 paper: "Under certain conditions an atom of hydrogen is attracted by rather strong forces to two atoms instead of only one, so that it may be considered to be acting as a bond between them. This is called a hydrogen bond."[23, 24]. Essentially, when a hydrogen atom is bound to a very electronegative

atom, the electronegative atom attracts electrons from the hydrogen, leaving the hydrogen molecule with a partial positive charge. This results in a dipole-dipole interaction known as a hydrogen bond. The atom that donates the electrons is the H-bond acceptor.

Both hydrogen bonds and covalent bonds are highly directional. Covalent bonds are also very stiff[25], and are generally much stronger, having a strength of around 100 kcal/mol – the strongest hydrogen bonds have a strength from 14 – 22 kcal/mol.[20] There are generally three kinds of hydrogen bonds: strong, moderate, and weak. [24]Of these bonds, the moderate hydrogen bonds are the most common, and are generally what is commonly thought of as a hydrogen bond. The strongest of the hydrogen bonds have a covalent-like nature and may have a strength that ranges from 14-22 kcal/mol. An example of the strong hydrogen bond is the hydrogen bond formed between F^- and HF (39 kcal/mol). The weak hydrogen bonds are electrostatic and are similar in strength (1-4 kcal/mol[24]) to van der Waals interactions, but are directional. One example of the weak hydrogen bond is the C-H to O/N bond.

Moderate hydrogen bonds, which are mostly electrostatic, are the most common hydrogen bond, and are the hydrogen bonds found in water and alcohols. Moderate hydrogen bonds have strengths ranging from 4-15 kcal/mol (with the O-H to O hydrogen bond having a strength of around 5 kcal/mol.) Now that the most common intermolecular interactions have been discussed, this chapter will discuss diffusion.

2.1.6 Diffusion

So far, this chapter has covered the structure and composition of atoms, and how they affect the forces between the atoms. This section will focus on diffusion, which is the transfer of mass because of the random molecular thermal motions discussed earlier. The simplest system to model diffusion is the dilute gas. Because a gas is less dense than a liquid, a dilute gas basically contains molecules which are moving about, but not really interacting with one another[26, 27]; gas molecules will occasionally collide with one another, but spend most of their time traveling in well-characterized velocities. Diffusion in low density gases is fairly well understood[26]. It is therefore possible to determine properties of a gas by assuming that the time gas molecules spend in contact with one another is very small in comparison with the time scale of the properties predicted[16, 27] (such as viscosity). Liquids, though, are a 'condensed material' – that is, the molecules of a liquid are always close to one another, and are always interacting. A molecule of a liquid may at any one time be interacting with its neighbors, which are, in turn, interacting with each other (the so-called many body problem)[28]. These interactions (discussed later) include electrostatic interactions, polarization forces, and quantum mechanical forces[28]. Therefore, while diffusion in a dilute gas is very well understood (see Chapman and Enskog), diffusion in a liquid is not entirely understood.

2.1.7 The Stokes-Einstein Equation

One way to look at diffusion is the motion of a molecule or solute through a continuum. This is a different approach than looking at diffusion from a molecular point of view, which is the approach that has been emphasized so far. Essentially, the continuum approach basically says that past a certain scale, it is possible to look at fluids as having a bulk property. For instance, think about density. Density is the mass per unit volume of a fluid. At a molecular length scale, however simply trying to measure a mass per unit volume of a fluid will not give a constant value: as discussed earlier in this chapter, molecules are always moving as a result of thermal motion. Thus, if the number of molecules inside a very small volume is measured as 'density', there will be significant fluctuation: density will not be constant. As the volume for which density is measured grows, the average number of molecules measured within will stabilize, resulting in a constant density. For all liquids and for gases at atmospheric pressure, the limiting volume is around 10^{-9} mm^3 [29] . So it's possible to think of a liquid as having a bulk property, and it's possible to extend that into modeling diffusion. The most common method of estimating diffusion coefficients is the Stokes-Einstein equation.

In 1905, Einstein derived equations for the motion of microscopically visible particles suspended in a liquid based on the molecular-kinetic theory of heat. Among the results of his equations was an equation for diffusion. [15] Einstein was able to

develop a relation for the diffusion coefficient of such a particle by examining dynamic equilibrium between the fluctuating force and the frictional, or drag force.

In 1851, Stokes, as part of his work on the effect of the internal friction of fluids on the motion of pendulums, published a paper which contained the drag force of a uniformly moving sphere whose velocity is small enough that the drag terms which are proportional to the square of velocity may be neglected.[30]

Einstein incorporated Stokes drag into his equation, resulting in what is known as the Stokes-Einstein equation,

$$D = \frac{k_B T}{f} = \frac{k_B T}{C \pi \eta R} \quad \textbf{(2)}$$

Where k_B is the Boltzmann constant, T is the temperature, η is the shear viscosity of the solvent, C is a constant which is dependent on the boundary condition (slip or stick), and R is the radius of the solute.[31]. While this equation is the most commonly used method for estimating diffusion coefficients in liquids, it is important to note that inherent in the assumption of Stokes drag is the continuum assumption – pendulums are much larger than air molecules. While this continuum approach is quite reasonable for a solute which is much larger than the solvent molecules, this assumption is no longer valid as the solute size approaches the size of the solvent molecules. Intuitively, this makes sense: a very large solute encounters a large number of solvent molecules as it moves. Enough solvent molecules collide and exert forces on the solute that it is possible to think of the solute as encountering an average bulk property – in this case,

the viscosity of the solvent. If, however, a solute is smaller than the solvent molecules, the number of solvent molecules that the solute will encounter and therefore interact with is not at all times constant. Now it's more difficult to argue that the drag on a molecule is related to a bulk property like viscosity. This is where the Stokes-Einstein equation starts to break down.

One modification to the Stokes-Einstein equation for small solutes is based on a reduced viscosity assumption [31], which states that $D \propto \eta^{-\alpha}$, where α lies between 2/3 and 1. [32, 33] Kowert examined the diffusion of O_2, biphenyl, anthracene, diphenylacetylene, diphenylbutadiyne, pyrene, perylene, coronene, and rubrene through a number of organic solvents including *n*-alkanes and found that α may increase with solute size, approaching the Stokes-Einstein limit ($\alpha = 1$) as the solute size becomes large as compared to the solvent[34-39]. This relationship has been tested by molecular dynamics simulation as well, for example by Harris[33], who showed that the molecular dynamics simulations of Meier *et al[40, 41]* of an idealized Lennard Jones fluid resulted in a self diffusion value of 0.921 ± 0.003 for α.

Zwanzig and Harrison[42] have argued that it is more accurate to describe this deviation from Stokes-Einstein diffusion in terms of an effective hydrodynamic radius reflective of the strength of solute-solvent interactions. They examined Pollack and Enyeart's[43] data for Xe (131 g/mol) diffusion in alkanes (72.15 g/mol – 226.44 g/mol) and argued that while the data for a small solute diffusing in a solvent of larger

molecules fits an equation of the form of viscosity to some power very well, the viscosity itself is also related to other physical parameters which might affect diffusion.

2.1.8 Diffusion in Liquids

As discussed earlier in the chapter, the molecules of a liquid are always interacting with each other, and this complicates theoretical predictions considerably. This section will present models for diffusion in liquids, including early activation energy models of the early 1900's, which (for reasons which will be discussed) have given way to the free volume theories which are used today. Because early models for diffusion in liquids were created by chemists, many early models for diffusion in liquid were based around the idea that matter rearranges following the surmounting of a potential energy barrier. These activation energy based models have been around since the early 1900's, and seemed to be supported by the fact that viscosity followed the form

$$\eta = \propto_{\eta} e^{\frac{\beta}{T}} \quad \textbf{(3)}$$

Over the normal range of temperatures generally explored (where η is viscosity, and α_{η} and β are temperature independent parameters). Eyring[44], for example, in 1936, published a theory based upon the idea that molecules passed through an intermediate 'transition state' in which they possessed a higher energy state as compared to those before or after the state. An equilibrium constant between the normal and 'activated' molecules could then be computed, and rate constants could then be computed. This model was applied by Eyring to the diffusion of heavy water into

light water, and a value related to a physical dimension of water obtained from the model, which seemed to suggest that this theory was correct[44].

A reason that activation energy based models of diffusion are no longer used for liquids, however, lies in the fact that one fundamental assumption of activation energy based theories is that the proportion of activated molecules should be very small[45]. Experiments have found activation energies for diffusive and viscous flow to lie in the region of 10-50 kJ/mol, with most values for mobile liquids lying in the 20 kJ/mol region. At 10 kJ/mol, approximately 20 percent of molecules would be in the activated state at room temperature[45]. Thus, at least in liquids, activation energy based theories for diffusion and viscosity have given way to free volume based theories, though activation energy based models persist in diffusion in solids[45].

A free volume based theory for diffusion in liquids was first proposed by Cohen and Turnbull in 1959[5, 46]. The Cohen and Turnbull free volume theory is based on the idea that liquid molecules may be thought of as hard spheres. At all times a liquid molecule is surrounded by a 'cage' of other liquid molecules. These molecules are in constant motion (with a frequency on the order of $10^{12} – 10^{13}$ Hz[47]), and these random fluctuations eventually produce an adjacent vacancy large enough for the diffusing molecule to move into[48]. The diffusion step, Cohen and Turnbull believed, was finished once a neighboring molecule occupied the previous location of the diffusing molecule. This model assumes that free volume is constantly being redistributed in a

liquid, and that diffusion does not require the overcoming of a potential energy barrier. In contrast, the activation energy theories essentially assume that the diffusing molecule has enough energy to physically displace neighbors[48].

Mathematically, the Cohen and Turnbull theory states that the total occupied volume of a liquid of N hard spheres of volume V* is NV*. If each sphere has, on average, free volume of V^f, the total volume of the liquid is

$$V_L = NV^* + NV^f \quad \textbf{(4)}$$

Cohen and Turnbull then developed a distribution function describing the probability of locating a free volume of sufficient size adjacent to a spherical molecule. The self-diffusion coefficient can then be written as:

$$D = Ae^{(-\gamma V^*/V^f)} \quad \textbf{(5)}$$

Where D is the self-diffusion coefficient, V* is the critical free volume size, A is a proportionality constant related to temperature, and γ is a correction factor for free volume shared by neighboring molecules.

The Cohen and Turnbull model was extended by Macedo and Litovitz in 1965 , as well as Chung in 1966[4, 48]. These authors argued that a molecule must still overcome attractive interactions prior to making a diffusive step. They therefore modified the Cohen and Turnbull diffusion coefficient prediction with an additional term:

$$D_{01} = D_0 e^{(-\frac{E}{RT})} \quad \textbf{(6)}$$

Where E is the activation energy necessary for a molecule to break free from its neighbors before it can occupy an adjacent free volume. Note that this is different from an overall activation energy for diffusion. This activation energy modification to the Cohen and Turnbull free volume theory will be used to find the difference in neighbor leaving activation energies for water diffusing through *n*-alcohols and water diffusing through the *n*-alkanes . Now that the general theories for diffusion in liquids have been discussed, the equation that describes droplet dissolution will be examined. This equation is the Epstein-Plesset equation.

2.1.9 Fick's Law and the Epstein Plesset Equation

Both diffusion and heat conduction are processes which result from random molecular motion. In 1855, Adolf Fick[49] first set out the equations of diffusion through analogy with the equations of Fourier, who had developed equations for heat transfer in 1822[50]. Fick's first law essentially states that the rate of mass transfer per unit area of a substance will be directly proportional to its concentration gradient through a constant of proportionality known as the diffusion coefficient. Mathematically, this is stated as:

$$J = -D\frac{\partial C}{\partial x} \tag{7}$$

Where J is the flux, D is the coefficient of diffusion, and C is the concentration.

Fick's second law (Equation 3) describes mass accumulation and can be derived by considering mass accumulation in an infinitesimally small volume through which diffusion is occurring in accordance with Fick's first law.

A single droplet in a dehydrating medium may be modeled as a spherical, symmetrical, constant-density droplet which loses mass solely through diffusion. For such a droplet, the change of radius R for a given mass loss is related by:

$$\frac{dm}{dt} = 4\pi R^2 \rho \left(\frac{dR}{dt} \right) \tag{8}$$

Fick's Second Law equation can be solved:

$$\frac{\partial u}{\partial t} = D\left(\frac{\partial^2 u}{\partial r^2} \right), \tag{9}$$

Where u is a transformed coordinate: $u = r(c - c_s)$, r is the distance from the center of the droplet, c is the concentration, and c_s is the saturation limit of the contents of the droplet in its surrounding environment.

For boundary and initial conditions: $\begin{matrix} u(r,0) = r\delta \\ u(R,t) = 0 \end{matrix}$, where $\delta = (c_i - c_s)$

The concentration gradient at the boundary of the droplet was previously solved and is given in the Epstein Plesset paper[3]::

$$\left(\frac{\partial c}{\partial r} \right)_R = \delta \left\{ \frac{1}{R} + \frac{1}{\sqrt{\pi D t}} \right\} \tag{10}$$

This is related, through Fick's first law, to the total mass flow from the droplet:

$$\frac{dm}{dt} = 4\pi R^2 D\left(\frac{\partial c}{\partial r}\right)_R = 4\pi R^2 D\delta\left\{\frac{1}{R} + \frac{1}{\sqrt{\pi Dt}}\right\} \quad \textbf{(11)}$$

Using the previous radius and mass relation, a relation for the radius versus time behavior of a water droplet in a dehydrating medium can be obtained. This is the Epstein Plesset equation:

$$\frac{dR}{dt} = -\frac{DC_s(1-f)}{\rho}\left\{\frac{1}{R} + \frac{1}{\sqrt{\pi Dt}}\right\} \quad \textbf{(12)}$$

Where f is defined as c_i/c_s, the ratio of initial concentration to the saturation concentration. The Epstein-Plesset equation forms the basis for the models for single droplet dissolution. This equation was shown to be valid for liquid droplet dissolution and gas bubble dissolution in a liquid medium, but holds only for the cases where bubble and droplet dissolution are a result of diffusion.

2.1.10 Hydrogen Bonding and Diffusion

A water molecule is composed of a single, comparatively large, oxygen atom covalently bonded to a pair of smaller hydrogen atoms, with an angle between the two O-H bonds of 104.52 degrees. Water is both a hydrogen bond donor and a hydrogen bond acceptor. Because of the geometry of the water molecule, it is highly polar, having a permanent dipole moment of 6.17×10^{-30} C m = (1.85 Debye), due to a partial negative charge on the oxygen, and a partial positive charge near the hydrogen atoms[22].

N-alcohols have a hydrophobic aliphatic group attached to a hydrogen bond-capable OH group (dipole moment from 1.7 (*n*-pentanol) to 2.0 Debye (*n*-octanol)[51]).

Thus, both water and alcohols can hydrogen bond, making the water-alcohol system ideal for studying the effect of this bonding on diffusion. *n*-Alkanes on the other hand have zero dipole moment, no capacity to hydrogen bond, and so represent the control system of the same hydrocarbon composition but lacking the -OH of the homologous alcohols.

Solute-solvent interactions, such as hydrogen bonding, have been found to affect the diffusion of a solute in a solvent. Easteal and Woolf examined the diffusion of short chain alcohols in water under various pressures and attributed initial increase in diffusion coefficient under increasing pressure as being due to the disruption of hydrogen bonded networks, allowing a solute to move while breaking fewer bonds[52]. Tominaga *et al* have examined the diffusion of cyclohexane and cyclohexanol in ethanol, methanol, and 1-hexanol, and similarly found the diffusion of cyclohexanol to be slower in alcohols as compared to that in cyclohexane[53], signifying that when a solute can hydrogen bond with the solvent, its progress through the solvent, by diffusion, is retarded.

Chen and Chan[54] used Taylor dispersion to measure the diffusion of various solutes in ethanol. They found that the solutes that were capable of hydrogen bonding diffused more slowly than non-associated solutes, and concluded that the retardation was equivalent to an increase in the equivalent van der Waals volume of a hydrogen bonding solute. They also compared this increase in van der Waals volume with the

van der Waals volume of the ethanol monomer and attributed this difference to solute-associated ethanol monomers. They calculated, using the Stokes Einstein equation, that phenols, on average, diffused with approximately 2.5 ethanol molecules, and that all aromatic amines diffused with approximately one ethanol molecule. This would suggest that a solute larger than the solvent molecules with which it is surrounded can effectively pick up the smaller solvent molecules and diffuse as a complex. In the same year, (1997), Chan *et al*[55] examined the diffusion of various pseudo-planar solutes in acetone and, using similar assumptions, concluded that all phenols on average diffused with approximately one acetone molecule and that all aromatic amines diffused with approximately 0.6 molecules of acetone, on average.

This slowing of diffusion due to hydrogen bonding has been used to investigate hydrogen bonding in dilute solutions, for example by Lu *et al*[56]. This is also supported by molecular dynamics simulations, which predict a slower diffusion coefficient for a solute which interacts attractively with the solvent, and a faster diffusion coefficient for a solute which interacts repulsively with the solvent[57], when compared to a model which had no interaction between solute and solvent.

Attempts have been made to modify the Stokes-Einstein equation to make the equation applicable to polar solute diffusion in alcohols and alkanes. Because a polar solute will have a different interaction with an alkane as compared to an alcohol, it becomes necessary to change the equation's boundary equation from the slip (C = 6) to

the stick condition (C = 4) to reflect this interaction[58]. Wakai and Nakahara, however, studying molecular diffusion using H-Fourier-transform pulsed field-gradient spin-echo NMR, found that this boundary condition change overestimated the friction ζ when the Einstein relation was applied to the diffusion coefficients of water in carbon tetrachloride, benzene, chloroform, dicholoromethane, acetonitrile, and acetone[59].

Wakai and Nakahara also examined the diffusion of different solutes in a variety of solvents, varying solute size, solute-solvent interaction, and solute polarity. They found that water molecules diffusing in organic solvents had an irregular dependence on viscosity, with, for example, a higher diffusion coefficient of water in acetonitrile as compared to acetone, despite acetonitrile's higher viscosity[59].

With this previous work (discussed above) in mind, the diffusion coefficients of water in *n*-alcohols and *n*-alkanes were measured. Previous experimental studies of small solute diffusion with hydrogen bonding have either focused on a single solvent with a variety of solutes or a variety of unrelated solvents with a single solute. The investigation concentrates on a single solute (water), diffusing in a series of homologous solvents which differ only in chain length and presence or absence of an –OH group. The effect of hydrogen bonding on diffusion for the case of water can be isolated. The relative simplicity of the technique and its analyses means that it is applicable to other solvent-solute systems for quantification of diffusion.

2.1.11 Hydrogen Bonding and Small Solute Diffusion in a Liquid

Diffusion of a small solute in a solvent with which it can hydrogen bond is an important, yet incompletely understood problem in liquids. The Stokes-Einstein equation, predicts that for a given particle radius, at known temperature, the diffusion coefficient is simply inversely proportional to the solvent viscosity. It is the most commonly used equation for estimation of the diffusion coefficient of a solute in a solvent[60]. However, for solutes smaller than the solvent, the Stokes-Einstein equation is of questionable validity, as the continuum assumption inherent in the Stokes drag equation no longer holds. In fact, experiments reveal that small solutes in a large solvent diffuse more quickly than predicted by the Stokes-Einstein equation. Furthermore, any attractive solute-solvent interactions, such as hydrogen bonding, would also affect the friction coefficient, and hence retard the motion of the solute through the solvent, lowering the diffusion coefficient[34, 35, 61]. In order to examine these effects in more detail, and to test the SE in systems with and without hydrogen bonding a new micropipette technique and analysis has been used to measure the diffusion of water in *n*-alcohols (with hydrogen bonding) and compared the results to that in *n*-alkanes (without hydrogen bonding).

As a water molecule is smaller than a molecule of n-alkane or n-alcohol, it can be can reasonably expected that diffusion behavior for water in both solvents will deviate from that predicted by the Stokes-Einstein model. Some experiments on solute diffusion

with hydrogen bonding have found that it retarded the motion of the solute as compared to a similarly sized and shaped solute incapable of hydrogen bonding. This data has been interpreted by some as the solute effectively diffusing as part of a solute-solvent complex.

One common experimental method of determining the diffusion coefficient of a liquid in another is the Taylor dispersion[60]. This method is based on laminar flow of the solvent, into which a pulse of immiscible solute is injected. The decay of this pulse is dependent on the diffusion of the solute in the solvent, and so, by measuring the shape of this pulse the diffusion coefficient of the solute in the solvent can be determined.

Another common method of experimental determination of diffusion coefficients is the diaphragm cell, which is comprised of two compartments of liquid of different concentration separated by either a porous membrane or a glass frit[60]. The diffusion coefficient is measured by determining the concentration present in each compartment after a given length of time. Easteal[62] used the diaphragm cell to study the diffusion of water in a variety of organic liquids, but did not extend his work to *n*-alkanes of chain length longer than hexane. Previous work on water diffusion in alcohols has similarly been limited to the shorter chain alcohols (up to *n*-butanol), in which water is more soluble and for methanol and ethanol, is miscible. These values are important and give us a point of calibration for the longer alkanes and alcohols studied here.

The method and analyses described in this chapter does not require any sort of flow, and the droplets are kept spherical by surface tension. Here, a technique for determining the diffusion coefficient of one liquid in another is presented, where the two liquids form an interface. This method is based on the observation of the dissolution of a microdroplet on the end of a micropipette. Because small microdroplets can be manipulated this way, the shrinkage of the droplet due to dissolution of the organic into the water can be measured in seconds to minutes.

As will be further described, a tens of micron-scale water droplet placed in an excess of pure *n*-alcohol or *n*-alkane solvent will lose mass because the water will dissolve completely into the solvent. This mass loss is visually observable in a light microscope as a reduction in the dimensions (diameter) of the droplet, and, assuming that mass transfer is governed only by diffusion, the time dependence of the mass loss is directly related to the concentration gradient of water at the boundary of the droplet. The gradient is, in turn, directly related to the solubility of water in the medium as well as the diffusion of water in that medium as it disperses in the medium away from the droplet interface. The relationship between diffusion, solubility, and the radius of the droplet forms the basis of the Epstein-Plesset equation initially developed to describe the *Stability of Gas Bubbles in Liquid-Gas Solutions*[3], but applied here for liquid-liquid systems.

The micropipette technique has been used in previous work by Duncan and Needham, which has shown that the Epstein-Plesset model[2] accurately predicts the radius versus time behavior of various two phase micro systems both for liquid-in-liquid[2] and gas bubble-in-liquid systems[1] from which mass is transferred purely through diffusion, and where the parameters of diffusion coefficients and solubility are known.

Because of the small size of the droplets (on the order of picoliters that can be suspended in hundreds of microliters of solvent), this method is ideal for the study of sparingly soluble solutes, such as in the case of water dissolving into longer chain *n*-alkanes, where typical solubilities are on the order of 10^{-8} M. This method bears conceptual resemblance to other methods of determining diffusion coefficient which are based on motion or decay of an interface.

In this chapter the diffusion of water in long chain alcohols and alkanes has been used to examine the effect of hydrogen bonding on small solute diffusion. By using a homologous series of alcohols and alkanes, solvent viscosities can be varied while maintaining similar intermolecular interactions within each series. While dispersion (van der Waals) interactions are present in both, water will hydrogen bond with alcohols and not with alkanes. Thus, diffusion of water molecules through long chain *n*-alcohols and *n*-alkanes allows the examination of the effect of hydrogen bonding on diffusion

behavior and quantify it. By using the same solute, any effects on diffusion from changes in solute shape or solute polarity are eliminated.

Constant diffusion coefficient is a low concentration approximation; in reality, diffusion coefficients tend to vary with concentration. This concentration dependent diffusion coefficient can change as much as hundreds of percent, and the form of this dependence is not always the same and is not always known [63]. To give an idea of the form of these relationships, two systems for which concentration dependent diffusion concentration are well characterized are urea in water and sucrose in water (as given in Cussler): urea's diffusion coefficient in water, for example, is $(1.380 - 0.0782\ c_1 + 0.00464\ c_1^2)*10^{-5}$; sucrose's diffusion coefficient in water is $(0.5228 - 0.265c_1)*10^{-5}$, where c_1 is the concentration of solute in moles per liter.[63] In any case, the Epstein-Plesset equation assumes that shrinkage of the droplet is governed by diffusive mass transfer at the boundary of the droplet. At the boundary of the droplet, the concentration of the contents of the droplet is assumed to be the saturation concentration, and it is at this concentration that diffusion is being measured. Since diffusion coefficient is not a constant, what we are actually measuring is the diffusion coefficient of the droplet material in the surrounding material at the saturation concentration. The saturation concentration of water in *n*-alkanes is quite low, and hence closer to infinite dilution, but this is not necessarily the case for water in the *n*-alcohols. While this holds true for any

method of measuring diffusion coefficient by observation of a moving interface, it is something that should be kept in mind.

2.2 Materials and Materials

2.2.1 Material Systems Studied

Table 1. Chapter 2: Material Systems Sudied

Material Systems Studied	
Droplet	Surrounding Solvent
Water	*n*-Pentane
	n-Hexane
	n-Heptane
	n-Octane
	n-Decane
	n-Undecane
	n-Tetradecane
	n-Butanol
	n-Pentanol
	n-Hexanol
	n-Octanol

The materials used were n-butanol (EMD Biosciences), n-pentanol (Sigma Aldrich), n-hexanol (Acros Organics), n-heptanol (Sigma Aldrich), n-octanol (Sigma Aldrich), n-pentane (Burdick & Jackson), n-hexane (Sigma Aldrich), n-heptane (Sigma Aldrich), n-octane (Sigma Aldrich), n-decane (TCI America), n-undecane (Sigma Aldrich), n-tetradecane (Sigma Aldrich), n-hexadecane (Sigma Aldrich), and deionized water. All solvents were dried of any dissolved water prior to experimentation using Type 3A molecular sieves (EM Science) by placing forty beads of sieve into the bottom of

a 20 ml scintillation vial, which was then covered with 15 ml of the solvent and sealed with a tight screw cap.

Water Solubility

All solubility values of water in the various *n*-alcohols were found in the literature[64, 65]. Solubility of water in the *n*-alkanes was calculated using an empirical equation obtained by **Tsonopoulos for alkanes from C_2 to C_{16}**[66]**:**

$$\ln x_w = \frac{-79.6677 - 6.6547CN}{9.5470 + CN} \quad \textbf{(13)}$$

where CN is the carbon numbers of a hydrocarbon and x_w was the mole fraction of water. The values obtained from the Tsonopoulos equation were compared to those values for water solubility in pentane, hexane, heptane, and octane available from literature[67, 68], and found to correspond well.

2.2.2 Experimental Methods

The Micropipette

The micropipette has been employed in the biological sciences since the early 1900's. A major problem in the early 1900's and late 1800's was the cultivation of cultures of a single spore. Many methods[69] were used, among them capillary tube based methods, beginning with Klebs in 1873, who used a fine capillary tube to observe replication in dilute suspensions of bacteria and spores, through to Hesler, who, in 1913, used a very fine capillary tube manipulated by hand to isolate single ascospores of Physalospora cydoniae. Similar, capillary tube based techniques were used by Holker

in 1919 and Hansen in 1926, who broke segments of the tube containing single spores and transferred them to growth media. Marshall A Barber, working on proving the microorganism theory of disease of Koch and Pasteur in 1904[70], used a micromanipulator fixed to the microscope stage to manipulate a micropipette (made by pulling a glass capillary using an ordinary Bunsen burner) or microneedle to handle bacteria in a microdrop on the underside of a coverglass placed over a moist chamber. This micropipette was used to remove single cells and transfer them to another culture, either by breaking off of the tip or depositing its contents into a test tube. A mercury column, heated with water to expand and contract, was used to control pressure in the pipette. Barber's apparatus was so complicated that it was not generally adopted[71]. However, he is generally credited with the technique of making a glass micropipette and manipulating it in the field of a compound microscope. Marshall Barber was successful in using the micropipette to induce disease in a mouse using a single anthrax bacillus[70].

Barber's method was later modified in 1923, by Peterfi, who used a platinum coil to heat the mercury column, and in 1922, by Chambers, who fitted a Luer syringe to the micropipette with a flexible tube. In 1954, Mitchison and Swann[72] became the first to measure physical properties of a cell by using a glass micropipette as part of what they called the 'cell elastimeter'. Pressure was controlled using a sea-water reservoir which was raised or lowered by a screw. This method was later refined by Rand and

Burton[73], who more carefully controlled the pressures involved (calibrating the device by measuring the pressure necessary to draw isobutanol into a water-filled pipette), before being perfected by Evans and Hochmuth.

Micropipette techniques have been used extensively by the Needham lab since the 1980s to measure and characterize the material properties of red cells, white cells, and giant lipid vesicles[74-81]. The micropipette has also been used to measure the permeability of lipid membranes, receptor-ligand mediated adhesion, molecular exchange, and other mechanical and thermomechanical properties that characterize a bimolecular membrane. The micropipette has also been applied to measurements of equilibrium and dynamic surface and interfacial tension.

Micropipette Manipulation System – The Two Chamber Method

Individual microdroplets were formed, manipulated and observed using a micropipette manipulation system. The micropipette technique for liquid microdroplets has been explained in a previous paper by Duncan[2]. Briefly, micropipettes were formed from glass capillary tubes, which were then microforged to provide a flat tip of about 8-10 microns internal diameter. These pipettes were then treated with hexamethyldisilazane (HMDS) to make them hydrophobic. The micropipette was then used to blow 50 μm diameter droplets of water into aniline, and aniline into water. Through observation of the radius of the droplet as the droplet dissolved into the

surrounding solvent, the mass flow from the droplet was measured and found to be well modeled by the Epstein-Plesset equation[2]

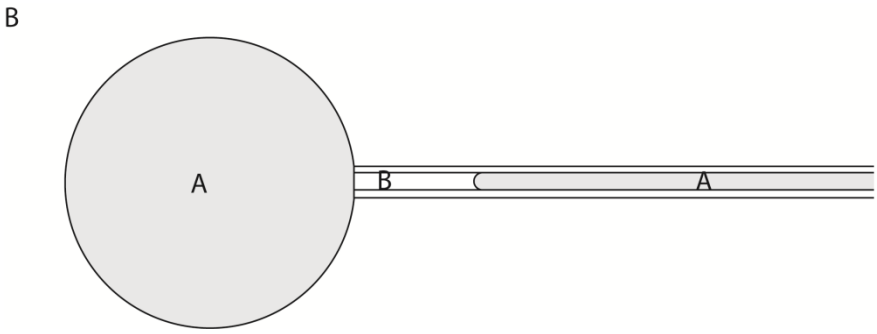

Figure 2. A droplet of material A is blown into an environment B using the single chamber method. The droplet is 'tapped off' or caught, leaving a 'plug' of material B between droplet and the reservoir of the liquid.

The standard micropipette technique involves backfilling the desired droplet material into a pipette, blowing out a droplet, and then separating it from the main reservoir of liquid by either 'tapping off' or separating and then catching the droplet.

The process of breaking off a single droplet is not always simple for all systems of interest, and sometimes can contain surfactants, which may affect the results. As surfactants occupy space at the interface, they clearly have the potential to affect mass transfer. In previous experiments, water droplets in pure decanol displayed wild surface oscillations, attributed to the Marangoni effect[82]. These oscillations disappeared with the addition of surfactant, so some affect of surfactant on droplet systems is clearly present. Certainly, for the more commonly studied problem of droplets in slow viscous flow, surfactant contamination has been shown to play a role, possibly through the elimination of internal circulation in the droplet (though others

argue that surfactant absorption to the surface is the cause of the reduction in mass transfer)[82]. Lee [83] studied mass transfer in a single drop extraction column and found a concentration dependent effect of Triton X-100 on transfer of acetic acid from acetic acid CCl_4 droplets into water. Because surfactant can affect mass transfer, experimental methods which eliminate surfactant are desirable.

Hence, a two chamber method was developed. This two chamber method allows a pipette to be placed into a chamber full of one liquid or solution of interest, loaded with enough material for a single droplet, then withdrawn with this liquid and blown into another chamber.

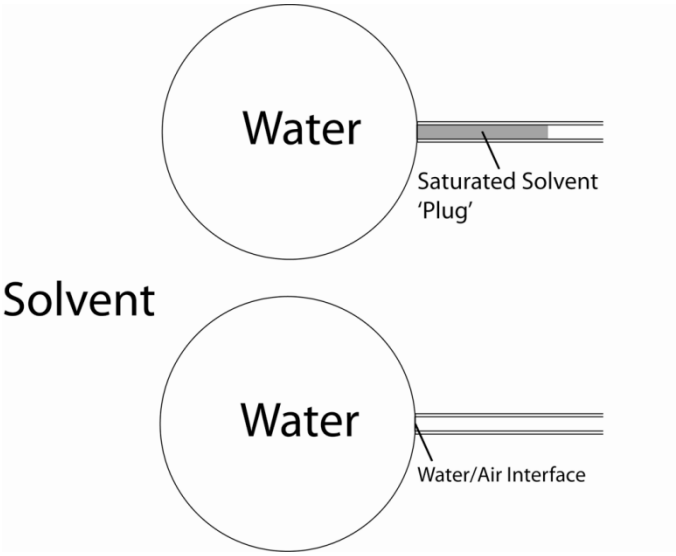

Figure 3. A droplet suspended on the end of a micropipette, both with (top) and without (bottom) a saturated plug. Without the presence of a saturated plug, water leaves the droplet both through the solvent and through the air behind it in the pipette. Since the volume of the air behind the droplet is quite small, the concentration of water in the air is high; hence, the rate of transfer of water through

Figure 3 (continued) the water/air interface is quite low. This rate can be calculated using certain geometrical assumptions.

Examining the geometry of the pipette and droplet shown in Fig. 3, it is clear that, while holding the droplet on the end of the pipette is a prerequisite for maintaining a diffusion limited process and for visual observation and recording of droplet dimensions as it dissolves into the surrounding medium, there is the possibility for water to also transfer out of the droplet through the water/air interface into the shaft of the pipette. Even though water vapor saturates the air space within the air-filled pipette, this transfer was found to be a source of error for the more slowly dissolving systems.

To eliminate this effect, a small amount of water-saturated *n*-tetradecane was drawn into the pipette prior to pulling water into the pipette. Because the tetradecane 'plug' behind the water droplet was saturated with water, water did not diffuse into the tetradecane, and hence left the droplet solely by diffusion into the anhydrous solvent. For the case of a droplet which transfers water both at the water/solvent interface and through an interface at the pipette, the mass flux can be split into two parts (for a saturated 'plug', $J_{pipette}$ is, of course, zero):

$$J_{total} = J_{water/solvent} + J_{pipette} \quad \textbf{(14)}$$

The surface area of a spherical cap of height h of a sphere with radius R is: (See Figure 4):

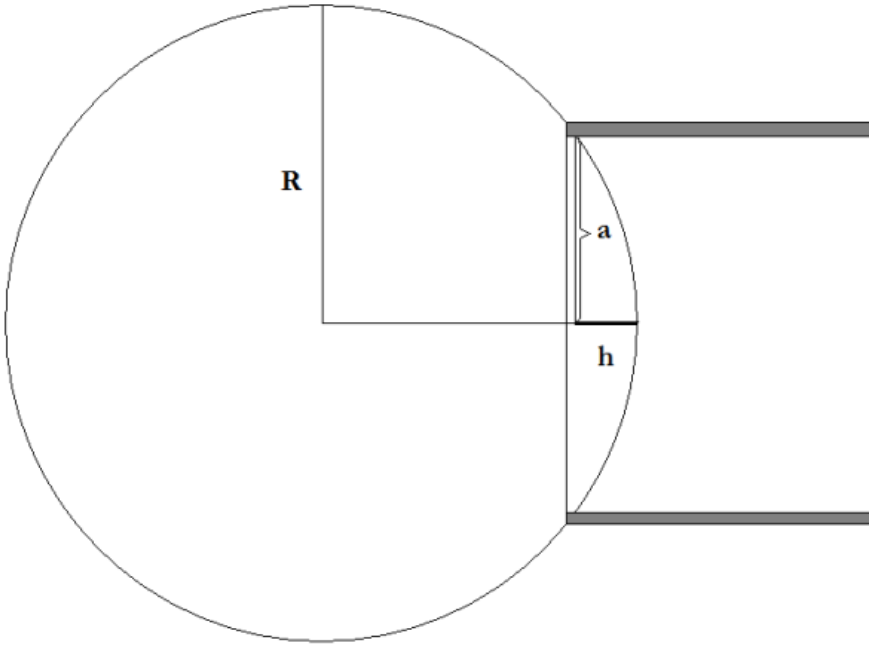

Figure 4. The surface area of a spherical cap of radius a and height h is given by equation ##

$$S_{cap} = 2\pi Rh \tag{15}$$

We can relate h to the radius of the spherical cap, a (physically the inner radius of the pipette), by using Pythagoras's theorem and recognizing that the length of the line from the center of the sphere to where a touches the boundary is the radius. We obtain:

$$\begin{aligned} h &= R - \sqrt{R^2 - a^2} \\ S_{cap} &= 2\pi R(R - \sqrt{R^2 - a^2}) \end{aligned} \tag{16}$$

The surface area of a spherical cap of height h of a sphere with radius R and cap radius a is:

$$S_{cap} = 2\pi R(R - \sqrt{R^2 - a^2}) \quad \textbf{(17)}$$

Mass leaving the spherical droplet into the solvent can now be assumed to exit through a spherical surface area reduced by this amount. The Epstein-Plesset equation can now be modified to obtain:

$$\frac{dR}{dt} = \frac{2\pi R\left(R + \sqrt{R^2 - a^2}\right)Dc_s(1-f)\left(\frac{1}{R} + \frac{1}{\sqrt{\pi Dt}}\right)}{4\pi R^2 \rho} \quad \textbf{(18)}$$

This modified equation, along with the water-saturated plug, now allows the obtaining of a more accurate curve-fit for droplet radius versus time, eliminating error due to transfer of water into air in the pipette. The liquid droplets were formed and held by the same micropipette in the center of the chamber, similar to the previous experiment by Duncan and Needham[2] and their diameters were measured versus time by using a calibrated video caliper system.

As mentioned above, the task is to form a single picoliter scale water droplet on the end of the pipet immersed in a microchamber of the organic solvent. Simply filling a pipet with water and trying to expel a single droplet proved very difficult because even though the pipet was treated to be hydrophobic on the outside, it did not have sufficient wetting characteristics for the water column in the pipet to pinch off and isolate the droplet. In the Duncan and Needham experiment, droplets were simply "tapped" off and, because of their neutral buoyancy, were readily recaptured. However, in these solvents the buoyancy difference prevented this delicate maneuver. Therefore, in a new

micropipet method, developed specifically for this kind of study, two standard optical glass cuvettes with a 2 mm path length (Nova Biotech, G-126) were arranged as shown in Fig. 5. Approximate dimensions are 40 × 10 × 2 mm^3 for a volume of about 0.8 mL. The temperature was controlled by the ambient air temperature and was nearly constant at 22 ± 1 °C in all experiments. (It should be noted that because temperature is controlled by ambient air temperature, localized temperature changes may occur for two liquids which have a very high heat of mixing. This is offset by the fact that the droplets are very small and the volume they are in is very large.) One cuvette was filled with water, the other with the organic solvent of interest. The fluid in the microchambers was held intact at the one open interface by surface tension. The advantage of the two-chamber approach is that the size of the droplet can be accurately controlled by how much water is drawn into the pipette and that is then expelled into the solvent in the other micro-chamber.

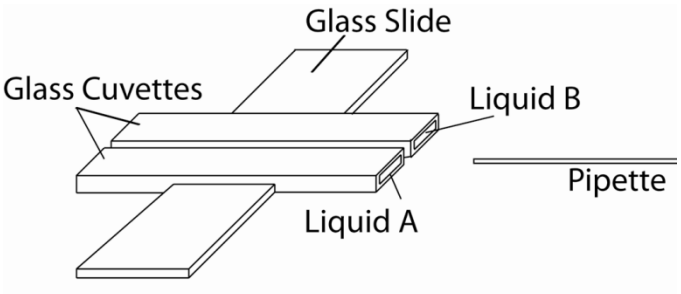

Figure 5. Two-cuvette system for micropipette based technique. This system allows the control of the amount of liquid A drawn into the micropipette. A droplet of liquid A can then be drawn into liquid B. In order to form a water droplet, the micropipette was first inserted into the water containing chamber. The desired

Figure 5. (continued) amount of water (~ .5 nanoliters) was drawn into the micropipette by slightly reducing the suction pressure, (micro to milli atmospheres negative pressure), re-zeroing the pressure, and withdrawing the micropipette and inserting it into the solvent-containing cuvette. A droplet was then blown out and held on the pipette tip with a small suction pressure, well below the pressure required to overcome its surface tension[84-86] and cause it to flow into the pipette. The droplet was then (Figure 7, continued) allowed to dissolve in the organic solvent and this reduction in diameter was then recorded on video tape for subsequent analysis. To preserve the anhydrous nature of the solvent medium, a new cuvette full of freshly anhydrous solvent was used for each micro-droplet experiment.

2.3 Results

Table 2 Diffusion coefficient of water in *n*-alcohols and *n*-alkanes: The diffusion coefficients of water in various *n*-alcohols and *n*-alkanes were obtained through use of the Epstein-Plesset equation.

Alkanes	Diffusion Coefficients (cm^2/s)	Alcohols	Diffusion Coefficients (cm^2/s)
n-Pentane	$12.5 \pm 0.58 \times 10^{-5}$	*n*-Methanol[i]	1.75×10^{-5}
n-Hexane	$8.97 \pm 0.76 \times 10^{-5}$	*n*-Ethanol[i]	1.22×10^{-5}
n-Heptane	$7.42 \pm 0.75 \times 10^{-5}$	*n*-Propanol[i]	0.61×10^{-5}
n-Octane	$5.38 \pm 0.43 \times 10^{-5}$	*n*-Butanol[i]	0.56×10^{-5}
n-Decane	$4.06 \pm 0.43 \times 10^{-5}$	*n*-Butanol	$0.44 \pm 0.06 \times 10^{-5}$
n-Undecane	$3.17 \pm 0.27 \times 10^{-5}$	*n*-Pentanol	$0.52 \pm 0.08 \times 10^{-5}$
n-Tetradecane	$1.88 \pm 0.21 \times 10^{-5}$	*n*-Hexanol	$0.35 \pm 0.03 \times 10^{-5}$
n-Hexadecane	$1.15 \pm 0.13 \times 10^{-5}$	*n*-Heptanol	$0.31 \pm 0.02 \times 10^{-5}$
		n-Octanol	$0.20 \pm 0.05 \times 10^{-5}$

[i] Values for diffusion coefficient of water in lower *n*-alcohols are obtained from MA Lusis, GA Ratcliff: Diffusion of Inert and Hydrogen-Bonding Solutes in Aliphatic Alcohols. Aiche Journal 17 (1971) 1492-&.

2.3.1 Radius Versus Time for a Dissolving Water Droplet in Solvent.

The radius versus time behavior of a water droplet dissolving in a surrounding solvent is shown in Fig. 6. The radius vs time curve was also fit to the Epstein-Plesset model. Having already shown that the EP model accurately defined the dissolution of

water into aniline where both solubilities and diffusion coefficients are known [87], and since the solubility of water in the various alcohols and alkanes was already known[64, 65], it was possible, using this simple data, to vary diffusion coefficients of a plotted Epstein-Plesset curve until a satisfactory fit was achieved. As Fig. 6 shows, dissolution times for a 40 micron diameter droplet are 10 times slower for alkanes than the corresponding chain length alcohol.

In order to test this method against already measured values from the literature, thirteen droplets of water were formed into a butyl alcohol solvent, in which the solubility and diffusion of water were already known[60], and their dissolution time recorded. Analysis of the data for the droplet resulted in an experimental value of 4.36 ± 0.57 x 10^{-6} cm^2/s. By comparison, a literature value for water in butyl alcohol[60] was found to be 5.6 x 10^{-6} cm^2/s. The experimental value for the diffusion of water in hexane, 8.97 x 10^{-5} cm^2/s was also found to be quite close to the value obtained by Easteal[62] of 9.5x10^{-5} cm^2/s.

Thus, the Epstein-Plesset equation was used to obtain values for the diffusion coefficient of water in C_5 – C_{16} *n*-alkanes and C_4 – C_8 *n*-alcohols, i.e., the solubility limit of the droplet material in the surrounding medium was known, and the radius versus time behavior of the droplet was measured, and so the diffusion coefficient of one material in the other could be deduced. The results are shown in Table I. All values in this table were measured by the micropipette technique except for the miscible pairs of water in

methanol, ethanol and *n*-propanol. These values were obtained from the paper by Lusis and Ratcliff[88].

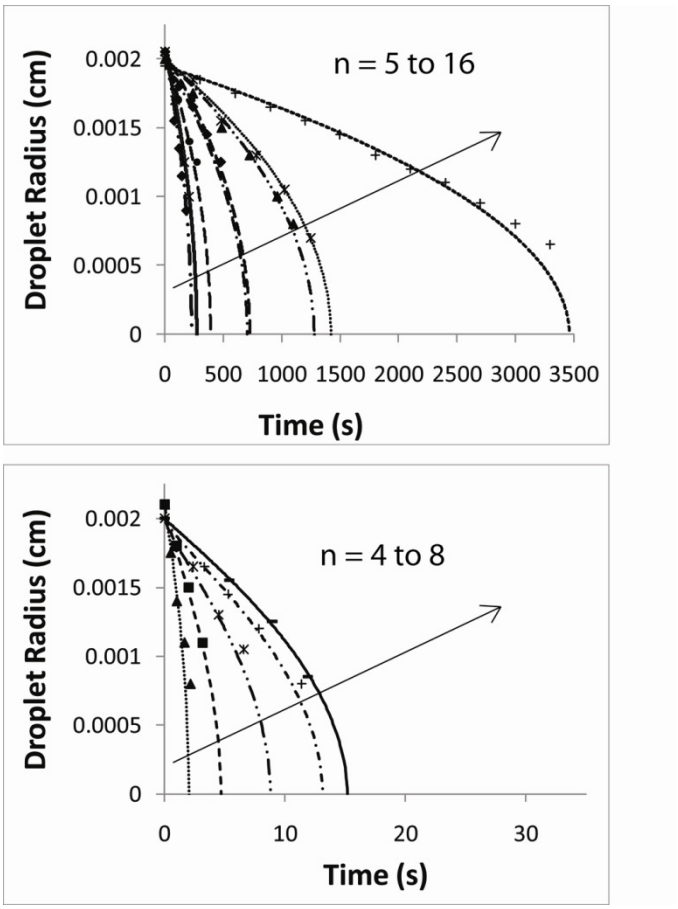

Figure 6. Example radius versus time plots of water droplets in n-alkanes and n-alcohols, fit to the Epstein Plesset equation (Equation 1). The arrows point in the direction of increasing carbon number. Lines are theoretical, and points are experimental. Increasing chain length results in a longer dissolution time within a series of homologous alkanes or alcohols.

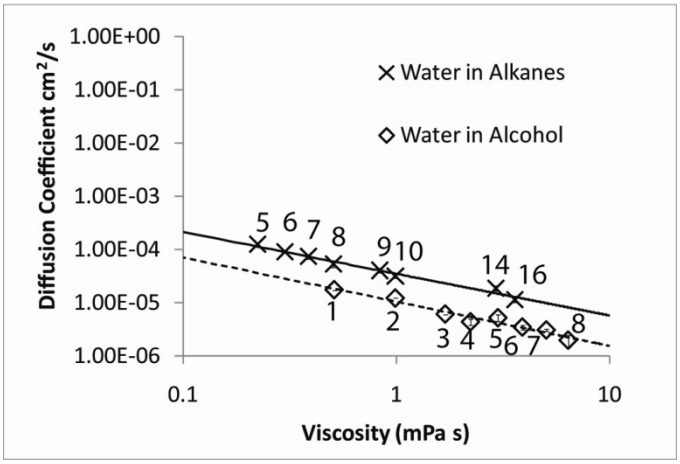

Figure 7. Diffusion coefficients for water in alkanes and alcohols derived from the droplet dissolution experiments. The number of carbons in each solvent is next to the data point. Diffusion coefficients for water in *n*-alkanes are always higher than for the corresponding chain length *n*-alcohol. The diffusion coefficient of water in an *n*-alkane is also higher than in an *n*-alcohol of similar viscosity. Also, in accordance with references 14-16, diffusion coefficient was found to be proportional to a fractional power of viscosity: $D \sim \eta^{-\alpha}$. For water diffusing in the *n*-alcohols $\alpha = 0.78$ (dashed line). For water diffusing in the *n*-alkanes, the value was $\alpha = 0.76$ (solid line). The error bars represent one standard deviation.

As listed in Table I and shown in Fig. 7, the diffusion coefficients of water in *n*-alcohols was generally an order of magnitude lower than the corresponding coefficient in *n*-alkanes of similar chain length despite the higher solubility of water in the alcohols. This difference in diffusion coefficient was most likely due to hydrogen bonding – alcohols are capable of hydrogen bonding to one another and water, while alkanes cannot form these bonds. This was in accordance with the results of studies which also found a decrease in diffusion coefficient due to the possibility of hydrogen bonding between a diffusing solute and the surrounding solvent[53, 55, 56, 59, 88-90].

Interestingly, plotting the diffusion coefficients of water in the various alkanes and alcohols (Fig. 7) did reveal a fractional power viscosity dependence as expected for the diffusion of a small solute: $D \sim \eta^{-\alpha}$. For water diffusing in the *n*-alcohols, α was 0.78. For water diffusing in the *n*-alkanes, α was 0.76. Relatively speaking each series does follow a reduced viscosity assumption.

2.4 Discussion

2.4.1 Small solute diffusion without hydrogen bonding: Comparison to other systems

If the diffusion of water in *n*-alkanes is compared to the diffusion of other small solutes in those same alkanes, it is found that their diffusion behavior is quite similar. Pollack and Enyeart[43] examined the diffusion of xenon (Xe) through the *n*-alkanes (*n*-pentane to *n*-hexadecane) at 20 degrees C. Xe is an inert gas incapable of hydrogen bonding. Pollack and Enyeart modeled Xe as a sphere of diameter of about 4.5 A, while water molecules are generally modeled as having a diameter of 2.75 A.

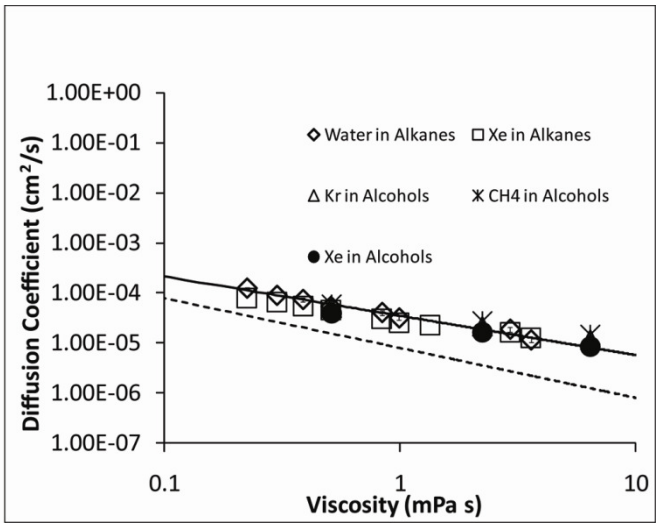

Figure 8. Diffusion of water in alkanes compared to the diffusion of other small non polar solutes (Xe, Kr, CH4) in polar (Alcohol) and non polar (Alkane) solvents. The power law is shown as a solid line. The Stokes-Einstein prediction for water in the *n*-alkanes is included as well (dotted line). Data for Xe diffusion in *n*-alkanes is taken from Pollack and Enyeart. Data for Xe diffusion in three *n*-alcohols from Chen *et al*.

If the diffusion coefficients of water in the alkanes are plotted versus viscosity, and compared with those for diffusion coefficients of Xe in the same alkanes (Fig. 8), they are found to be similar. This is to be expected because neither Xe nor water can hydrogen bond with the *n*-alkanes, and each solute molecule is considerably smaller than the solvent molecules.

Chen *et al*[54] examined the diffusion of Xe in the *n*-alcohols. Xe is not capable of hydrogen bonding, so the diffusion behavior of Xe in an *n*-alcohol of similar viscosity is expected to be similar to that of Xe in an *n*-alkane (unlike what was found for the diffusion of water in *n*-alkanes versus *n*-alcohols). This is, indeed, the case.

The diffusion of other, similarly sized non-hydrogen bonding molecules in *n*-alcohols is also similar to the diffusion of water in alkanes. The diffusion of krypton (Kr) in *n*-alcohols is similar to the diffusion of water in the *n*-alkanes. The diffusion of methane (CH_4) in *n*-alcohols is also similar to the diffusion of water in the *n*-alkanes (Fig. 8).

Interestingly then, each of these systems deviates from the Stokes Einstein prediction in agreement with the reduced viscosity model of small solute diffusion. Pollack and Enyeart found α=0.686 for Xe in the *n*-alkanes.

2.4.2 Activation Energy and Free Volume

Recall the Macedo-Litovitz and Chung activation energy based modifications to the Cohen and Turnbull free volume theory (Equation 6):

$$D_{01} = D_0 e^{(-\frac{E}{RT})} \quad \textbf{(6)}$$

The curve fit for water diffusing through *n*-alkanes (non-hydrogen bonding) revealed the relationship: $4x10^{-5}\eta^{-.782}$. For the alcohols, the power law relationship was found to be $1x10^{-5}\eta^{-.761}$. Assuming that the viscosity dependence of both diffusion processes is roughly identical (as is expected by Harris[33]), it becomes possible to write the ratio of the relationships:

$$\frac{D_{hydrogen\ bonding}}{D_{without\ h-bonding}} = \frac{1x10^{-5}\eta^{-.761}}{4x10^{-5}\eta^{-.782}} = \frac{D_0 e^{(-\frac{E_{ah}}{RT})}}{D_0 e^{(-\frac{E_a}{RT})}} \quad \textbf{(19)}$$

Where E_a is the activation energy for water to break free from an *n*-alkane, and E_{ah} is the activation energy for water to break free from an *n*-alcohol.

$$.25 = e^{(\frac{E_a}{RT} - \frac{E_{ah}}{RT})} \quad \textbf{(20)}$$

Taking the log of both sides yields:

$$\ln(.25) = \frac{E_a}{RT} - \frac{E_{ah}}{RT} \quad \textbf{(21)}$$

Which in turn, gives us

$$-1.39\text{RT} = E_a - E_{ah} \quad \textbf{(22)}$$

$$E_{ah} = E_a + 1.39\text{RT} \quad \textbf{(23)}$$

Thus, the activation energy for breaking free from any interactions with neighboring molecules under free volume diffusion with hydrogen bonding, E_{ah}, is greater than the activation energy for non-hydrogen bonding diffusion, E_a by approximately 1.39RT, which, at 25 degrees C, is approximately 3.5 kJ/mol. This value is not an absolute value, but rather the difference in activation energy entirely due to the difference between water's interaction with an alkane, and water's interaction with an alcohol. 1.39 RT, is, of course, quite small, and deserves further discussion.

While moderate hydrogen bonds, as discussed above, generally have total magnitudes of 4 – 15 kcal/mol, or around 16.7 – 62.8 kJ/mol, Smith *et al* estimated the energy required merely to break water's hydrogen bond with another water molecule (leaving the molecules in the same position, with no change in electrostatic interaction) to be 6.3 kJ/mol, using x-ray absorption spectra of supercooled and normal liquid

water[91, 92]. (The energy to break and separate two water molecules is larger: approximately 23.3 kJ/mol). Assuming that the Macedo-Litovitz/Chung theory of free volume diffusion with an included activation energy is correct, there are three plausible explanations: that, on average, due to the small size of the solute, fewer than one hydrogen bond is formed for each water molecule surrounded by much larger molecules (which can only hydrogen bond at the -OH group), that the water-alcohol hydrogen bond is weaker than the water-water bond, or some combination of the two. The strength of the hydrogen bond could be checked with computation.

An interesting future experiment would be to repeat these experiments with water diffusing in alcohols with –OH groups located in different locations and with water diffusing in polyalcohols. Should the difference in neighbor-leaving activation energies increase in discrete steps in accordance with the number of –OH groups of the poly-alcohols, this would be an excellent indication that this activation energy is directly related to the strength of the hydrogen bond. Should the location of the –OH group change the estimate for neighbor-leaving activation energy, this would be a clear indicator that the geometry of the problem, and not the strength of the hydrogen bond, affects this value. One possible difficulty lies in appropriate solvent selection: polyalcohols tend to be miscible with water.

A possibility is that the small solute makes brief and non-optimal contact with the –OH groups, resulting in effectively a lower activation energy. Experiments with

hydrogen bonding solutes of approximately the same size as the solvent should reveal whether this lowered activation energy is related to the small size of the solute. The other extreme of this case is also a possibility: that the small solute is surrounded by so many –OH groups that it can hop easily from one to another, in a way similar to how protons move in water.

2.4.3 Small solute diffusion and the inclusion of hydrogen bonding

When water diffuses through an *n*-alcohol, its diffusion behavior shows a power law with viscosity, but the absolute rate of diffusion is significantly smaller than its diffusion in the same chain-length n-alkanes. Thus, in line with the findings of Skipp and Tyrrell[93], Easteal and Woolf[52], and Tominaga et al[53], solute-solvent interactions, such as hydrogen bonding, do reduce the diffusion of a hydrogen bonding solute in a solvent. This could be due to an increased residence time, as the water molecule binds briefly to the OH on the larger alcohol, or possibly being due to the diffusion of a hydrogen bonded solute-solvent complex, diffusing as one species.

If data for the smaller water molecule (molecular volume of 30 A^3 [94]) is compared with that of the non-hydrogen bonding but larger organo tins (molecular volume of 114.9 A^3 for tetramethyltin[87]) in the same alcohols, diffusion of water in *n*-alcohols closely resembles that of several of the organo-tins in *n*-alcohols. This is notable because the organo-tins, being a single atom of tin surrounded by four alkanes, are much larger molecules than water. Thus water molecules diffuse in alcohols at the

same rate for the same viscosity as a larger non-hydrogen bonding solute. This could imply that water molecules do indeed pick up a solvent molecule or two and carry it, thus slowing its diffusion. If this were the case, increasingly slower diffusion for water in the larger alcohols would be expected. However, the effective hydrodynamic radius of water diffusing in n-alcohols is not observed to increase with increasing solvent chain length, as might be expected if an increase in effective radius was due to temporary association with solvent molecules, and the same power law fits for all systems.

2.4.4 Diffusion of 1-hexyl-3-methylimidazolium tetrafluoborate in 1-pentanol

Zhu et al used a similar Epstein-Plesset based method to measure diffusion coefficients of 1-hexyl-3-methylimidazolium tetrafluoborate ((Hmim)(BF4)) in 1-pentanol. The value obtained by Zhu et al was 1.87×10^{-10} m^2/s, which was compared with their Wilke-Chang prediction of 2.31×10^{-10} m^2/s. Zhu et al concluded that this slower diffusion was due to cluster formation of ((Hmim)(BF4)).

This conclusion is problematic. The Wilke-Chang equation is a semi-empirical equation, and the citation used, Su *et al*[95], is not necessarily expected to provide an exact prediction, as the correction factor was based on diffusion of alkylimidazolium tetrafluoroborates and hexafluorophosphates in water, and not 1-pentanol. Zhu further uses a value of 1.0 for the solute-solvent interaction parameter in the Wilke-Chang equation. This value corresponds to a non-hydrogen-bonded solvent. 1-pentanol, however, has an OH-group, and will hydrogen bond, as is seen here.

It is insufficient to argue that any deviation from the expected Wilke-Chang value is due to hydrogen bonded cluster formation of (Hmim)(BF4). For Zhu's conclusion to be correct, it is further necessary to argue that (Hmim)(BF4) forms aggregates in 1-pentanol, but not in water.

Even supposing that the Wilke-Chang equation's prediction is accurate and that no aggregate formation occurs in other systems, the experimentally obtained value for diffusion is 1.87×10^{-10} m^2/s, as compared to the Wilke-Chang prediction of 2.31×10^{-10} m^2/s. Zhu's proposed cluster is at least twice the size of a single (Hmim)(BF4) molecule. Should such a cluster diffuse as a group, its diffusion coeffcient should differ correspondingly.

2.5 Summary and Conclusion

The diffusion of water in both alkanes and alcohols shows deviations from the classical Stokes-Einstein model for a solute diffusing in a solvent, and follows a power law dependence on solvent viscosity (water in alkanes $\alpha = 0.78$, and water in alcohols $\alpha = 0.76$) that closely matches the reduced viscosity assumption. This power law dependence on viscosity of water in alkanes was similar to other non-hydrogen bonding solutes like Xe in the same alkane series. However, for a hydrogen bonding system like water in alcohols, water diffusion (at the same viscosity) was slowed reflecting a possible retardation of water diffusing in alcohols because of hydrogen bonding between the water and the OH group. Since water diffusion in alcohols is as slow as

that for a larger (but non-hydrogen bonding) organo tin, this slower diffusion could be interpreted as an increase in hydrodynamic radius where hydrogen bonding allows the smaller solvent to carry with it one or more solvent molecules. However, the fact that the effective hydrodynamic radius of water did not increase with increasing solvent chain length, leads us to conclude that the slower diffusion of water in alcohols compared to alkanes is simply due to a longer residence time for water at the alcohol OH group due to a higher energy of activation for breaking free from its neighbors before a diffusive step.

3. Two component droplet dissolution

3. 1 Introduction

Chapter three will discuss an extension to the Epstein Plesset equation discussed in chapter two. In chapter two, the Epstein Plesset equation was discussed for systems in which a pure droplet dissolved in a pure surrounding liquid. In this chapter, a modification to the Epstein-Plesset equation was used in order to extend the equation to systems of a single droplet containing a mixture of liquids dissolving in a pure liquid. Based upon the concentration gradient at the edge of the droplet and the diffusion coefficient of the droplet material in the surrounding medium, an expression can be derived for the mass flow which can be related to the change in the dimensions of the droplet through the density.

The mass transfer expression obtained from the Epstein-Plesset equation is:

$$\frac{dm}{dt} = D(c_0 - c_s)\left\{\frac{1}{R} + \frac{1}{\sqrt{\pi D t}}\right\} \quad \textbf{(24)}$$

Where D is the diffusion coefficient of the droplet material in the surrounding medium, R is the radius of the droplet, t is the time, c_0 is the initial concentration of the droplet material in the surrounding medium, and c_s is the saturation concentration of the droplet material in the surrounding medium. Since what is measured in the experiment is the diameter of the microdroplet versus time, this expression can be made more practical and turned into to the equivalent expression for the change in radius over time through the definition of density as mass per volume:

$$\frac{dR}{dt} = \frac{Dc_S(1-f)}{\rho}\left\{\frac{1}{R} + \frac{1}{\sqrt{\pi Dt}}\right\} \quad \textbf{(25)}$$

Where f is the ratio of the initial concentration of the droplet material in the surrounding medium c_0 over the saturation concentration of the droplet material in the surrounding material c_s, and ρ is density. This is the Epstein-Plesset equation as used by Duncan and Needham [2] for single component droplets, (e.g., either aniline droplet dissolving in water or a water droplet dissolving in aniline, and in Chapter Two (published in Su *et al[96]*), for water droplets dissolving in alkanes and alcohols.

Similar assumptions can now be used to extend the Epstein Plesset equation. First assume that two miscible liquids in a droplet mix ideally and are homogenously distributed throughout the droplet, including its interface. According to the Epstein Plesset equation, mass transfer due to diffusion from of a pure droplet is related to the concentration gradient at the boundary and the surface area through which mass is transferred. The surface area available to each component of the droplet can be assumed to be in proportion to the volume fraction that each component occupies in the droplet.

The total mass flux into the surrounding area, J_{total}, will be equal to

$$J_{total} = J_{liquid\,1} + J_{liquid\,2} \quad \textbf{(26)}$$

Where $J_{liquid1}$ and $J_{liquid2}$ are the mass flux of each component of the droplet. From the Epstein Plesset derivation, the concentration gradient at the edge of the droplet is given by:

$$\left(\frac{\partial c}{\partial r}\right)_R = (c_i - c_s)\left\{\frac{1}{R} + \frac{1}{\sqrt{\pi D t}}\right\} \quad \textbf{(27)}$$

Where c_i and c_s are the initial and saturation concentrations of the droplet material in the surrounding medium, respectively.

From Fick's first law, the mass flux from the droplet is proportional to the concentration gradient through the diffusion coefficient. The mass transferred by this mass flux is, in turn, proportional to the surface area through which the flux occurs, which can be assumed to be proportional to the volume fraction of the components. Hence, the mass flux of each component *i* is

$$\frac{dm_i}{dt} = A_{frac_i} D_i (c_i - c_s)\left\{\frac{1}{R} + \frac{1}{\sqrt{\pi D_i t}}\right\} \quad \textbf{(28)}$$

Where A_{fraci} is the area fraction of component i and D_i is the coefficient of diffusion of component *i* in the surrounding medium. These mass fluxes can be related to volume changes through the density of each component, which can, in turn, be related to the radius of a spherical droplet. Naturally, for the case for which a single liquid comprises the entirety of the droplet, this collapses back to the original Epstein-Plesset equation.

3.1.1 The Gibbs Surface Excess

The previous section addressed a modification to the Epstein Plesset equation to make it suitable for to describe the dissolution of droplets consisting of a mixture of liquids. This modification made the assumption that the mixture of liquids within the droplet will distribute homogenously, even at the surface. Homogenous distribution

doesn't always happen in a droplet, however. While an ideal mixture will mix homogenously throughout a droplet, non-ideal mixtures may exhibit a non-uniform concentration. In the case of a non-ideal mixture with differential adsorption at the interface, a surface excess can occur, and so the primary assumption of the model no longer holds true unless this surface excess is taken into account.

As described in Fawcett's *Liquids, Solutions, and Interfaces* [97], an example of a surface excess is a water and propanol system containing both liquid and gas phases (Figure 9). If concentration of alcohol is measured throughout the system (moving in the x direction), it will be found that this concentration will be constant in the bulk of the liquid phase. Closer to the interface, however, the concentration of the alcohol will rise, before falling to the lower concentration that propanol possesses in the gas vapor phase. This is due to the hydrophobic nature of the carbon chain in propanol. While this effect is small for most circumstances where the surface area/volume ratio is small, this effect can become appreciable if the area/volume ratio is increased, such as is in the case of a fine dispersion[97].

As will be derived below, following a combination of the derivation given in Fawcett[97] and that given in Jaycock[98] the Gibbs surface excess is reflected in a change in the behavior of the interfacial tension with respect to the log of concentration. The Gibbs free energy of a multicomponent system which can exchange matter with its surroundings and can change its area A is[98]:

$$dG = -SdT + VdP + \sum_i \mu_i dn_i + \gamma dA \quad \textbf{(29)}$$

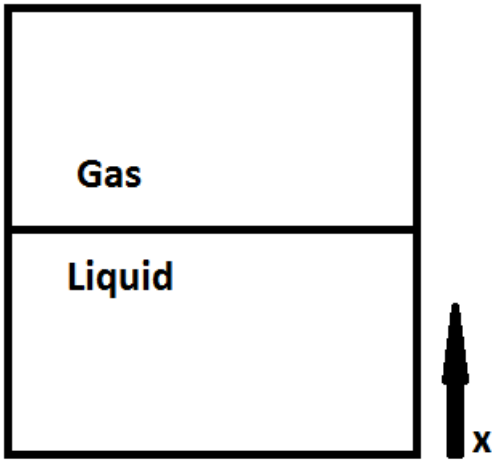

Figure 9. One example of a system in which there is a surface excess is a propanol and water system which contains both gas and a liquid.

Where S is entropy, T is temperature, V is volume, P is pressure, G is Gibbs free energy, μ is the chemical potential, and γ is the interfacial tension, defined as

$$\gamma = \left(\frac{\partial G}{\partial A}\right)_{T,P,n_i} \quad \textbf{(30)}$$

Chemical potential, μ is defined as

$$\mu_i = \left[\frac{\partial G}{\partial n_i}\right]_{n_{j,T,P,\gamma}} \quad \textbf{(31)}$$

So

$$G = \sum_i \mu_i n_i \quad \textbf{(32)}$$

And

$$dG = \sum_i \mu_i dn_i + \sum_i n_i d\mu_i \quad \textbf{(33)}$$

Subtracting this equation from equation 60 yields

$$SdT - VdP + Ad\gamma + \sum_i n_i d\mu_i = 0 \quad \textbf{(34)}$$

This is essentially the Gibbs-Duhem equation for an interphase. At constant temperature and pressure, this equation becomes:

$$-Ad\gamma = \sum_i n_i d\mu_i \quad \textbf{(35)}$$

Now, defining a surface excess

$$\Gamma_i = \frac{n_i}{A} \quad \textbf{(36)}$$

Where Γ_i is the amount of species I in a unit area of the interphase. Thus, the Gibbs adsorption isotherm is:

$$-d\gamma = \sum_i \Gamma_i d\mu_i \quad \textbf{(37)}$$

For a two component system, this gives:

$$-d\gamma = \Gamma_1 d\mu_1 + \Gamma_2 d\mu_2 \quad \textbf{(38)}$$

Remembering the Gibbs Duhem equation

$$x_1 d\mu_1 + x_2 d\mu_2 = 0 \quad \textbf{(39)}$$

Where x_i is the mole fraction of component i in the bulk of the solution,

$$-d\gamma = \left(\Gamma_1 + \Gamma_2 \frac{x_1}{x_2}\right) d\mu_1 = \Gamma_1^{(2)} d\mu_1 \quad \textbf{(40)}$$

Where $\Gamma_1^{(2)}$ is the surface excess of component 1 relative to component 2. For a sufficiently dilute solution, Henry's Law holds so that

$$d\mu_1 = RTdlnc_1 \quad \textbf{(41)}$$

Where c_1 is the concentration of component 1. Thus, for a dilute solution:

$$\Gamma_1 = -\frac{1}{RT}\left(\frac{\partial \gamma}{\partial lnc_1}\right) \quad \textbf{(42)}$$

Therefore, to test for the presence of a surface excess, it is possible to measure the change in interfacial tension with concentration of the solutions. Since the assumptions of the model require that there be little to no surface excess, the interfacial tensions of the selected systems: ethyl acetate/butyl acetate with water and butyl acetate/amyl acetate with water were measured with varying concentration. The method used relies on a specialized tapered micropipette technique which is based on the Laplace-Young equation, which will be discussed in the next section.

3.1.2 The Laplace-Young Equation

As discussed in the previous section, a surface excess will be reflected in a change in the interfacial tension between two liquids. This interfacial tension can be measured using a specialized tapered micropipette. The basis for this is the Laplace-Young equation, the derivation of which will be given below, following the derivation given in Fawcett[97]. Assume a spherical gas bubble in a liquid, where the pressure of the gas inside the bubble is P_g and the pressure inside the liquid is P_l. Should additional gas be introduced into the bubble, the volume of the bubble will increase, as will its surface area. This means that a certain amount of P dV work will be done against surface tension forces, or, mathematically:

$$\gamma dA = \left(P_g - P_l\right)dV \qquad \textbf{(43)}$$

Where γ is the surface tension of the gas bubble, A is the area of the gas bubble, and V is the volume of the gas bubble. The volume of a sphere, V, is $4\pi r^3/3$, and the surface area of a sphere, A, is $4\pi r^2$. Hence, $dV = 4\pi r^2 dr$, and $dA = 8\pi r\, dr$.

The expression relating dV and dA is:

$$dA = \frac{2dV}{r} \quad \textbf{(44)}$$

Combining this expression with the previous equation, and expression $P_g - P_l$ as ΔP gives the Laplace-Young equation:

$$\Delta P = \frac{2\gamma}{r} \quad \textbf{(45)}$$

3.2 Materials and Methods

3.2.1 Material Systems Studied

Table 3. Chapter 3 Material Systems Studied

Material Systems Studied	
Droplet	Surrounding Solvent
Ethyl Acetate Butyl Acetate Amyl Acetate Ethyl Acetate/ Butyl Acetate Butyl Acetate/ Amyl Acetate	Water

Butyl acetate (99.5% pure) was obtained from Sigma, and ethyl acetate(99.9% pure) and amyl acetate (99.5% pure) were purchased from Mallinckrodt. Deionized

water was purified through a Branstead Nanopure Life Sciences (UV/UF) ultrapure water system.

3.2.2 Experimental Methods

Measuring Interfacial Tension with a tapered pipette

Interfacial tension can be measured using a tapered pipette method, as used by Lee and Needham[99]. Essentially, two immiscible fluids are successively introduced into a tapered pipette. A curved interface forms at the junction of these two fluids. The radius of curvature of this curved interface can be measured, and is related to the interfacial tension through the Laplace-Young equation.

Radius of curvature of the interface was measured using the same geometrical assumptions as used in Lee and Needham. Briefly, a similar micropipette pipette setup as was used for water droplet dissolution experiments as detailed in chapter two was used in this experiment, though a more sharply tapered pipette was used. (Solenoid setting on the David Kopf pipette puller was 90; this is much higher than the value of 60 used for droplet dissolution.) Two chambers were used – essentially, the solvent mixture was drawn into the micropipette, in one chamber, then transferred into the other chamber, which contained saturated water. Previous interfacial tension measurements involved pure systems, however, interfacial tension measurements of ethyl acetate/butyl acetate mixtures with water were complicated by the volatility of ethyl acetate. This volatility can result in changing ethyl acetate/butyl acetate

concentrations during the experiment. In order to combat this change, saturated plugs were used, and all inter-chamber transfers were preformed as quickly as possible. A plug consisting of water saturated with butyl acetate and ethyl acetate was drawn first into the pipette, followed by the saturated solvent. This plug prevents evaporation of the ethyl acetate through the air/solvent interface.

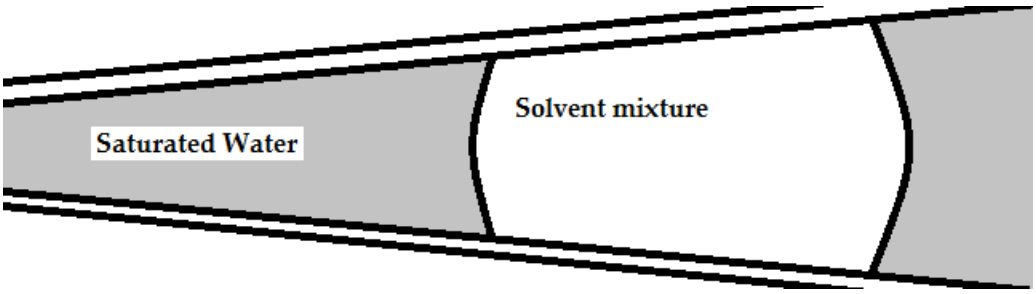

Figure 10. Illustration of a plug in a tapered micropipette (not to scale). A saturated water plug was used to prevent evaporation up the micropipette. This was necessary because of the high volatility of ethyl acetate.

Care must be taken to ensure that the plug is of sufficient length, both so that the diffusion of ethyl acetate through the plug does not occur, and so that the air space behind the plug becomes saturated with ethyl acetate. When forming a plug, it is important to remember that because the pipette is sharply tapered, the plug will shrink in length as it is moved away from the tapered area. It is better to have more plug material than less, as evaporation will not become evident until after the experimental data is analyzed.

One the micropipette containing the solvent mixture is inserted into the chamber containing saturated water, the pressure can be manipulated using the syringe in order

to move the curved interface. Increasing the pressure using the syringe results in the solvent moving towards the pipette's outlet, and decreasing the pressure results in the solvent moving away from the exit of the pipette. Record the curved interface using the video recorder, and then advance the interface along the pipette, adjusting the pipette so that the interface remains visible. Measurements may only be taken when the interface is stationary. As this procedure is very sensitive to minor motions in the interface, it may be helpful to place a mark on the video monitor to ensure that the interface is not slowly moving. Measurements should be taken both 'forwards' and 'backwards' – that is, with the interface being advanced towards the exit of the pipette, and with the interface moving away from the exit of the pipette.

The radius of curvature of the curved interface can be measured by measuring two dimensions of the interface, marked in Figure 12 as X and Y (Figure is from the measurement of the surface tension of water from Lee and Needham, 2001). While previous interfacial tension measurements involved pure systems, and hence were not concerned about evaporation and maintenance of the appropriate concentration, interfacial tension experiments required careful control of the solvent concentration.

The radius of curvature corresponds to the radius of curvature of the spherical cap at the tip of the curved interface. Geometrically, this radius can be defined as:

$$R_c = \frac{(Y/2)^2+X^2}{2X} \quad \textbf{(46)}$$

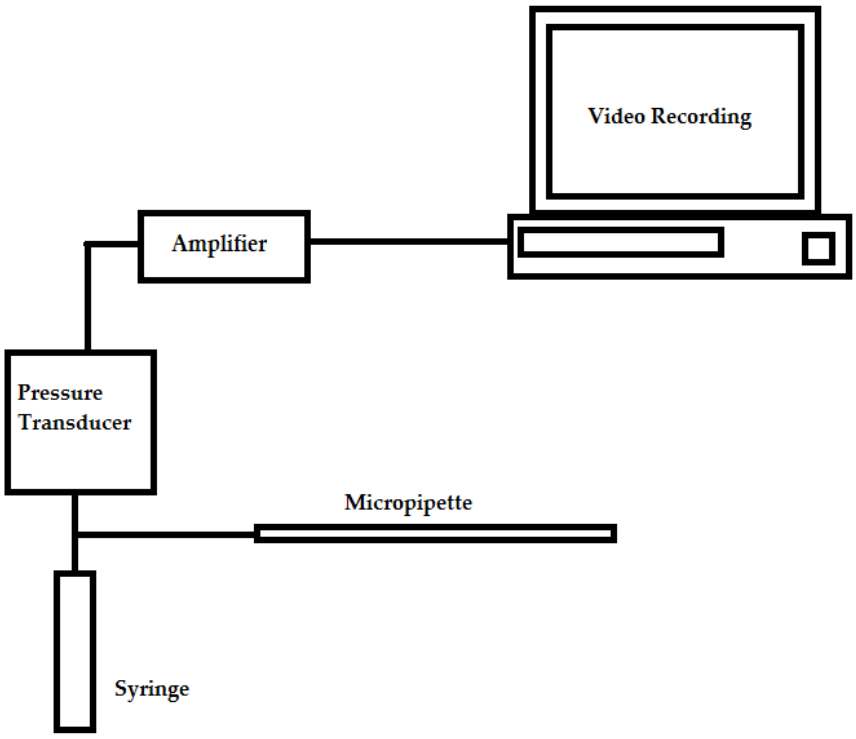

Figure 11. Schematic of experimental setup. Pressure is applied using a syringe. This pressure goes to the micropipette and to a voltage transducer, where it is translated into a voltage. The voltage from the pressure transducer is amplified and then recorded.

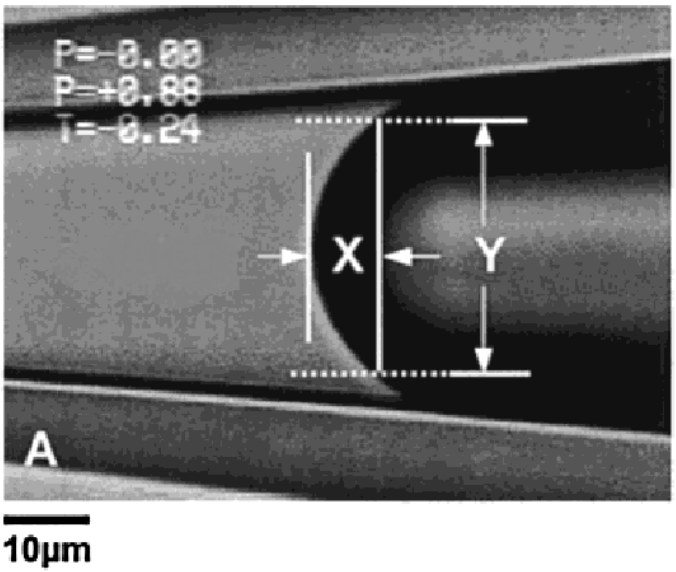

Figure 12. Measurement of surface tension of water and air, from Lee and Needham, 2001. The radius of curvature of the interface can be measured using the height and width of a spherical cap, as described in the text.

This radius can be used to find an interfacial tension through application of the Laplace-Young equation. Surface tension can be then taken from the slope of the line $dP/d(1/R_c)$. (It is theoretically possible to obtain the measurement from a single point, but as argued by Lee and Needham, using the slope of the line allows for a more accurate measurement for surface tension, regardless of the user's ability to measure absolute R_c, as long as the user is consistent.) Note that deviation from literature values occurred once $1/R_c$ reached a region of around 0.1 1/m, corresponding to a small pipette diameter, possibly due to the difficulty of accurately measuring R_c at small pipette diameter.

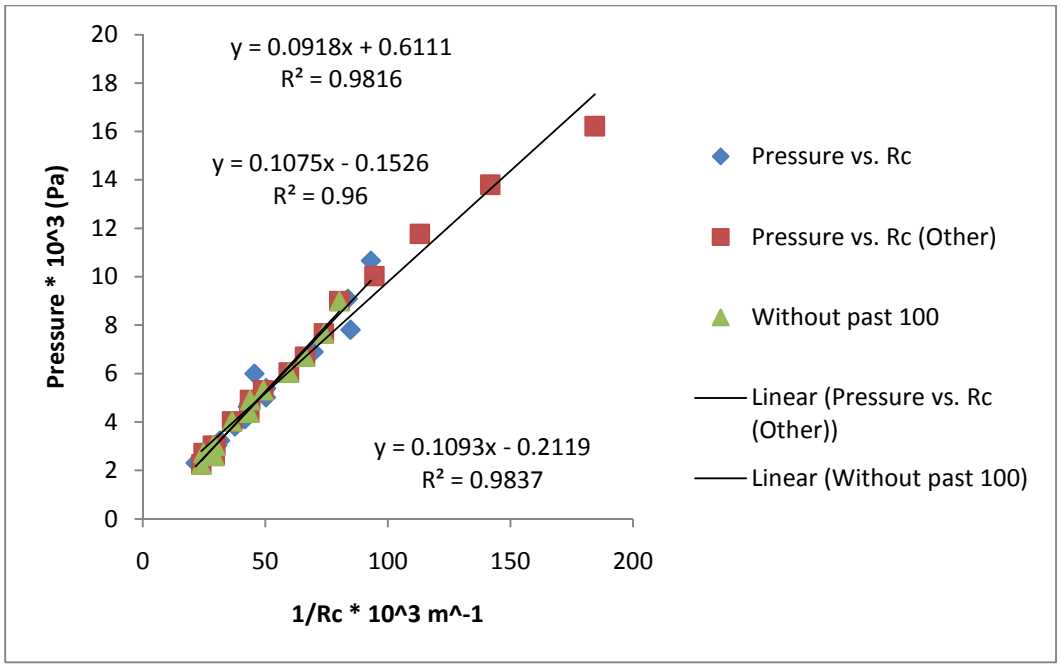

Figure 13. Surface tension measurement of water and decane. Three trials are represented: triangles and diamonds indicate two trials which did not exceed 1/Rc of .1 m. Squares indicate a trial taken to 1/Rc of .184. Note deviation from other experimental trials.

Measurement of the curved interface should not be performed at very small pipette diameters. The interfacial tension of water and decane was measured using the tapered pipette technique (Figure 13). When interfacial tension was calculated using only data points corresponding to pipette radii greater than ten microns, an interfacial tension of 52.4 mN/m +/- 0.6 was measured. Including all data points resulted in a significantly lower measurement of 45.9 mN/m. In comparison, the Lee and Needham value for water and decane was 51.2 +/- 0.4, which is similar to other values found in the literature[99].

A pipette diameter less than ten microns is not necessary for interfacial measurement, however, choice of tapered pipette exit diameter does have some bearing on the experiment. A small final diameter requires a larger pressure to move, but may allow for easier manipulation of the interface. A larger exit diameter is much more sensitive to small fluctuations in pressure, but is less prone to error due to slow movement of the interface. In the end, the experiments carried out in Chapter three were conducted using a small exit diameter pipette, though theoretically the large exit diameter pipettes should work if sufficient care is taken to ensure that the interface is not moving during the measurement. (Experimentalists may wish to mark the video screen and observe the interface for a prolonged period of time).

Using the U-bend Manometer

The tapered pipette method for measuring surface tension is relies upon an accurate pressure measurement for calibration. In order to measure pressure, pressure must be recorded from a sensor. Generally, this is done by translating the pressure into an electrical voltage, which is then recorded. In this case, a pressure transducer (Validyne Model DP15-24N154A) uses deflection of a diaphragm to measure the pressure. The transducer then outputs a voltage. This voltage is amplified, and then recorded onto videotape along with video of the procedure.

Figure 14. Syringe attatched to the pressure transducer. Pressure is applied using the syringe. This pressure goes to both the micropipette and the pressure transducer, which converts the pressure into a voltage.

The U-tube manometer was invented by Christiaan Hyugens in 1663, through the principles upon which U-bend manometer are based have been known at least since the time of Galileo, who analyzed a similar u-bend "in order to enlighten certain practical mechanicists who, based on false premises, sometimes attempt impossible endeavors." Blaise Pascal, in his *Traitte de l'equilibre des liqueurs*, published in 1663 (a year after his death) invented a hydraulic lift which was based on a similar principle.

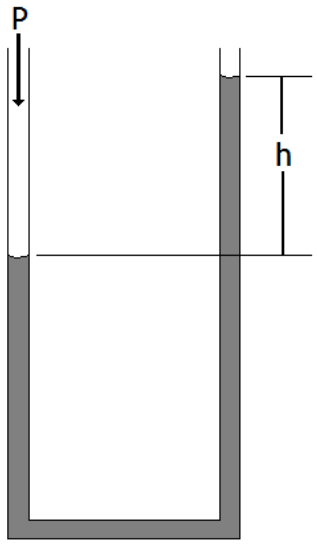

Figure 15. U-bend manometer.

A u-bend manometer essentially consists of a U-shaped tube filled with a liquid (in this case water), one end of which is open to the atmosphere, and is hence at atmospheric pressure. Pressure is applied to one end of the tube, causing a rise in the liquid level in the other side of the tube. At static equilibrium, Newton's first law tells us that all of the forces on the liquid must be balanced, and because the tube is of constant diameter and hence constant cross-sectional area, the pressures must be equal. Hence, in order for static equilibrium to exist, the pressure exerted on one end of the tube must be balanced by the weight of the column of fluid of height h in the other end of the tube.

The pressure difference is related is therefore related to height h, the difference in the fluid levels in each arm of the manometer. This pressure difference can be expressed in mmH_2O, which in turn can be easily converted into Pa.

In order to calibrate the pressure gauge, the pressure sensor must first be zeroed. This can be accomplished by exposing the gauge to atmospheric pressure, generally through the opening of one or more valves. The left-most knob can be slowly turned until the pressure reading is zero. One side of the U-bend manometer can then be attached to the system, in lieu of the micropipette. Pressure can be exerted upon the manometer (a 60 mL syringe can be used in place of the 10 mL syringe generally used for micropipette experimentation). At this point, it is possible to adjust the gain such that the voltage reading corresponds to a multiple of ten of the pressure. A calibration curve should be established by taking readings from the u-tube manometer and recording the corresponding voltage.

Figure 16. The signal from the pressure transducer is amplified using the Validyne Model CD15 Carrier Demodulator. The zero may be adjusted by using the knob on the left, and the gain by the knob on the right.

Figure 17 The signal from the pressure transducer is amplified (white box) before being input into the video recording unit (top of photograph). See Figure 17 for a close up view of the pressure transducer.

When adjusting the gain, the experimentalist should be cautioned that voltage transducers are generally only linear in their mid-range[100], and that any readings close to either extreme (in this case +/- 1.970) are likely to be inaccurate.

Droplet Dissolution

The dissolution of a pure liquid droplet into a liquid environment in which the droplet material is soluble has been previously studied by the Needham lab, using a micropipet technique capable of forming and manipulating single microdroplets with volumes on the order of tens of picoliters, as explained earlier in this thesis. This work has now been extended to encompass microdroplets comprised of a mixture of two miscible liquids. Two systems were chosen: ethyl acetate/butyl acetate mixtures, and butyl acetate/amyl acetate mixtures. Chemical structures are shown in Fig 1.

As can be seen from Fig. 18, ethyl, butyl, and amyl acetate are all molecules with a polar acetate group and a carbon chain. Ethyl, butyl, and amyl acetate differ only in the length of the carbon chain, with ethyl acetate having a two carbon chain, butyl acetate having a four carbon chain, and amyl acetate having a five carbon chain. Because these molecules all posses the same polar acetate group, each molecule should have similar adsorption to the droplet interface with water, and hence the same area per molecule normal to the interface. The longer carbon chain results in a lowered solubility in water, which, in turn (since the diffusion coefficients are similar) results in a slower rate of mass transfer. In this chapter, a new modification to the Epstein Plesset equation for mass transfer of two miscible liquids (ethyl and butyl acetate, butyl acetate and amyl acetate) from a single liquid microdroplet dissolving into a second immiscible solvent (water) is presented.

Mass transfer in a system of many droplets is a common occurrence in liquid-liquid extraction processes, but is difficult to model en masse. It is expected that an understanding of the mass transfer in a single droplet system will bring new insight to such thermodynamically complex systems. Nauman[101], for example, in 1974, proposed a simple droplet diffusion based model for micromixing, based on the idea that the mixing of one liquid into another can be modeled by the dissolution of a large number of uniform spherical droplets diffusing into a liquid with a suitable average concentration.

Liquid-liquid extraction processes have been used in analytical chemistry since 1892, when Rothe[102] described an extraction method based on the differing solubilities of ferric chloride (soluble) and manganous, nickelous, chromic, and aluminium chlorides (insoluble) in ether in the presence of hydrochloric acid. Since then, liquid-liquid extraction processes have been widely used for a large number of purposes, including the formation of polymer microspheres through solvent evaporation[103-109], in uranium production[110] and, in a new innovation, the formation of glassified protein microspheres[111].

While this chapter focuses on liquid-liquid systems, the ostensibly similar problem of evaporation of a multi component droplet has previously been considered in the literature, mostly in connection with fuel combustion, due to the importance of the combustion of fuel mixtures. Early authors, such as Wood *et al[112]* found that liquid

vaporization of a miscible binary droplet followed a batch distillation process, with the components of the droplets leaving in order of highest volatility first. Cheng *et al*[113] examined the evaporation of sessile microdroplets of ethanol-water mixtures on gold surfaces modified with self-assembled monolayers and found evidence that droplet evaporation of an ethanol-water mixture proceeded in distinct stages: the first, in which primarily ethanol evaporated; the second, in which both ethanol and water evaporated; and the third, in which only the water evaporated. Experiments with sessile droplets of ethanol and water were conducted by Sefiane *et al[114]*, and similar evaporation regimes were found. However, batch distillation has been found to poorly describe the actual vaporization of other multicomponent droplets, especially where diffusion of components within the liquid droplet proceeds on a time scale longer than vaporization of the components[115]. For example, Widmann and Davis[116] suspended single 10 micron levitating droplets of 1-bromotetradecane and 1-iodododecane to study aerosol behavior and found good agreement with a theoretical prediction based upon an ideal solution. The problem of multi-component droplet vaporization differs from the problem of droplet dissolution, however, as dissolution of one liquid into another generally proceeds more slowly than vaporization of a liquid into a gas. Batch distillation has been found to be a poor model for dissolution of a mixed-liquid droplet; instead all components of the droplet leave at the simultaneously, but in proportion to the amount of material present at the interface of the droplet.

The study of the dissolution of two component droplets in another liquid has been primarily focused on interfacial turbulence which can rapidly increase mass transfer[117], and is hence of great interest to those seeking to optimize industrial processes. This spontaneous interfacial turbulence is not exhibited in the experimental systems presented in this chapter (though has been observed using the micropipette in other systems, for example in the dissolution of a pure droplet of water in *n*-decanol.)

'Spontaneous interfacial convection' upon the mixing of two liquids was first observed by James Thomson[118] in 1855, who found that the addition of some 'strong spirituous liquor' to a glass of water would result in rapid motion away from the alcohol. Kostarev[119] studied the dissolution of 2-15 mm cylindrical droplets of chlorobenzene and isopropanol in water inside a Fizeau interferometer in order to visualize the two dimensional flows within the droplet (flows within a spherical droplet are difficult to visualize). Isopropanol is miscible with water, and this system was subject to capillary jets which are observed neither in the ethyl acetate/butyl acetate droplet system nor in the butyl acetate/amyl acetate system. As the micropipette technique is capable of experimentally generating clean, spherical liquid/liquid interfaces of any immiscible system, the technique is uniquely suited to study the onset of interfacial turbulence, and may be applied to this problem in the future. Because of the greater interest in this spontaneous interfacial turbulence, the purely diffusive

dissolution of droplets of a liquid mixture in another liquid remains relatively unexplored, and is addressed in the current chapter.

A new model, based upon a modification to the Epstein Plesset equation, is presented for single particle dissolution of a multi component droplet and which approximates this amount by assuming ideal homogenous mixing. This model is tested through an extension of the micropipette-based method talked about in Chapter 2.

An ideal solution can be best approximated by systems in which intermolecular interactions between neighbors are as close as possible to intermolecular interactions between like molecules. This forms the basis for the selection criteria of experimental systems: ethyl acetate, butyl acetate, and amyl acetate differ only in the length of their carbon chain.

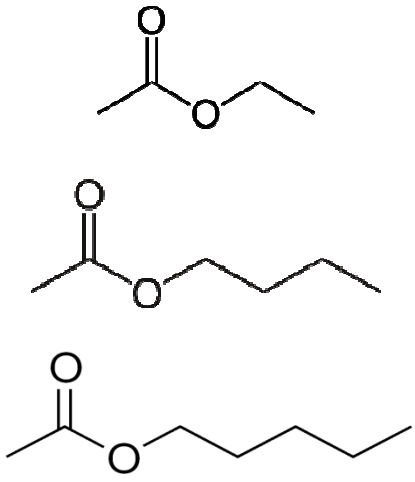

Figure 18. Chemical structures of (from the top) Ethyl Acetate, Butyl Acetate, and Amyl Acetate

Diffusion Coefficient Measurement

The experiments were conducted using a two chamber technique (Fig 2), that can be mounted on a microscope slide, as previously described in Chapter Two and Su *et al*.[96] Briefly, two chambers were employed; one containing the droplet liquid, and the other the surrounding liquid.

By inserting the micropipette into the cuvettes in the correct order, an amount (10 pico liters) of plug material was drawn into the micropipette, followed by 20 pico liters of droplet material. This plug material then served to prevent evaporation of the droplet material out of the rear of the micropipette. After moving this front-filled micropipet to the adjacent cuvette, the droplet material was then blown into the cuvette containing the surrounding medium, and the dissolution of this droplet was observed through the microscope and its diameter vs time was measured using calibrated video calipers.

The concentration of the droplet material is not important for droplets containing a single component, as the concentration of a pure liquid is always the same. The same is not true, however, for droplets which contain more than one component. In this case, all mass transfer processes occurring throughout the experiment must be carefully monitored.

One possible source of error due to mass transfer during the experiment arises from the fact that the two chamber cuvettes are, by necessity, open to the outside environment. While this is not a problem for pure systems, or for liquids which are not

particularly volatile, problems arise for systems which are more volatile and will evaporate into the surrounding environment. This can result in not only inaccurate initial concentrations, but possible inhalation hazard as well. The current microscope setup involves open cuvettes and is not operated in a personal protective device such as a fume hood. As an example, the current National Institute for Occupational Safety and Health limit for chloroform is 2 ppm for a 60 minute period, which is well below the detectable odor threshold. While exposure will be affected by ventilation and circulation of air within the room, the current microscope setup requires the operator to be in close proximity to the cuvettes. The use of a saturated solvent plug is therefore an easy and sensible safety measure for solvents such as chloroform.

In order to eliminate this source of error, it is possible to put a non-volatile plug of immiscible liquid at the entrance to the cuvette that contains the droplet material. This plug should be saturated with the droplet material. This will greatly slow the transfer of mass from the cuvette to the surrounding environment. While some plug material may diffuse into the cuvette, selection of the appropriate material should ensure that this quantity is minimal.

Thus, in order to prevent evaporation of volatile droplet material from the microchambers and also through the back of the micropipet, an immiscible solvent plug was included in the first chamber, as shown in Fig 16.

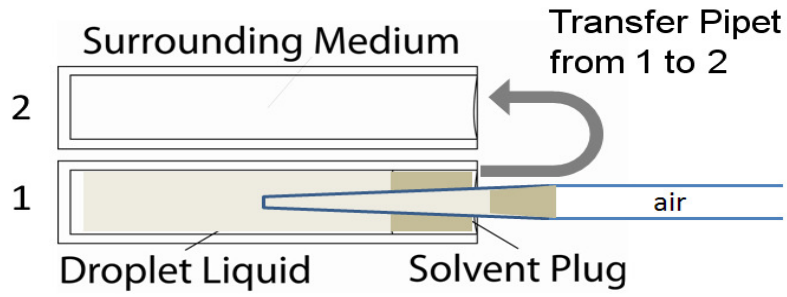

Figure 19. Two cuvettes, side by side, illustrating the immiscible solvent plug. Since the droplet liquid must be kept at a constant concentration, and the droplet liquid may be volatile, a saturated solvent plug is first drawn into the micropipet followed by the desired droplet liquid to avoid evaporation. The loaded pipet is then simply transferred from chamber 1 to chamber 2 and the droplet is blown out into the desired surrounding immiscible liquid

An item of concern is mass transfer during the droplet's 'blowing out' phase: the period of time during which the droplet is being created. Droplet creation is quite fast when using the two chamber technique (0.1 - 0.5s), but for other techniques, including single chamber techniques, mass transfer can become appreciable during blowing out, especially when one component is extremely soluble in the surrounding medium (such as ethyl acetate in water).

It is therefore necessary to estimate the quantity of mass transfer that occurs during the 'droplet formation ("blowing out") process. This quantity can be estimated by applying this multicomponent droplet model. A value for mass lost at each time point may be obtained by measuring the radius of the droplet during the 'blowing out' process, finding the total surface area available, and applying Equation 55.

3.3 Results and Discussion

In order to use this model, diffusion coefficients of ethyl, butyl, and amyl acetate in water were measured using the technique explained in Chapter 2. This technique is based on observation of the radius of a dissolving pure spherical droplet of solvent in water. Since solubility of these acetates is known from the literature, diffusion coefficient can be obtained directly from a curve-fit of the Epstein Plesset equation to the experimental data. The results are summarized in Table 4.

Table 4. Solubility values for ethyl acetate from[120]. Solubility of Butyl acetate from[121]. Solubility of Amyl Acetate from[122]. Diffusion coefficients as measured using the method described in Chapter Two and Su et al[96]. Density values from[123].

Chemical	Density (g/cm^3)	Solubility in Water (g/cm^3)	D in Water (cm^2/s)
Ethyl Acetate	0.895	8×10^{-2}	8.65 x 10-6 (+/- 9×10^{-7})
Butyl Acetate	0.879	7.8×10^{-3}	7.61 x 10-6 (+/- 4×10^{-7})
Amyl Acetate	0.859	2.2×10^{-3}	9.14 x 10-6 (+/- 6×10^{-7})

Interfacial tension of Ethyl Acetate/Butyl Acetate Systems

Interfacial tensions of Ethyl Acetate/Butyl Acetate mixtures with water were measured using the tapered pipette method. Unfortunately, despite the use of multiple solvent plugs, the high volatility and fast diffusion of ethyl acetate made accurate control over the concentration of the mixture difficult.

As a result, the trend in change of surface tension with respect to mol fraction of ethyl acetate has been difficult to determine. While it is possible that this relationship is linear, confirmation of this will require a method which is able to more carefully control the relative concentrations.

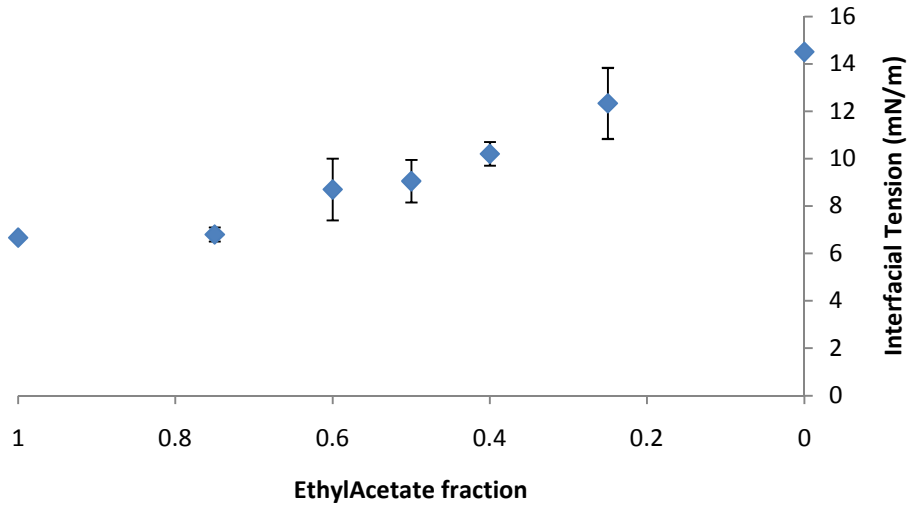

Figure 20. Interfacial tension of ethyl acetate/butyl acetate mixtures and water. Pure ethyl acetate is at the left, and pure butyl acetate is at the right.

Droplet Dissolution Models and Experiment

Droplets consisting of a mixture of ethyl acetate/butyl acetate and butyl acetate/amyl acetate were blown into water. Ethyl acetate, butyl acetate, and amyl acetate are all quite soluble in water (see Table 1)[121]. Comparison of the data to the modified Epstein-Plesset model shows that both components of the droplet are diffusing from the droplet at the beginning of the droplet. In contrast, in previous literature, such as the batch distillation process such as was observed by Wood *et al* for evaporation of a droplet mixture, each mixture component left in order of its volatility. If the ethyl

acetate/butyl acetate mixture droplets dissolved in water in a similar manner, one would expect all of the ethyl acetate to leave, followed by all of the butyl acetate. This is clearly not the case.

For cases such butyl acetate/amyl acetate (Fig 9-11), where the solubility of the materials is not very different (See Table 4; butyl acetate's solubility in water is 7.8×10^{-3} g/cm^3, and amyl acetate's solubility in water is 2.2×10^{-3} g/cm^3), both materials clearly leave at the same time. For droplet mixtures where one material is extremely soluble in the surrounding environment and the other is not particularly soluble (for example a system like droplets of chloroform and decane dissolving in water), the model will approach the batch distillation observation.

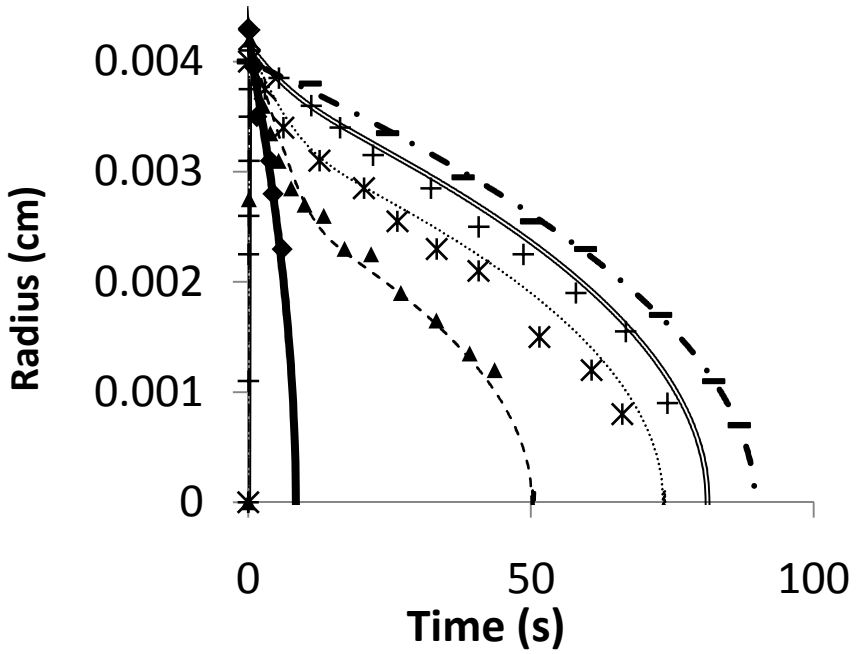

Figure 21. Experimental Ethyl Acetate/Butyl Acetate droplet dissolution compared with model predictions in order of increasing amount of butyl acetate.

Figure 21 (continued) From left to right: Pure ethyl acetate droplet, 3:1 ethyl acetate/butyl acetate, 1:1 ethyl acetate/butyl acetate, 1:3 ethyl acetate/butyl acetate, and pure butyl acetate.

From the theoretical comparisons to the experimental data (Fig. 21 and 22), the model predicts droplet dissolution quite well. As expected, droplets containing a mixture of ethyl acetate and butyl acetate dissolve more slowly than a droplet of pure ethyl acetate, and more quickly than a droplet of pure butyl acetate (Fig 21.) Similarly, droplets containing a mixture of butyl acetate and amyl acetate dissolve more slowly than a droplet of pure butyl acetate, and more quickly than a droplet of pure amyl acetate (Fig 22.)

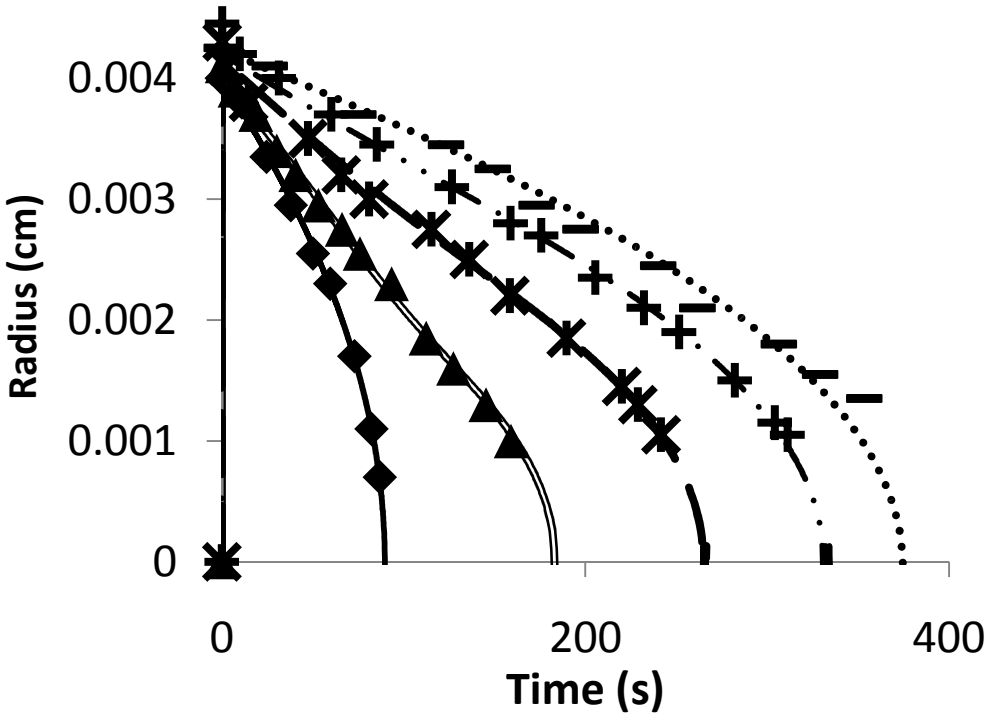

Figure 22. Experimental Butyl Acetate/Amyl Acetate droplet dissolution compared with model predictions in order of increasing amount of amyl acetate. From left to right: Pure butyl acetate droplet, 3:1 butyl acetate/amyl acetate, 1:1 butyl acetate/amyl acetate, 1:3 butyl acetate/amyl acetate, and pure amyl acetate.

Dissolution times can also be graphed against droplet composition, for droplets of the same initial diameter. As can be seen from the graph, dissolution times increase nonlinearly with composition; a droplet of 1:3 ethyl acetate/butyl acetate has a dissolution time very similar to that of a pure butyl acetate droplet. Similarly, a droplet of 1:3 butyl acetate/amyl acetate has a dissolution time very similar to that of a pure amyl acetate droplet.

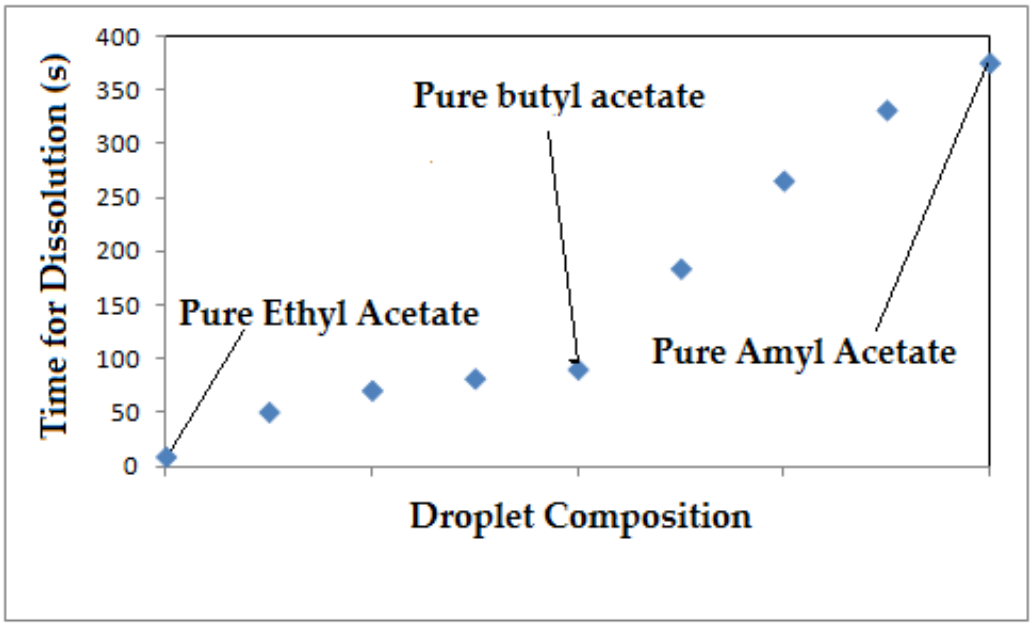

Figure 23. Time for dissolution of (R=45 um) droplets dissolving in water. From left to right: Pure ethyl acetate, 3:1 ethyl acetate/butyl acetate, 1:1 ethyl acetate/butyl acetate, 1:3 ethyl acetate/butyl acetate, pure butyl acetate, 3:1 butyl acetate/amyl acetate

3.5 Conclusion

A modification to the Epstein Plesset equation based upon a reduced surface area approximation has been presented and evaluated experimentally. This modified equation models the dissolution of a liquid droplet mixture in a liquid environment in which both components of the droplet are soluble. Additionally, a modification to the two-chamber method, as previously laid out in Su *et al[96]* is presented which allows for the study of multi-component droplets.

This model has been shown to work quite well for the ethyl acetate/butyl acetate and butyl acetate/amyl acetate systems. Care should be taken, however, in applying the model to systems where the assumptions of homogenous mixing does not hold true. In the case where there exists a surface excess of one component of the droplet, this model is expected to fail. Similarly, in any case where slow diffusion causes concentration gradients within the droplet, deviation from the model is expected.

4. Structure Formation in a Solute-Containing Dissolving Droplet

4.1 Introduction

As described earlier, if a droplet of an organic solvent is immersed in a liquid in which it is soluble but immiscible, the droplet will shrink as solvent leaves diffusively. If this droplet contains a solute, structures may form as the concentration of the solute within the droplet increases, and the solute glassifies or precipitates. Rickard and Needham[124], for example, dehydrated droplets of protein solution in an organic environment to obtain glassified protein microspheres. The removal of solvent from other solute-droplet systems may create different structures as well; in some cases, the formation of a shell-like structure which crumples upon physical disruption of the structure is observed.

These structures are likely to be due to a difference in rates of diffusion within the droplet and without – if solute diffusion inside the droplet is slow, the concentration gradient inside the droplet will be very steep. At some critical concentration, it is expected that precipitation inside the droplet will occur. For a sufficiently steep gradient, a shell may form. If the diffusion of the solute within the droplet is fast as compared to dehydration of the droplet, the gradient may be relatively shallow. Thus, a bead may form.

It may be possible, then, to control the structure of the solute in a dehydrated droplet by varying the rate of dehydration of the droplet. The structure of the solute

may greatly affect, for example, the release profile of a drug. It is also possible that a similar mechanism may result in different polymer concentration profiles in polymer microspheres formed using a solvent removal technique. Since formation of structures in a dehydrating droplet is a significant problem in spray drying and combustion, this problem has been previously considered for droplets which have been dehydrated in air.

Other methods used to study drying droplets

The glass filament approach, used notably by Charlesworth and Marshall in 1960 (Charlesworth, Marshall, Evaporation from drops containing dissolved solids) was one of the earliest of the methods used to study droplets. A droplet was placed on the end of a very thin glass filament, and its deflection was used to measure its mass. Thermocouple wires were inserted into the droplet to measure the temperature of the droplet as it dried. Droplet volumes were approximately 2×10^{-3} mL.

The nozzle method, employed by Audu and Jeffreys in 1975 (Audu, Jeffreys, The Drying of Droplets of Particulate Slurries) was another early method used to study evaporating droplets containing a solute. A droplet was suspended at the end of a nozzle and constantly rotated so that a crust of uniform thickness would be formed. One drawback of this technique is that only part of the droplet is exposed to the drying medium at any one time, which complicates theoretical modeling of this process.

Previous models of shell or bead formation

Previous models of shell or bead formation models concluded that shell or bead formation is due to concentration gradients which form within the droplet as it dries. While the initial concentration of solute within the droplet is expected to be uniform, as solvent is removed and the droplet dries, the concentration at the boundary of the droplet is expected to rise. This increase in concentration at the boundary will lead to a mass flux towards the center of the droplet, where the concentration is lower, through the process of diffusion. The steepness of this gradient is expected to be reflected in the formation of shells or beads.

Jayanthi *et al* theorized that the creation of shells or beads was related to the difference between the saturation concentration and the supersaturation concentration. A concentration gradient will always be present in a drying droplet, and precipitation will occur once a critical supersaturation concentration is reached (CSS). If, when the CSS is reached, the rest of the droplet is above the supersaturated concentration, precipitation will occur throughout the droplet and a bead will be formed. If, however, when the CSS is reached, the rest of the droplet is below the saturation concentration, a bead will be formed.

While the water droplet in air and the droplet dissolving in a liquid solvent share many similarities, there are many differences as well. Evaporation of a water droplet in air is quite fast compared to droplet dissolution in a solvent; the diffusion of water in a

gas is expected to be much faster than the diffusion of water in a liquid. Temperature based convection and evaporation is important in combustion processes, while both are ignored in this case for the simplicity of the model.

This micropipette-based method allows the continuous monitoring of dissolution of the droplet as liquid leaves, something that is difficult for other methods, which do not allow visual observation and involve liquid-in-gas droplets, which evaporate at a much faster rate than these liquid-in-liquid droplets.

Model for concentration within a dehydrating droplet

The formation of these structures is assumed to be due to diffusive processes within the droplet. Using an approach similar to Meadly[125], who considered the problem of solute diffusion within an infinite flat plane, solute diffusion within a spherical droplet with a shrinking boundary is modeled. As a previous model for an evaporating droplet, convective transport within the droplet is ignored or treated as a higher effective diffusion coefficient within the droplet. This approach is similar to the solution by Gardner[126].

The shrinking of one droplet in another medium has been previously shown[2] to be accurately modeled by the Epstein-Plesset equation[3]. This problem is approached by first considering the diffusion equation (or Ficks' Second Law) in spherical coordinates:

$$\frac{\partial c}{\partial t} = \frac{D}{r^2}\frac{\partial}{\partial r}\left(r^2 \frac{\partial c}{\partial r}\right) \quad \textbf{(47)}$$

A coordinate transform is now performed:

$$\eta = \frac{r}{R(t)} \tag{48}$$

This gives:

$$\frac{\partial^2 c}{\partial \eta^2} = \frac{\eta R R'}{D}\frac{\partial c}{\partial \eta} + \frac{R^2}{D}\frac{\partial c}{\partial t}\Big|_{\eta} - \frac{2}{\eta}\frac{\partial c}{\partial \eta} \tag{49}$$

The Epstein Plesset equation states that the droplet will shrink according to the equation:

$$\frac{dR}{dt} = -\propto \left(\frac{1}{R} + \frac{1}{\sqrt{\pi D t}}\right) \tag{50}$$

The second term is neglected to simplify the solution:

$$\frac{dR}{dt} = -\frac{\propto}{R} \tag{51}$$

The Epstein Plesset equation is now incorporated into the partial differential equation:

$$\frac{R^2}{D}\frac{\partial c}{\partial t}\Big|_{\eta} = \frac{\propto \eta}{D}\frac{\partial c}{\partial \eta} + \frac{\partial^2 c}{\partial \eta^2} + \frac{2}{\eta}\frac{\partial c}{\partial \eta} \tag{52}$$

With boundary conditions:

$$\frac{\partial c}{\partial \eta} = 0 \; at \; \eta = 0 \tag{53}$$

$$\frac{D}{R}\frac{\partial c}{\partial \eta} + c\frac{dR}{dt} = 0 \; at \; \eta = 1 \tag{54}$$

Or, combining the Epstein-Plesset equation with the boundary condition:

$$D\frac{\partial c}{\partial \eta} - c \propto = 0 \; at \; \eta = 1 \tag{55}$$

The entire equation can now be solved numerically through a finite difference method.

4.2 Materials and Methods

4.2.1 Material Systems Studied

Table 5. Chapter 4 Material Systems Studied

Material Systems Studied	
Droplet	Surrounding Solvent
Albumin Solution Catalase Solution	n-Pentanol

4.2.2 Methods

Numerical Solution

As presented in the Appendix, first order ordinary differential equations like the Epstein Plesset equation can be solved readily by using an explicit finite difference method. A similar finite difference approximation to a second derivative can be found by using a Taylor series expansion.

For g(x):

$$g(x+h) = g(x) + hg'(x) + \frac{h^2}{2}g''(x) + \frac{h^3}{6}g'''(x) + \ \ldots \quad \textbf{(56)}$$

$$g(x-h) = g(x) - hg'(x) + \frac{h^2}{2}g''(x) + \frac{h^3}{6}g'''(x) + \ \ldots \quad \textbf{(57)}$$

Addition of these two equations reveals:

$$g(x+h) + g(x-h) = \ 2g(x) + h^2 g''(x) + O(h^4) \quad \textbf{(58)}$$

And thus:

$$g''(x) = \frac{g(x+h)-2g(x)+g(x-h)}{h^2} + O(h^2) \quad \textbf{(59)}$$

Where $O(h^n)$ indicates terms on order of h^n. $O(h^2)$ means that this approximation is second order accurate; or, in other words, that there is a certain amount of error due to these approximations, and that this error is on the order of h^2. Thus, the smaller the value for h, the smaller the error.

C Coding

The code used to solve this problem is included in the Appendix. While the program is fairly straightforward, some discussion of the reasoning behind some of the particular coding choices made may be useful to newer programmers who face similar computing resource restrictions, and now follows.

Because accuracy of the solution increases with smaller time and space step sizes, a time step of .002 seconds and a space step of .02 cm were chosen. Given the time scales of these experiments (tens of seconds), one consequence of the small time and step sizes is the generation of a great deal of data.

While the relatively simple solution of the Epstein Plesset equation can be easily accomplished using common spreadsheet software, the amount of data generated precludes any method which stores all of the generated values in memory (such as Excel, or the use of a very large array), unless an extremely powerful computer is used. Hence a C program was chosen to implement the numerical solution to this equation.

The solution methods used use the calculated values of one time step to predict the values at the next time step. Hence, it is only strictly necessary to maintain in memory two sets of values at any one time: one 'old' set, and a 'new' set, which is calculated from the 'old' values. Once the values at the next time step have been calculated, the 'old' values can be written to a file and replaced with the 'new' values. This greatly reduces the amount of memory required to execute this program.

Even this method, however, results in the generation of data files which may be on the order of tens of megabytes. While the storage of these files is not problematic, given the specifications of computers of today, loading these large files into graphing software can become problematic.

Fortunately, while solutions must be calculated in increments of .002 seconds, it is unnecessary to write these results to a file at such short intervals. Thus, by writing the data to the file every 2500 timesteps (or every 5 seconds), a smaller subset of the data which is easier to display can be obtained.

Additionally, computational load can be reduced by computing commonly used values once and using the result as a different variable, rather than re-computing the value at each time step. For example, in the program, the square of the initial radius features in the equation to be solved. By obtaining a value for the square of the initial radius instead of calculating this square every time the equation calls for it, it is possible to save a great deal of computational load.

4.3 Results and Discussion

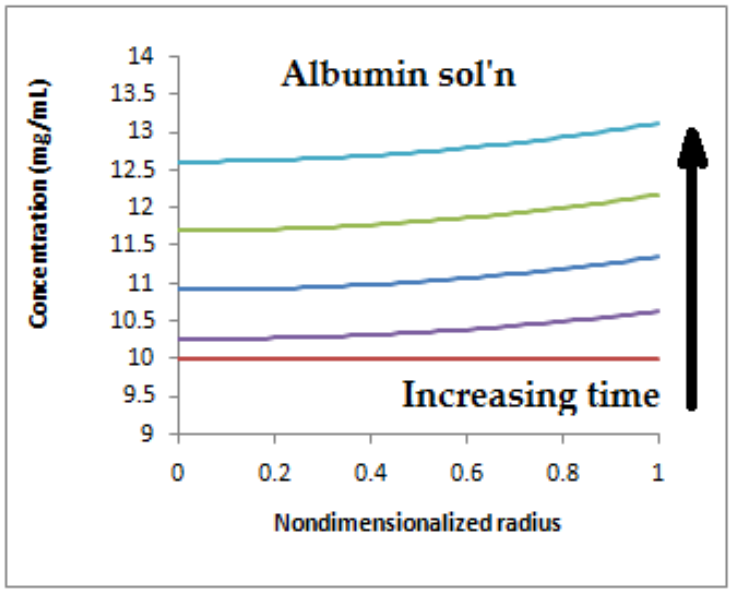

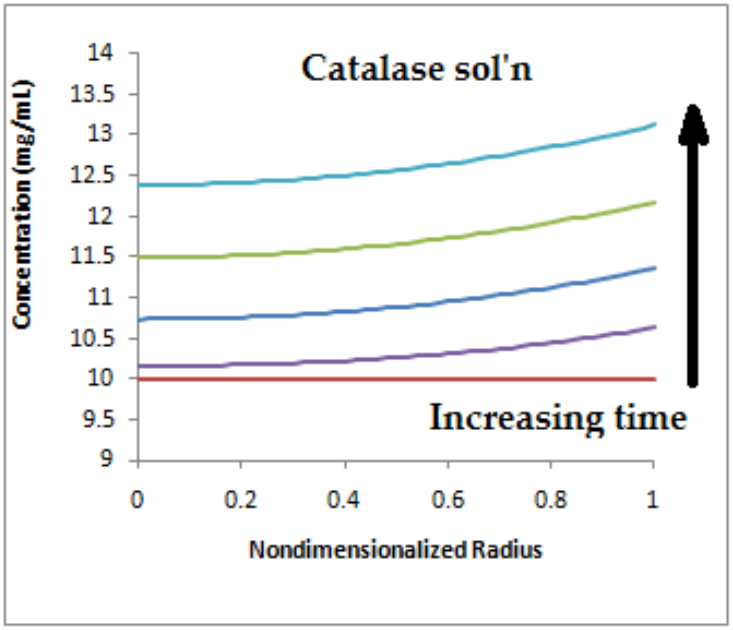

Figure 24. Time evolution of a concentration profile inside a droplet at ten second intervals. Left is albumin (diameter of 72 A), right is bovine catalase (diameter of 105 A). Red is t = 0s, purple is t = 10s, dark blue is t = 20s, green is t = 30s, light blue is t = 40s. Diffusion coefficients were estimated using the Stokes-Einstein equation.

One problem that is now encountered is the appropriate selection of experimental system. The critical supersaturation concentration of proteins is not available in the literature, if at all. While numerical simulations of the dehydration of albumin and bovine catalase yielded results in keeping with qualititative expectations, a lack of literature data prevented quantitative evaluation of the model.

4.4 Conclusion

While qualitatively the observed behavior of a dissolving droplet matches the solution of this partial differential equation, a more quantative fit is difficult to obtain. This is due to the difficulty in locating values for critical supersaturation for proteins in the literature. Thus, quantitative validation of this model awaits selection of an appropriate experimental system.

5. Delivery of protein suspensions

5.1 Introduction

One of the inventions that has resulted from the dehydration of solute containing microspheres has been the formation of glassified beads of protein and peptide. Proteins and peptides are large (1000 Da to more than 200,000 Da) molecule drugs that have been used for therapy since 1922, when insulin was first discovered[8-10], and possess greater specificity and selectivity than any non-biological small molecule drug[7] (< 600 Da). There are three primary classes useful for pharmaceuticals: enzymes (of which there are approximately 3000), hormones (of which there are approximately 150), and antibodies (of which, based on the number of receptors, there are approximately 3500 possible targets[7].) In comparison to this number of possible drug-able proteins, as of late 2009, there were only approximately 150 approved commercially available protein products and nearly 20 antibody products available[127].

One of the difficulties in working with proteins is that, in contrast with other drugs, they are fragile–even when protein is kept in a cool, dark, sterile aqueous environment, it will degrade after a few weeks[7]. One method that has been used to stop this degradation is lyophilization (freeze-drying). Lyophilization can damage protein both with freezing stresses: selective crystallization of buffer salts during freezing can lead to pH shifts, some proteins can cold denature, and exposure to the ice-water interface can damage protein; and drying stresses, in which dehydration-induced

structural changes can occur[127]. A new dehydrating technology for proteins and peptides, *microglassification*, has been developed, which gently removes water and has been shown to return some test proteins back to their original functional activities after rehydration.

Due to poor absorption through other routes, most protein and peptide pharmaceuticals must be delivered as an injection. Conventionally, proteins such as monoclonal antibodies (for example Rituxan® and Herceptin®, both approved for the treatment of cancer) are delivered through an IV, but this requires frequent administration at a hospital[11]. The subcutaneous route is an alternative that may allow for home administration and improved patient compliance, but is limited by a maximum volume of 1.5mL. Protein has a limited solubility[128], and it may be therefore difficult to achieve the desired dose in 1.5mL[11]—Rituxan®, for instance, has a dose of 375 mg/m^2[129]. Further, even if soluble, the highly concentrated solutions required to achieve the desired dose would have a prohibitively high viscosity. Intravenous delivery of proteins is limited to high volume dilute injections, partially due to the high viscosity of concentrated solutions of protein.[130] One way to overcome these problems is to deliver the protein as a suspension. Insulin has been approved for delivery as a crystalline suspension[131], and crystalline suspensions of mAbs (which require a dose of anywhere from 100mg to 1g) have been explored for delivery as well[132].

Chick and Lubrzynska[133], for example, found the viscosity of egg-albumin in water solution to increase from 1.22 times that of water at a concentration of 3.016% by weight to 9.99 times that of water at 28.15%. A high viscosity solution is difficult to pass through a needle, and is hence impractical for injection; a low concentration solution may have a lower viscosity, but much more volume, and may therefore similarly be impractical for injection.

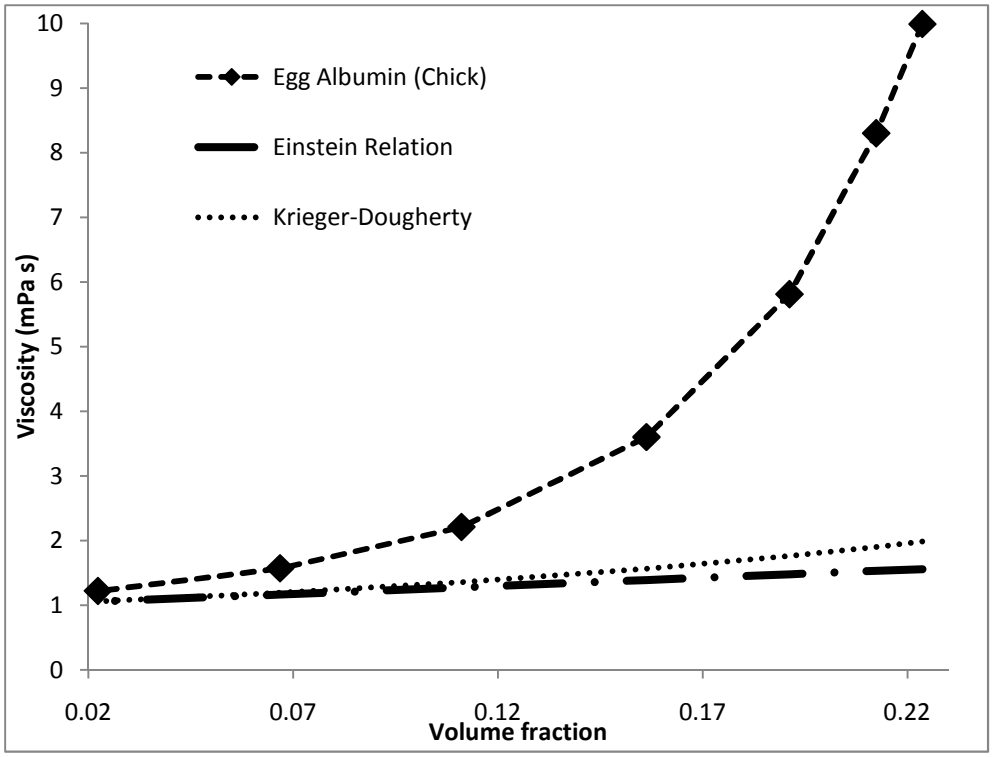

Figure 25. Viscosity of egg albumin solutions vs. Einstein and Krieger-Dougherty predictions at the same volume fraction. Solution viscosity is much higher than suspension viscosity.

As illustrated in Figure 25, one solution, then, is to inject the protein as a suspension. Viscous suspensions of bovine somatotropin in sesame oil and a suspension of bovine growth factor releasing analogue in miglyol oil have been delivered through a 14-16 gauge needle[130]. The preferred needle gauge for injection into humans is 25-27; a higher gauge indicates a smaller needle, and a smaller needle is correlated with decreased discomfort. Miller *et al* [130] dry milled lyophilized lysozyme microparticles using a marble mortar and pestle. Viscosity of the suspension was found to closely follow the Krieger-Doughety model with a coefficient of 2.5. Plotting the predicted viscosity of an equivalent suspension according to the Krieger Dougherty prediction reveals that the suspension viscosity is much lower (see Figure 25). As will be explained later in this chapter, this equation may not hold strictly true (as the suspension may be non-Newtonian), but this discussion is intended as a useful starting point.

One possible application of the technology which creates glassified microspheres of protein is the incorporation of these glassified microspheres into a protein suspension. A suspension of glassified protein microspheres would allow us to deliver a large overall concentration of protein without a large suspension viscosity.

5.1.1 Empirical correlation for injectability

Allahham *et al* determined an empirical correlation for the amount of force necessary to inject a viscous fluid, using an Instron machine[134].

$$F = \eta K \left(\frac{L}{D^4}\right) S + f \qquad \textbf{(60)}$$

Where f is the frictional force due to the syringe, L is the length of the capillary, D is the diameter of the capillary, S is cross-head speed, and K is a constant. The length and diameter of a syringe needle are already set, and the speed at which the plunger of the syringe will be depressed cannot be increased without increased patient discomfort. Thus, viscosity is an important parameter, and one that can be varied in order to improve the injectability of the suspensions. Because viscosity is an important concept for this application, the next section will discuss viscosity.

5.1.2 Viscosity of Suspensions

Since the viscosity of the suspension is an important parameter for an injectable, it is important to discuss viscosity. In order to discuss viscosity, viscosity must first be defined. Viscosity is commonly thought of as a measure of the resistance to flow of a fluid. As illustrated in Figure 26, if two parallel plates of area A with a liquid of viscosity η between them are a distance z apart, and the bottom plate is held fixed while the upper plate is acted upon with force F, in the steady state, the upper plate will move with a constant velocity, u. If a uniform velocity gradient occurs between the two plates, the liquid behavior is simple and the liquid is Newtonian[135].

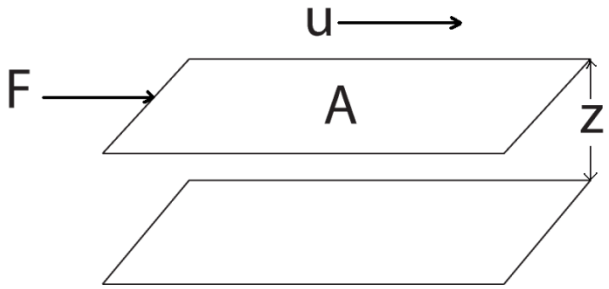

Figure 26. An illustration of the parallel plates example for Newtonian viscosity

Newton's law states that for this system (Figure 26),

$$F = \eta A du/dz \tag{61}$$

Where η is the coefficient of viscosity.

Viscosity of a dilute gas is fairly well understood, with Maxwell first deriving a theory for viscosity based on the kinetic theory of gases in 1860. Essentially, consider a system, such as the system above, in which a velocity gradient is present. Molecules adjacent to the bottom fixed plate will collide and lose momentum. Molecules in a plane above this plane will collide with those molecules, losing momentum, and so on. Thus, in order to keep motion constant, a force must be maintained.[27, 135] The theories for viscosity in liquids are currently unfinished[135], but the general molecular origins have been established. Recall that since liquid is a condensed state, the molecules of a liquid are constantly interacting with one another. Unlike in a gas, these intermolecular interactions play a much larger role in viscosity than simple momentum transfer due to molecular collisions, as in a gas. Thus it is these intermolecular interactions which cause

neighboring molecules to lose momentum, and which require a force in order to maintain constant motion.

The most commonly used theoretical estimate of the viscosity of a dilute suspension is the Einstein equation, which is based solely on the excluded volume of spheres. The derivation of this equation is somewhat complicated, and was originally presented by Einstein in 1906 in a paper entitled *Elins aeue Bestimmung der Molekuldimensdone* [136]. For those who are unable to read German, however, alternate derivations can be found in the literature, for example by Lauffer[137].

Essentially, the derivation begins by considering Newton's definition of viscosity using two parallel planes of area 1 with 1 cm distance between them. If the viscosity of the liquid is η, the force necessary to generate a velocity gradient, du/dz, of 1 is also η. In one second, the plane will move 1 cm, so the work per second is also η.

Spheres can then be added. The work per cm^3 per second necessary to maintain an average velocity gradient of one in the liquid given that the spheres do not contribute to the gradient is

$$W_1 = \frac{\eta_0}{(1-\Phi)} \quad \textbf{(62)}$$

Where Φ is the total volume of the spheres, and η_0 is the viscosity of the fluid without the spheres.

The work per cm^3 per second necessary to maintain a velocity gradient of one given the flow past the spheres is:

$$W_2 = \frac{1.5\eta_0}{(1-\Phi)^2} \quad \textbf{(63)}$$

Total work per cm^3 per second (adding the two equations) gives us η:

$$\eta = \frac{\eta_0}{(1-\Phi)} + \frac{1.5\eta_0}{(1-\Phi)^2} = \frac{\eta_0(1+0.5\Phi)}{(1-\Phi)^2} \quad \textbf{(64)}$$

This is often approximated by:

$$\frac{\eta}{\eta_0} = \frac{1+0.5\Phi}{1-2\Phi+\Phi^2} \quad \textbf{(65)}$$

Or:

$$\frac{\eta}{\eta_0} = 1 + 2.5\Phi + 4\Phi^2 + 5.5\Phi^3 + \ ... \quad \textbf{(66)}$$

Which, neglecting higher terms, becomes

$$\frac{\eta}{\eta_0} = 1 + 2.5\Phi + O(\Phi^2) \quad \textbf{(67)}$$

This is the most commonly used form of the Einstein equation for viscosity of a dilute suspension.

Note that this derivation is only strictly valid for dilute suspensions of rigid non-interacting hard spheres, where a diluate suspension is defined as one in which the disturbance around one sphere is assumed to not affect the others. For more concentrated suspensions, a number of approaches have been attempted, but the most common is the approach of Dougherty and Krieger [138]. The following derivation largely follows that given in Goodwin's book [135].

Dougherty and Krieger began by differentiating the Einstein equation:

$$d\eta = 2.5\eta_0 d\Phi \quad \textbf{(68)}$$

For a suspension with volume fraction Φ and viscosity η(Φ), this equation becomes:

$$d\eta = 2.5\eta(\Phi)d\Phi \tag{69}$$

This equation can then be integrated to give the increase in viscosity:

$$\int \frac{d\eta}{\eta(\Phi)} = 2.5 \int d\Phi \tag{70}$$

A correction factor is then used to take into account the fact that in order to form a suspension of higher concentration, new particles must replace solvent, and not other particles:

$$\int \frac{d\eta}{\eta(\Phi)} = 2.5 \int \frac{d\Phi}{\left(1-\frac{\Phi}{\Phi_m}\right)} \tag{71}$$

Where Φ_m is the maximum concentration at which flow can occur (which depends on the geometry of the particle.) Integration of this equation given that η(Φ) goes to η_0 as Φ goes to 0 gives:

$$\frac{\eta(\Phi)}{\eta_0} = \left(1 - \frac{\Phi}{\Phi_m}\right)^{-2.5\Phi_m} \tag{72}$$

This is the Dougherty Krieger equation, which has been used previously in this section to predict the viscosity of a concentrated suspension of noninteracting spheres.

5.1.3 Pouiselle's Law

Pouiselle's law describes the flow of a viscous liquid through a cylindrical tube and can be derived directly from Newton's Law. The derivation that follows comes largely from that given in Lauffer[137]. A pressure, P, applied to a cylindrical core of

liquid with viscosity η in a tube of radius r will cause a force of $\pi r^2 P$ on the liquid core, causing it to flow. When steady flow occurs, this force is balanced a force given by Newton's law, given a tube of length L filled with a liquid of viscosity η and a radius r_1:

$$\pi r^2 P = -2\pi r L r \eta \frac{\mathrm{du}}{\mathrm{dr}} \quad \textbf{(73)}$$

where u is velocity.

$$-\pi r^2 P dr = 2\pi r L r \eta \mathrm{du} \quad \textbf{(74)}$$

$$\mathrm{du} = -\frac{P}{2L\eta} r dr \quad \textbf{(75)}$$

Hence,

$$\mathrm{u} = -\frac{P}{4L\eta} r^2 + C \quad \textbf{(76)}$$

Applying the no-slip boundary condition (At $r = r_1$, $u = 0$), gives:

$$\mathrm{u} = \frac{P}{4L\eta}(r_1^2 - r^2) \quad \textbf{(77)}$$

The distance that each cylinder of radius is u, and the volume associated with that cylinder is

$$u \cdot 2\pi r dr \quad \textbf{(78)}$$

The volumetric flow rate, V, is the amount of volume flowing through the cylinder in one second, and can be obtained by integration:

$$\mathrm{V} = \frac{\pi P}{2L\eta} \int_0^{r_1} (r_1^2 r - r^3)\, dr \quad \textbf{(79}$$

$$\mathrm{V} = \frac{\pi P r_1^4}{8L\eta} \quad \textbf{(80)}$$

This is the familiar Pouiselle equation. This equation describes flow through a cylindrical tube, and is therefore important in order to understand the basic principles behind measurement of viscosity through the use of capillaries.

5.2 Materials and Methods

Viscosity can be measured in a wide variety of ways, including capillary viscometry (other methods include parallel plate viscometers, which work on the basis of the definition of the viscosity, given earlier in this chapter). Capillary viscometers (see Figure 27) are based on the Pouiselle equation, above, which provides a relationship between the rate of flow of a liquid, the geometry of a cylindrical tube, and its viscosity. By comparing the amount of time taken for a liquid to pass between two marks with the amount of time taken for a liquid of known viscosity to pass between the two marks, the viscosity of the measured fluid can be obtained. Note that care must be taken that the viscometer be set up in exactly the same way between measurements, as a slight angle will result in repeatable but incorrect results. Further, this method is not ideal for the measurement of viscosity of suspensions, which may settle during the (often lengthy) measurement. For this reason, a syringe based system, which is faster and reflects the actual injection mechanism, was used for the measurement of viscosity.

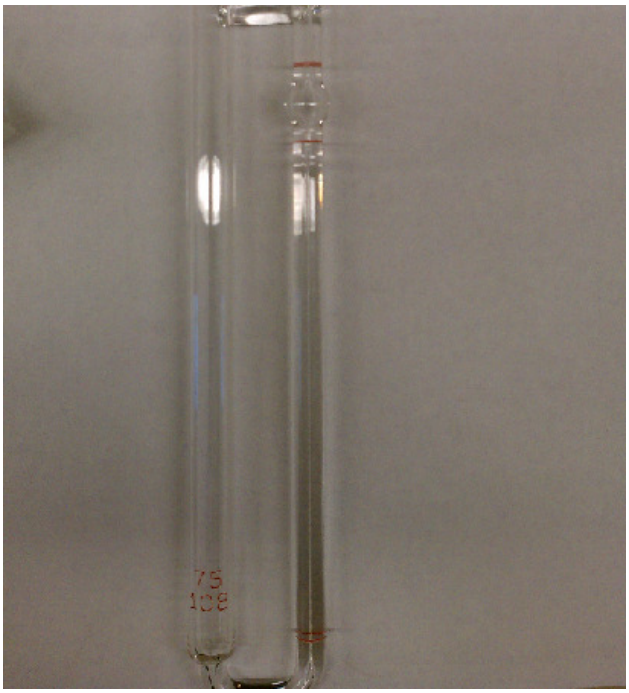

Figure 27. Capillary Viscometer. The amount of time it takes for a fluid to pass between the two marks is compared to that of a calibrating fluid, typically water. Since the viscosity of water is known (1 cP at 25 degrees C), the viscosity of the desired liquid can be obtained.

5.2.1 Viscosity measurement using a syringe based method

Vicsosity of several liquids was measured according to the procedure of Shire *et al*[11, 139]. Shire *et al* found that the time necessary for a 1 mL syringe to fill after the plunger was moved to the 1 mL mark was directly proportional to the viscosity of the liquid. This method of viscosity measurement works on the same principle as the capillary viscometer: the Hagen-Pouiselle equation states that flow through a pipe is proportional to the radius to the fourth power and pressure difference, and indirectly proportional to the length of the pipe and the viscosity of the fluid.

Hence, if liquid is drawn through the same capillary – or in this case, the needle of a syringe, the volumetric flow rate will change with the viscosity of the liquid. As volumetric flow rate is the volume that passes through a surface in a given amount of time, the amount of time necessary for 1 mL of fluid to fill a 1 mL syringe should reflect the viscosity of the liquid passing through the syringe needle.

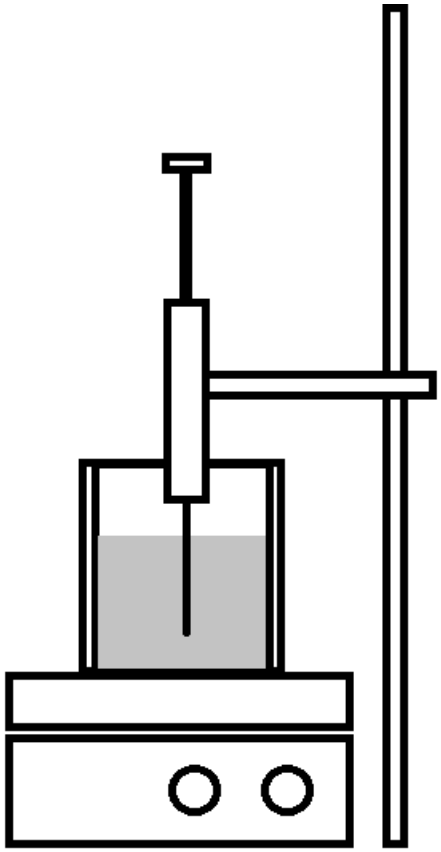

Figure 28. Schematic of measurement system (not to scale). A 1 mL syringe was mounted vertically above a beaker containing the fluid whose viscosity was to be measured. The fluid was stirred using a magnetic stirrer. The plunger of the 1 mL syringe was drawn to the 1 mL mark, and the amount of time taken for the syringe to fill measured. This was found to be proportional to the viscosity of the liquid.

The primary advantages of this method are that it is easy, requires little equipment, and the testing of the viscosity of the injectibles in a system which closely resembles its intended use. This system is not, however, expected to be as accurate as more controlled methods, such as parallel plate or rotational methods. The operator is required to withdraw the plunger of the syringe repeatedly, and might not repeat the procedure in exactly the same way each time. Further, if the densities of the liquids vary greatly, this method may not be ideal, as this changes the force balance between two compared systems. Certain solvents may also break down the polymers which comprise the syringe and plunger, resulting in variability of results.

A 26G5/8 B-D Sub-Q needle, of the type commonly used for subcutaneous injection, was luer-locked to a 1 mL B-D syringe. The end of the needle was submerged in a beaker filled with the solvent whose viscosity is to be measured.

Some solvent was first drawn into the syringe, and the syringe inverted in order to remove air from the barrel of the syringe. The syringe was then clamped vertically such that the tip of the needle was well below the surface of the liquid. Simultaneously, the timer was activated and the plunger was withdrawn to the 1 mL position. The time necessary for the liquid to fill the barrel of the syringe was recorded.

In order to test this method the viscosity of various liquids was measured. These liquids were water, *n*-pentanol, *n*-octanol, and *n*-decanol, which ranged in viscosity from

1 mPa s (water) to 11.05 mPa s (*n*-decanol). The procedure described above was repeated ten times for each liquids, with the same syringe used for five trials.

The viscosity of suspensions of glass beads in water was then measured using the same technique. 325 mesh (approximately 44 micron diameter) glass beads (MO-SCI Specialty Products, GL-0191 Class IV) were obtained from MO-SCI Specialty Products and suspended in water at volume fractions of 10, 25, and 50%. Suspensions were stirred during testing using a magnetic stirrer.

5.3 Results and Discussion

The syringe based method was quite successful for the measurement of pure liquids. As illustrated in Figure 29, the relationship between the viscosities of water, *n* pentanol, *n*-octanol, and *n*-decanol (which are known) and time taken to fill a 1 mL syringe is quite linear (R^2=.9971), and was used for calibration. Unfortunately, as can be seen from the graph (Figure 30), measured suspension viscosities differed from the Krieger-Doughtery prediction. While the measured viscosity of the suspension was somewhat close for the lower volume fractions, the sample which was 50% v/v glass beads was significantly less viscous than predicted. This is likely due to local suspension inhomogenity due to rapid settling of these large glass microspheres. It is also possible that the underlying assumptions of the Krieger-Dougherty model fail for our system; in reality, suspensions are quite rarely comprised of non-interacting ideal hard spheres, and it is possible that this suspension is non-Newtonian. For this reason,

alternate measures of viscosity should be explored, such as plate or rotating viscometers. Settling (discussed in the next section) will still be an issue in those viscometers, so appropriate material choice (PLGA, protein) will be still important.

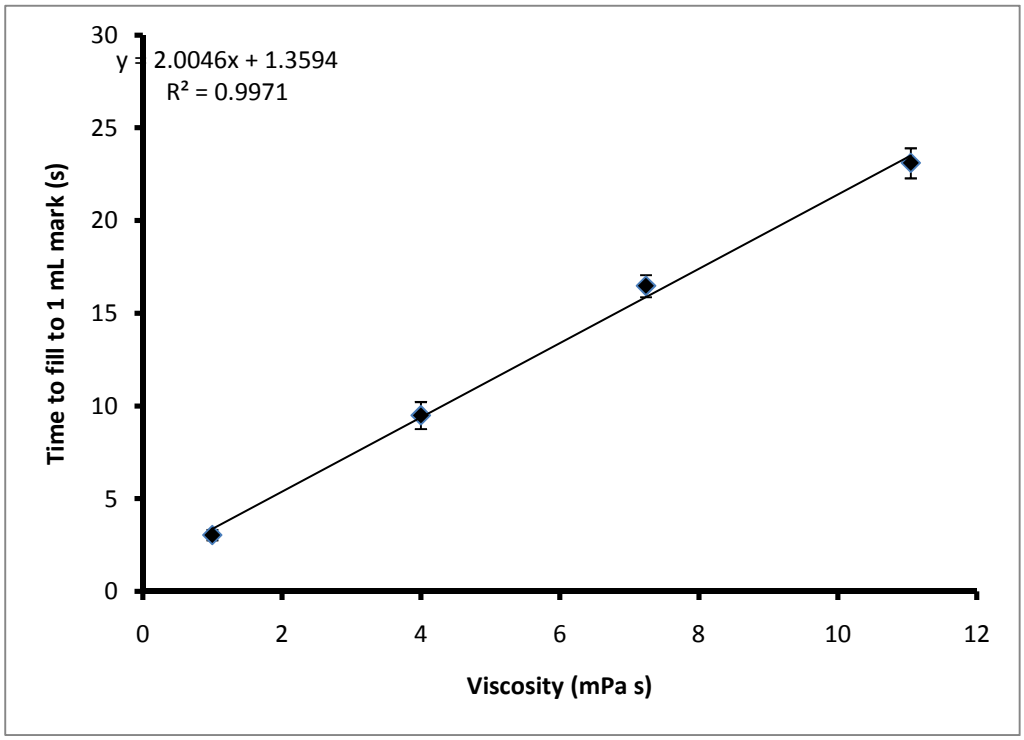

Figure 29. The viscosities of water, n-pentanol, n-octanol, and n-decanol were measured using the method of Shire et al. Each liquid was drawn into a 1 mL syringe through a 26G5 B-D SubQ needle. As expected, the relationship between time taken to fill a syringe and the viscosity of the liquid was linear.

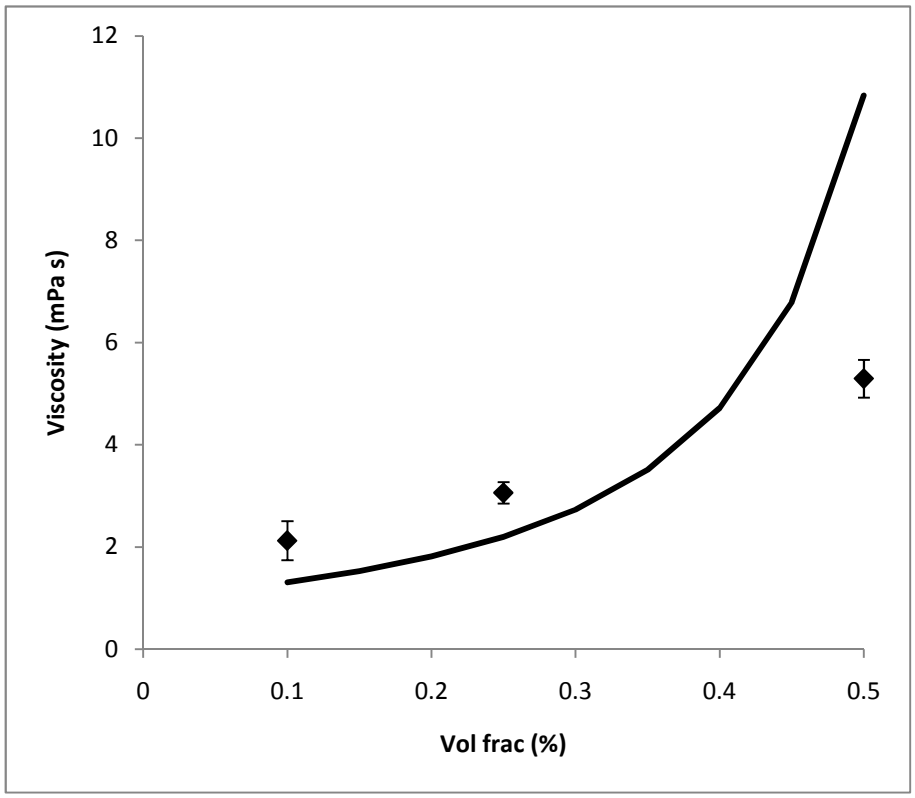

Figure 30. Viscosity of glass bead suspensions was measured using the syringe method as described in Shire et al. The solid line is the Krieger-Doughtery prediction for viscosity, while the points are experimental measurements, calibrated according to the previous figure.

5.3.1 Settling velocity of a particle in a fluid

One problem that became apparent in the glass bead experiments was settling. Despite the magnetic stirring of the glass and water suspension, rapid settling was observed. This settling results in non-uniformity of the suspension throughout the sample, which in turn, causes inconsistent viscosity measurement.

Settling is, of course, the result of the difference between two forces: the force of gravity, which pulls the glass spheres downwards, and the drag force and buoyancy, which oppose the motion of the sphere. The settling velocity is governed by the equation:

$$V = d^2 \frac{(\rho_s - \rho_l)g}{18\eta} \quad \textbf{(81)}$$

Where V is the settling velocity, d is the Stokes' diameter, ρ_s and ρ_l are the densities of the solid and the liquid respectively, g is the acceleration due to gravity, and η is the viscosity of the liquid.

Hence, to reduce settling, different materials can be chosen. Glass has a density of approximately 2.4 – 2.5 times that of water. PLGA microspheres, however, have a density of approximately 1.2 times that of water, so settling is expected to be slower. The density of dry albumin is somewhere around 1.2-1.3 times that of water[133]. Further, the choice of suspending medium has the potential to affect settling as well, both due to the affect of the viscosity of the suspension medium as well as its comparative density. Further testing is required.

5.4 Conclusion

Thus, using this new micropipette technology, glassified microparticles of protein can be created. These microparticles can be used as suspensions of protein which have much less viscosity than equivalent concentrated solution. Because the viscosity of a liquid is directly related to its injectability, the ability to create suspensions of microglassified protein allows the delivery of high concentrations of protein in a form which can easily pass through a needle. Measurement of the suspension viscosity will require further experiment, as the glass beads used as a model system settled too rapidly, despite the presence of constant stirring. It is recommended that different materials be used to test this system, including the use of microglassified beads of consistent size (if possible – this will be discussed in the next chapter), or perhaps PLGA microspheres, which are less dense than the glass used in these experiments.

6. Microdroplet Size Control

6.1 Introduction

The sizes of the glassified microspheres are governed by the initial sizes of the microdroplets generated. A number of methods have been attempted in order to generate a large number of microdroplets with desired specifications – some applications may call for a monodisperse population of microdroplets (size distribution of the glassified beads may affect drug release, for example), while for others, the size distribution of microspheres may not be important at all (if, for example, the glassified microspheres are to be dissolved prior to use.) A number of methods have been attempted in order to generate these populations, and they are reviewed here for the benefit of future researchers.

The methods for generating microdroplets can be roughly separated into two general categories: bulk methods and capillary methods[12, 13]. Each method has advantages and disadvantages, which will now be discussed.

6.1.1 Bulk Methods

Bulk methods are very common and simple means of generating droplets. In a bulk method, two liquids are brought together and one liquid (the one that is to be divided, known as the dispersed phase) is broken up into smaller parts inside the other (known as the continuous phase). This is generally accomplished through a shear or turbulent flow. Common bulk methods of preparation include stirring, mixing,

shaking, homogenization, and static mixing. While this allows for a large number of droplets to be formed, the inhomogenous nature of the environment results in a wide distribution of droplet sizes.

Two processes are important in the preparation of microdroplets in bulk: droplet breakup[14] and droplet growth[140]. Both of these processes are largely correlated with the size of the droplet; growth rate decreases with increasing droplet size, while droplet breakup decreases with decreasing droplet size. Ostwald ripening, in which material from droplets diffuses through the suspending medium to other droplets, may also occur; however, as Ostwald ripening occurs on a longer time scale, it will not be discussed in this chapter.

For droplet breakup, two scenarios are important: droplet breakup in shear flow and droplet breakup in turbulent flow.

A droplet placed in shear will, depending on the viscosity ratio of the two liquids, begin to elongate. A very viscous droplet sheared by a continuous medium which is much less viscous will deform less than a comparatively less viscous droplet in a continuous medium[140]. Thus, to break up droplets, the continuous phase should be more viscous than the discrete phase.

Experimentally, a droplet formed of a material that is less viscous than the continuous phase will, when placed in simple shear flow, elongate and eventually break up, once surface tension is no longer able to compensate for the action of the shear.

Commonly, when droplet breakup in shear occurs, daughter 'satellite droplets', much smaller than the droplet, are formed[140]. (Similar 'satellite droplets' are also responsible for the Harkins-Brown correction in the measurement of interfacial tension.)

Droplets may also break up in turbulent mixing, such as occurs in high pressure homogenization. In turbulent breakup, velocity fluctuations in the continuous phase near the droplet induce surface oscillations, resulting in breakup if the energy of the oscillations is sufficient to balance the surface energy gain caused by droplet breakup. For the study of the turbulent breakup of droplets, it is often useful to examine the ratio between the kinetic energy and the surface energy:

$$We = \frac{\rho u^2(d) d}{\sigma} = \frac{\rho C_1 \varepsilon^{2/3} d^{5/3}}{\sigma}. \quad \textbf{(82)}$$

This constant, We, is a dimensionless number known as the Weber number, where ϱ is the density of the droplet material, u(d) is the velocity of the surface of the droplet, d is the equilibrium diameter of the droplet, σ is the surface tension of the droplet, C_1 is a system dependent constant, and ε is the energy dissipation per unit of mass and time[140].

Droplet growth during mixing can occur when two droplets collide and coalesce. Not all droplet collision results in coalescence and droplet growth, however, clearly minimizing droplet collision will likewise result in decreased coalescence. Therefore, droplet collision should be avoided for a homogenous droplet population.

6.1.2 Capillary Methods

Capillary methods rely upon the stretching of a single fluid thread[141]. As a fluid thread is stretched, because the tendency of a system is to minimize its surface energy, it will spontaneously transition from a single cylindrical thread to a group of spheres. This phenomenon was first studied by Lord Rayleigh[142] in 1878, and this instability bears his name.

The total capillary energy of a column of fluid of volume V is

$$E_C = 2\pi RL\gamma = \frac{2\pi V\gamma}{R} \quad \textbf{(83)}$$

Where γ is the interfacial tension, L is the length of the column, and R is the radius of the column.

In comparison, a collection of N droplets of radius R′ and volume V has capillary energy of

$$E = 4\pi R'^2 N\gamma = \frac{3\gamma V}{R'} \quad \textbf{(84)}$$

Therefore, the system of droplets is more energetically favorable under conditions

$$R' \geq \frac{3}{2\pi} R \quad \textbf{(85)}$$

Thus, a fluid thread will tend to form a string of droplets under certain conditions. Experimentally, the radius of these droplets have been found to be roughly 1.85 times the radius of the fluid thread.

6.2 Methods and Materials

6.2.1 Bulk Methods Explored in Lab

A number of methods to generate droplet emulsions have been explored in the Needham lab. One of the earliest methods attempted was the use of an Avestin hand-held extruder, shown in Figure 31.

Figure 31. The Avestin hand-held extruder.

The Avestin hand-held extruder consists of two glass gas-tight syringes, each mounted to a separate plastic piece. A filter of the desired pore size can be inserted

between the two plastic pieces, and the device sealed. Liquid may then be transferred from one syringe through the filter to the other syringe.

An Avestin hand held extruder was used to process solutions of 1 mL of decane (dispered phase) in 10 mL of 10 mM SDS (continuous phase). Filters of 50 – 250 nm pore size were used and final droplet size was measured on a Brookhaven Instruments Corporation ZetaPlus particle sizer, using light scattering. Curiously, the final droplet size of the emulsions was unrelated to filter size. Further, droplet size was the same even with no filter present.

One explanation for this phenomenon is that the droplets, rather than being formed at the filter pores, were effectively being formed at the 'nozzle' located at the end of the syringe. Another possible explanation is that droplet size was limited by surfactant concentration. Since a dispersion of constant volume increases in surface area as it is more finely divided, fewer surfactant molecules are available per droplet as the droplet size is reduced.

Figure 32. Re-usable syringe filter. (Top) Assembled. (Bottom) Disassembled.

The re-usable syringe filter shown operates in a similar fashion as the hand held extruder. A syringe may be Luer-locked to the upper half, and the contents expelled through a filter, which is mounted on a wire mesh. Unlike the Avestin hand-held extruder, the syringe filter allows only one 'pass'.

1 mL of decane was blown into a 10mM solution of SDS using a 10 mL B-D syringe. No matter how rapidly the plunger of the syringe was depressed, very large droplet of decane, with diameters on the order of the size of the exit tube of the syringe

filter, were observed. Thus, even if droplets on the order of the size of the filter pores are being created, coalescence and droplet growth occur.

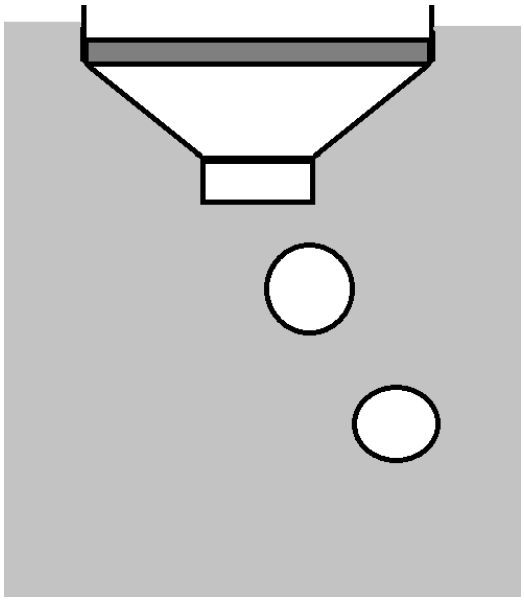

Figure 33. Cutaway view of syringe filter. The droplets are immediately forced into contact with one another in a confined space after the filter. This results in a high rate of droplet collision. Droplet collision results in droplet coalesence.

It may seem intuitive that if droplets with diameters on the order of the orifice diameter can be formed using capillary methods, a filter should act in the same manner, only in parallel. One complication with this, however, is that droplet coalescence is related to droplet collision. This is intuitively obvious – in order for two droplets to merge, they must first make contact. Thus, creation of a large number of small droplets in a confined space, such as occured in a re-usable syringe filter (Figure 32, Figure 33), resulted in droplets much larger than the filter's pore size.

Static mixing is another bulk method for preparing dispersions. A tube static mixer consists of a cylindrical tube in which a helical blade has been affixed (Figure 34). The flow within a static mixer should, in theory, be quite predictable, and therefore the droplets created accordingly less disperse. However, the droplet distribution obtained with the use of a static mixer was polydisperse, and comparable to the distribution obtained when using a filter based system.

Figure 34. Koflow Stratos Static mixer. A helical static blade is set into a cylinder.

Ultrasonics have been reported to allow for the creation of fairly homogenous populations of droplets. When attempted using a bath sonicator, polydisperse emulsions were created.

6.2.2 Capillary based methods

Capillary based methods have also been explored for the creation of monodisperse populations of microdroplets and microparticles. As the laboratory has the capability to create very small diameter (4-10 micron) glass micropipettes, some of the first

experiments involved the generation of microdroplets by forcing solution through a glass capillary.

A quick reference to Pouiselle's law will show that the pressure difference necessary to achieve a given volumetric flow rate increases with the fourth power of the radius of the pipette. Unfortunately, the pressure difference needed to drive an appreciable flow through the micropipette exceeded the ability of the seals of the micropipette apparatus to maintain the liquid within. While the laboratory routinely 'blows' droplets using picoliters of material, these micropipettes contain much less material. Loading the micropipette with many times that amount results in an increased force necessary to drive the flow, as discussed in the previous chapter (Pouiselle's law); doubling the length that the fluid must flow doubles the required pressure to maintain the same volumetric flow rate.

Needle based capillary methods have been previously used[12] to generate microdroplets. Theoretically, at a certain flow regime, jetting should occur, resulting in formation of a monodisperse population of microdroplets with sizes on the order of the orifice size. Flow of the exterior solvent, of course, may not only result in earlier droplet formation, and therefore smaller droplets, but also may also enhance mass transfer at the droplet interface, resulting in earlier droplet glassification as compared to a method which lacks flow. Glassified microbeads are, of course, more resistant to droplet coagulation as well as droplet breakup.

A 10 mL syringe was used to force protein solution through a 30 gauge needle. This syringe was vertically fixture using a standard ring stand with the needle submerged under the surface of decanol, which was contained in a 50 mL beaker. The solvent was stirred using magnetic stirring. Both stationary and vibrating needles were used to test this concept. Needle vibration was induced through action of a 6 volt electric motor controlled through a variable rheostat.

While the droplets were observed to be fairly uniform as they emerged from the end of the needle, three factors contributed to the non-uniformity of the final dispersion. One important factor is that the flow rate through the needle was controlled through hand depression of the plunger. While this method is simple and inexpensive, it lacks the controllability and repeatability necessary to create a truly uniform dispersion. Further, because the solvent within the beaker was stirred in order to increase the mass transfer rate between the protein solution and the solvent, the droplet experienced shear forces. Droplet breakup was occasionally observed, through this was dependent upon droplet size and stir rate. Lowering the stir rate to avoid droplet breakup, however, resulted in insufficient removal of water from the microdroplets, leading to droplet coalescence and polydisperse droplet formation.

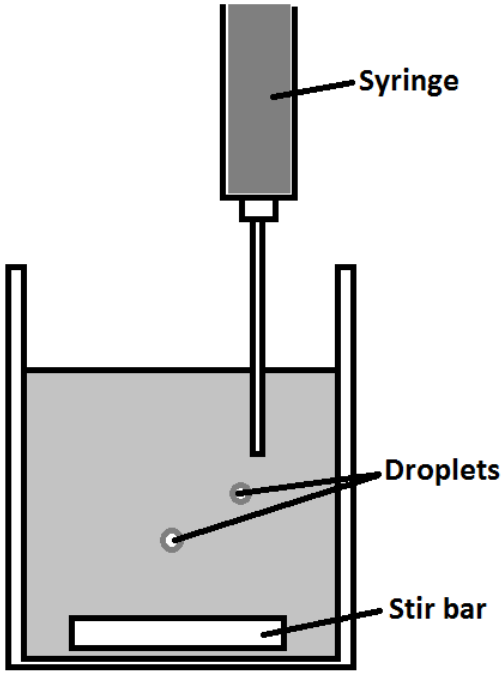

Figure 35. A syringe was used to form droplets of aqueous protein solution inside an organic solvent environment. (Not to scale.) The solvent was stirred using a magnetic stir bar. Rapid stirring resulted in droplet breakup resulting in polydisperse droplets; slow stirring resulted in droplet coalescence at the bottom of the beaker.

In order to provide a more uniform dehydration environment, a needle and tube apparatus was devised. In this apparatus, a syringe pump, attached to a 60 mL B-D syringe (because of space and size requirements), was set up to allow flow of solvent through thirty two feet of Tyvek tubing. At one end of the tube, a 30 gauge needle, mounted on a 10 mL syringe was used to pierce the wall. At the other end of the tube was set a collection beaker.

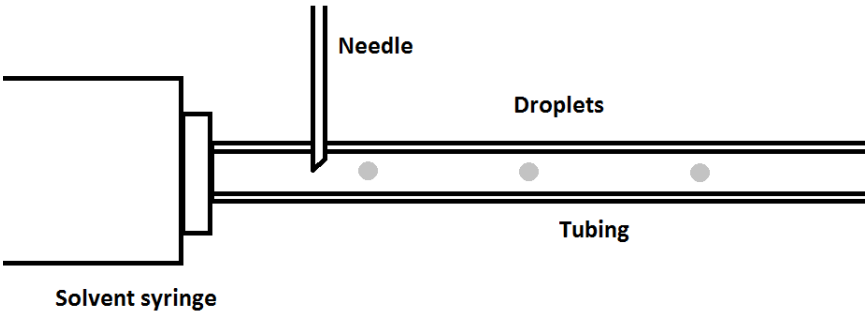

Figure 36. Syringe and tubing microfluidic device. In order to provide a more uniform dehydration environment, droplets were formed in a flowing stream of solvent.

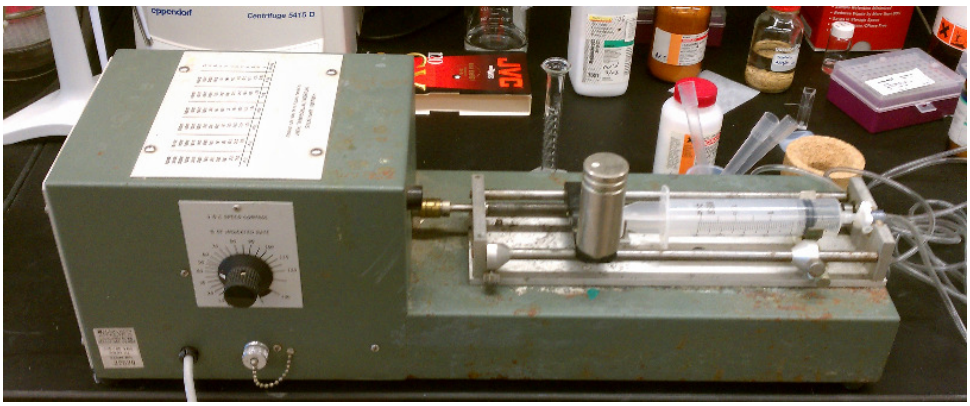

Figure 37. Harvard Apparatus 906 Syringe pump with emplaced 60 mL syringe.

The syringe pump available (Harvard Apparatus 906) was incapable of providing a sufficient infusion rate to create a very strong flow. This limited the amount of organic solvent that could be introduced. Further, the 10 mL syringe used to introduce protein solution into the organic solvent was operated by hand, reducing repeatability. Nonetheless, this method represents the most controllable out of the methods attempted. This method should be further explored, with multiple, more controllable syringe pumps.

Conclusion

Many methods of generating a highly monodisperse system of microdroplets were attempted. Two primary classes of droplet generation exist: bulk methods and capillary based methods. Bulk methods commonly create polydisperse populations of microdroplets, but can create microdroplets quite quickly, while capillary or microfluidic methods can create monodisperse droplet populations, but have a much lower through-put. As expected, all of the bulk methods attempted, including filter based methods, resulted in polydispersity.

Capillary based methods involving syringes and stirring resulted in polydispersity due to inhomogeneity of the drying environment. Insufficiently fast stirring resulted in protein solution microdroplets falling to the bottom of the drying vessel and coagulating. Fast stirring resulted in inhomogeneity due to droplet breakup. In order to create a homogenous drying environment, an attempt was made to dry the droplets in an excess of solvent in an extremely long tube. This method has promise, but will require the purchase of equipment which is currently unavailable in this laboratory.

7. Future Work

The primary focus of this thesis has been to model the dissolution of a liquid droplet in a surrounding liquid medium. At such a small scale, and with the droplet at the end of a micropipette, the mass transfer in and around this droplet is governed solely by diffusion. What follows now are recommendations for future work based upon work in this thesis.

7.1 Dissolution of Pure Liquid Droplets

Comparing the diffusion coefficients of water in *n*-alkanes with the diffusion coefficients of water in *n*-alcohols revealed that the diffusion coefficient of water in the *n*-alcohols was lower than in the analogous *n*-alkanes. This was attributed to hydrogen bonding. Applying the Macedo-Litovitz and Chang activation energy based modifications to the Cohen and Turnbull free volume theory to the diffusion coefficient relationships observed for water diffusion in the *n*-alcohols and the *n*-alkanes, the difference in activation energy for escaping neighboring molecules could be calculated to be approximately 1.39RT higher for water in the *n*-alcohols, which is lower than the energy for a moderate strength hydrogen bond, such as is commonly found for alcohols and water. One possible explanation is that this represents water, on average, making less than one hydrogen bond at each diffusion step. This is especially likely in the light of water's small size in comparison with the solvent through which it diffuses.

Other possibilities exist. It is also possible that in this system, water diffuses in a 'bucket chain' method, in which it forms a new hydrogen bond before making the diffusive step. Another, though unlikely, possibility is that this measurement reflects the strength of the water-alcohol hydrogen bond. In order to conclusively ascertain the meaning of this difference in activation energies, additional experiments are proposed. Repeating this experiment with secondary alcohols should allow for the measurement of any possible geometry effects. Additionally, repeating this experiment with poly-alcohols could allow us to determine whether the strength of the hydrogen bond is, indeed, being measured; if the difference in activation energy increases in a discrete step if water is allowed to form two hydrogen bonds, this would open the possibility that this measurement does indeed reflect the bond energy. One possible difficulty with experimentation with water and poly-alcohols, however, is that our experiments require immiscibility, and many water/poly-alcohol systems are miscible.

7.2 Dissolution of Mixed Liquid Droplets

A model was then proposed for the dissolution of droplets of liquid mixtures. In this model, each component of the liquid droplet was assumed to diffuse from the droplet in accordance with the area it occupies at the surface. This model was tested using ethyl acetate/butyl acetate droplets and butyl acetate/amyl acetate droplets. To test for the possible presence of a surface excess, the surface tension versus concentration

relation of ethyl acetate/butyl acetate was plotted, however, due to the volatility of ethyl acetate, these tests were inconclusive.

This model should be used for practically relevant applications, such as the formation of a polymer or protein bead through solvent evaporation. Further, theoretically, there is no reason that this model should not work for any n component droplet system. This work should be tested for mixtures of three or more components. As this model's assumptions require homogenous mixing within the droplet, it would be interesting to examine systems for which this model does not hold. Deviations from this model may result in interesting information about the interaction between the components of the droplet.

Additional work is required for the measurement of surface tensions of volatile systems using the micropipette technique. Even the use of very large plugs did not result in consistent experimental results, due to the high volatility of ethyl acetate.

7.3 Shell Formation in a Solute-Containing Dissolving Droplet

The next system considered was dissolution of droplets containing a solution. As the concentration of material within the droplet rises, precipitation may occur. In some cases, droplet dissolution resulted in a shell, in others, a bead. Following the work of Meadley[125], who considered the concentration of material within an evaporating infinite planar surface, an equation for the concentration within a shrinking droplet was proposed. This equation was solved numerically, however, because of the difficulty in

finding critical supersaturation concentrations for proteins, only qualitative agreement was obtained. Future work in this area will deal primarily with the selection of an appropriate experimental system, which may not be an easy task.

7.4 Application: Analysis of Injectable Suspensions

Suspensions of glass beads were tested using a syringe based viscosity measurement method, as described in Shire *et al*[11, 130]. While this method proved quite capable of the measurement of the viscosity of various solvents, the measurement of suspension viscosities was complicated by settling of the glass spheres. This settling resulted in an inhomogenous distribution of spheres within the sample, even despite constant stirring, and with the short experiment times. As the density of glassified protein is three times lower than that of silica glass, the use of microglassified samples might improve these results.

7.5 Microdroplet Size Control

One reason for the use of glass beads was to ensure consistent size control over the suspension. As microglassified beads are generated from dehydration of a protein solution droplets, final microglassified bead diameter is largely dependent upon initial protein solution droplet diameter.

Two broad categories of droplet generation exist: bulk methods, such as stirring, and capillary methods, which include microfluidics. In general, bulk methods allow for the processing of large amounts of material in a short time, but due to the

inhomogenous local environment tend to have a broad droplet size distribution. Capillary methods, on the other hand, generate droplets through the stretching of a fluid thread, and can generate extremely consistent droplet sizes. The tradeoff with capillary methods is that throughput is generally much lower than in bulk methods.

A number of methods for generating microdroplets in the laboratory have been attempted, and are summarized for the benefit of future students. These methods included bulk methods, including stirring, shaking, and homogenization, all of which generated wide distributions of droplet sizes. Filter based methods, did not generate the desired size distributions, largely due to droplet coagulation immediately after the filter. Capillary based methods were based largely around a fine, 30 gauge syringe needle, and resulted in mixed results. Only one syringe pump was available, and it was antiquated, incapable of providing a useful range of flow rates. These methods do, however, have some promise, and deserve further exploration, should the equipment become available.

Appendix A: Micropipette Experimentation

A1. Micropipette Pulling

Micropipettes are generally made by pulling on a glass capillary tube. Historically, the earliest micropipettes were hand-pulled[143] while being heated in a Bunsen burner flame. The micropipettes formed from this process were of extremely variable quality, even after quite a bit of practice, with one pair of researchers, Nastuk and Hodgkin, reporting in 1950 that only 5% of their tips were suitable for use. It is for this reason that mechanical pipette pullers were developed.

The first pipette puller was described by DuBois in 1931, based on observation of an expert hand pipette-puller, and was a horizontal pipette puller. A platinum wire filament was used to heat a capillary, and a powerful spring was used for the actual pulling itself. The spring automatically began to pull once the glass was heated to a certain temperature, thus resulting in a more controlled temperature at pulling onset. Pulling began slowly (to help create a shorter tip) and then quickened (to make a fine tip). The tip was then removed from the heating element, and a guide rod was used to ensure that the pulling was straight.[143]. These are all features which have been incorporated into every pipette puller designed since.

One difficulty in horizontal pipette pulling is that if the pulling velocity is not sufficiently high, the tip may sag, resulting in a curved pipette. In 1956, Winsbury described a vertical pipette puller designed specifically to avoid tip sag. Vertical pipette

pullers have the limitation that their tips may be very fine, as they cannot pull with less force than produced by gravity. Other modifications to pipette pullers include the air-jet micropipette puller, which immediately cools the tip after cooling. This allows short, fine tips, which are desirable in some biological applications.

The Needham laboratory employs the David Kopf Model 700c vertical pipette puller, though a horizontal W-P Instruments MPI PUL-1 is also available. Should a user desire to use the horizontal pipette puller for their experiments, they should bear in mind that more effort must be taken to ensure proper alignment, and that low pull speed may result in curvature of the pipette's tip.

The David Kopf Model 700c, as with all vertical pipette pullers, places tension upon a glass capillary tube. Electricity is supplied to the heater coil, which results in heating. As tension is always applied to the capillary, pulling begins as soon as the temperature of the glass capillary allows the glass to flow.

In order to create a micropipette using the David Kopf Model 700c vertical pipette puller, a glass capillary tube (A-M Systems, Inc., Catalog # 635500, Glass, Standard, .75mm x .4 mm, 6") is first clamped into the pipette puller. The topmost clamp should be applied to the glass capillary tube, then the bottom clamp should be lifted from its resting place and clamped onto the bottom of the glass capillary tube. If two micropipettes are to be made from a single tube, care should be taken that the center of the glass capillary tube is aligned with the center of the heating coil. The power

switch is located at the lower right on the face plate of the machine. Activation of this switch should also turn on an orange light, indicating that the puller is ready.

Both heat and pulling speed can be set on the pipette puller. A red line has been drawn on the heating dial, indicating where previous attempts have burnt out the coil (David Kopf Instruments Model 710 Nichrome Heater Coil). Avoid exceeding the red-line limit unless you have a different coil installed in the machine. Varying pulling speed and heating can vary the final shape of the pipette. For these experiments, coil and speed settings of 60 and 60 were used.

Once you are ready to begin pulling of the pipette, briefly depress the black activation button located on the faceplate of the machine. The rest of the process proceeds automatically. Care should be taken when removing the newly formed pipettes from the machine, as the tips are very fragile and will break at even the slightest contact. Very little pressure is required for this very small tip to penetrate skin. Ensure that the pipette puller is turned off when it is no longer needed.

A2. Microforging the Micropipette's Tip

The tip of the micropipettes should be flat. Random breakage, however, will result in an unpredictable, jagged pipette tip. For this reason, a microforge is employed.

The microforge comprises a microscope set up horizontally, a heating element, and a stage upon which the pipette can be clamped. Upon the heating element, which is a 'v' shaped wire, is mounted a single bead of glass (Ferro Corporation, CF 7570 0010

Electronic Glass). This glass bead is composed of a glass which has a lower melting point than the glass of the micropipette. By allowing heated glass from the bead to flow up into the micropipette through capillary action, the pipette can be broken under controlled conditions, creating a flat surface.

In order to use the microforge, both the illuminator lamp and the heating element must be turned on. Clamp the newly create micropipette onto the stage on the right hand, laying the pipette into the groove and using the screw to secure the pipette to the stage. Depress the foot pedal to begin heating the bead.

Advance the micropipette forward by turning the knob to the right of the stage. Continue to do this until the tip of the micropipette is visible through the microscope. At this point, adjust (using the knobs at the left hand side of the heater holder) the position of the glass bead so that the tip of the micropipette is aligned with the equator of the sphere. Advance the micropipette a short distance into the heated glass bead, then release the foot pedal to allow the glass bead to cool.

As the glass bead cools, it should break off the very tip of the micropipette. Retreat the micropipette from the glass bead and depress the foot pedal to heat the bead once more. Once the bead melts, advance the (now open) tip of the micropipette a short distance into the bead and allow the melted glass to flow up micropipette until it reaches the point at which you want the glass to cleanly break. At that point, release the

foot pedal. The pipette will break on its own as the glass cools, an event that is accompanied with a faintly audible sound.

A3. Replacing the Glass Bead

After a great number of pipettes have been microforged, the user may notice that the properties of the glass in the glass bead may have changed, as the glass bead now contains a significant amount of pipette glass. In order to change the glass bead, turn on the heater element of the microforge and depress the pedal until the bead is melted. Using a disposable wooden implement, remove the glass bead.

Now, keeping the pedal depressed, use a spatula to dust the 'v'-shaped wire with glass powder (Ferro) until the bead is once more of the desired size. When the bead has reached the desired size, release the pedal and put away the glass powder. The microforge's glass bead has now been replaced.

A4. Creating a Hydrophobic Pipette

While glass capillary tubing is an ideal material for the creation of micropipettes, it is also a hydrophilic material. This can cause a great deal of difficulty for systems in which water is the droplet phase, as the droplets will spread on the surface of the micropipette instead of creating a spherical droplet.

For this reason, the glass pipettes can be treated with hexamethyldisilane to make them hydrophobic. This substance is quite toxic, so extreme caution should be used in handling this chemical. This procedure should only be performed in a fume

hood. Proper protective equipment, including goggles, gloves, and a laboratory coat should be worn during this procedure.

A5. Conducting a Micropipette Experiment

When conducting a micropipette experiment, it is of utmost importance that care be taken when handling a micropipette. As stated above, the slightest contact with any other surface will render the pipette's tip broken, and the tip easily penetrates skin. An intact tip should be barely visible to the naked eye. Absence of this very fine tip means that the tip is broken. Also keep in mind that the micromanipulators are extremely delicate and easily damaged. Do not drop a micromanipulator, and avoid placing a great deal of force on the pipette chuck's holder.

The micromanipulators are pneumatic, working on air. The pipette itself is placed on a special holder that transmits air from an external source into the pipette itself while also allowing it to be mounted in a chuck on the micromanipulator. This chuck is mounted on an extremely delicate miniature bellows, which ruptures easily and is expensive to repair. For this reason, the tube leading from the pipette holder should always be put into the strain relief clip. Do not mount and un-mount the holder while the micromanipulator is attached to the stage. As the holder is held in with a screw, be very cautious when mounting and un-mounting the holder.

In order to perform a micropipette experiment, the micropipette must first be loaded. The micropipette must first be measured and then shortened to the desired

length using a diamond scribe. We then mount the micropipette into its holder in preparation for loading.

This can be accomplished in a number of ways, but is most simply accomplished by applying negative pressure (commonly, using an attached 10 mL syringe) to the micropipette as the tip is immersed in the liquid to be loaded. As the pipette's diameter is quite small, this procedure can take some time. If your pipette fills quickly, there is a good chance that the tip has broken and is now unsuitable for experiment. Varieties of loading holders are available throughout the lab; hand loading, while possible and not requiring special equipment, is only recommended for those with a steady hand, as it is quite easy to break a pipette's tip during this process.

Having loaded the micropipette, the pipette and holder must be mounted to the micromanipulator. Remove the micromanipulator from the microscope and, using a finger to stabilize the mount, carefully insert the holder. Tighten the screw to secure the holder into the mount. Now slide the micromanipulator back onto its post.

At this point it may be useful to view the pipette and objective lens from overhead to center the pipette's tip. It may be easier to locate the barrel of the pipette, and from there, the tip. Also, you may wish to sight along the pipette holder to ensure that the pipette tip is neither too low nor too high to enter the desired chamber. Find the pipette tip visually in the microscope and verify that it remains intact.

Fill the desired chamber with the outer phase liquid and place the chamber onto the holder. Advance the chamber onto the pipette. You are now ready to begin your pipette experiment.

Appendix B: Numerical Solution

The solution of ordinary differential equations is a common problem is science and engineering. There are two primary ways by which ODE's can be solved: analytically and numerically. Analytical solutions are generally much preferred but can only be preformed for ODE's of certain form.

If an ODE cannot be solved analytically, numerical methods may be used. Many numerical methods exist, the simplest method of which are the Euler type methods. The Euler method for solving differential equations is based on the approximation of a derivative. A derivative is defined as the slope of a function at a point. The limit definition of a derivative is:

$$\frac{dy}{dx} = \lim_{h \to 0} \frac{y_{x+h} - y_x}{\Delta h} \quad \textbf{(A1)}$$

Euler's method essentially states that given knowledge of dy/dx and y_x, the limit h -> 0 can be approximated with a very tiny Δh, which should allow the calculation of yx+h. This is equivalent to saying that since the slope of a function at a point is known, if the function can be approximated as a line and advanced a very small amount, a close approximation of the next point in the function can be found. Hence, Euler's method can be written as:

$$y_{n+1} = y_n + hf(x_n, y_n) \quad \textbf{(A2)}$$

Euler's method, despite its simplicity, has several drawbacks. Euler's method has an error on the order of $O(h^2)$ – that is to say, the step's error is proportional to the

square of the step size. Other methods are more complicated, but have higher order error, making them generally preferred.

While a fourth order Runge Kutta method was tested, no improved accuracy over a simple to implement Euler's method was found. Programs were written, both in MATLAB and in C, to solve the Epstein-Plesset equation, but eventually, a solution to the Epstein Plesset equation was implemented in Microsoft Excel. While this is slower and more memory intensive than MATLAB (which is in turn, much slower than C), Excel allows for a friendly user interface and eliminates the need for repeated compilation and execution.

This solution was implemented in Excel as follows: It is possible to simplify the Epstein Plesset equation into the form:

$$\frac{dR}{dt} = -\propto \left(\frac{1}{R} + \frac{1}{\sqrt{\pi D t}}\right) \qquad \textbf{(A3)}$$

Notice that α should be calculated once, as it remains constant. Calculating α for each step is unnecessarily computationally expensive. One cell is initialized with the initial time: 0, and another with the initial radius. (Care must be taken so that units are internally consistent; for most of the spreadsheets, all lengths were calculated in centimeters.)

Once the value for the radius at time t = 0 is known, in accordance with the formula for Euler's method, the value for the radius at the next time step is simply the value of the previous time step added to the value of dR/dt at the current time,

multiplied by the size of the time step. This can be repeated until the radius reaches zero. Once the radius reaches zero, the equation becomes unphysical, and will tend to oscillate.

Care must be taken when selecting a time step – too small of a time step may be unnecessarily computationally expensive, and may run in to round errors.

Appendix C. Miscibility and Immiscibility

In order for the micropipette to be an applicable to an experimental system, the system must have an interface. This means the liquids must be immiscible. Water and oil is the most common example of an immiscible system: if olive oil is poured into a pot of water (at room temperature), a distinct layer of oil will form on top. A common example of a room temperature miscible system is water and ethanol; many common alcoholic beverages are based entirely on this concept. The reason that water and oil form separate phases, while water and ethanol does not (at room temperature) lies in the intermolecular interactions between the molecules.

The following derivation is from Dill's *Molecular Driving Forces*.[144] A lattice model can be used to model a mixture. N_A molecules of substance A and N_B molecules of substance B, both of which are of the same size, can fill a three dimensional lattice of N sites:

$$N = N_A + N_B \quad \textbf{(C1)}$$

The number of ways in which these molecules can be arranged is

$$W = \frac{N!}{N_A! N_B!}. \quad \textbf{(C2)}$$

The Boltzmann equation states

$$S = -k \ln W. \quad \textbf{(C3)}$$

Where k is Boltzmann's constant (k = 1.380662 x 10^{-23} J/K), W is the *Wahrscheinlichkeit* (German for probability), or the frequency of occurrences of a state, and S is the entropy of the mixture.

Stirling's approximation states

$$\ln n! \approx n \ln n - n \quad \textbf{(C4)}$$

So W can be re-written as

$$N! = N \ln N - N \quad \textbf{(C5)}$$

$$N_A! = N_A ln N_A - N_A \quad \textbf{(C6)}$$

$$N_B! = N_B ln N_B - N_B \quad \textbf{(C7)}$$

Which means:

$$\Delta S_{mix} = -k(N \ln N - N_A \ln N_A - N_B ln N_B)$$

$$= -k(N_A \ln N + N_B \ln N - N_A \ln N_A - N_B ln N_B) \quad \textbf{(C8)}$$

Or, in terms of mole fractions,

$$\Delta S_{mix} = -k(N_A \ln x_A + N_B ln x_B) \, . \quad \textbf{(C9)}$$

If the free energy of mixing is:

$$\Delta F_{mix} = -T\Delta S_{mix} \, , \quad \textbf{(C10)}$$

then the solution is considered ideal; in other words, if mixing is governed solely by the entropy of mixing, and no other entropies, such as changes in volume, structuring, or ordering in the solution the solution is ideal. Further, in an ideal solution, there is no change in total internal energy of the mixture upon mixing – the

total internal energy, U, of the system depends only upon the intermolecular interactions. In an ideal mixture, the interaction between molecules of different types is the same as the interaction between molecules of the same type, so this internal energy does not change upon mixing.

A lattice model can be used to estimate the energies of mixing which result in solution nonideality. Given a solution of molecules of A and B particles, the total energy of a system is

$$U = m_{AA}w_{AA} + m_{BB}w_{BB} + m_{AB}w_{AB} \quad \textbf{(C11)}$$

Where m_{AA} is the number of AA bonds, m_{BB} is the number of B bonds, m_{AB} is the number of AB bonds, and w_{AA}, w_{BB}, and w_{AB} are the contact energies of the corresponding interactions. The number of contacts is not known because of the many possible configurations of the system, so it is common to express the number of bonds with the number of neighbors of each particle in the lattice. Assuming each particle has z sides, then the total number of sides of particles of types A and B are

$$zN_A = 2m_{AA} + m_{AB} \quad \textbf{(C12)}$$

$$zN_B = 2m_{BB} + m_{AB} \quad \textbf{(C13)}$$

Hence, the total interaction energy U is

$$U = \left(\frac{zN_A - m_{AB}}{2}\right) w_{AA} + \left(\frac{zN_B - m_{AB}}{2}\right) w_{BB} + m_{AB}w_{AB} \quad \textbf{(C14)}$$

It is possible to estimate m_{AB} through the use of the Bragg-Williams 'mean field' approximation, which essentially assumes that the particles are mixed as randomly and uniformly as possible.

Given the mean field assumptions, the likelihood that a molecule of A has a B neighbor is

$$p_B = \frac{N_B}{N} = x_B = 1 - x \quad \textbf{(C15)}$$

Since each A molecule has z neighbor sites, the average number of AB contacts per A is the probability multiplied by the number of sites. Hence, the number of m_{AB} contacts is

$$m_{AB} = \frac{zN_AN_B}{N} = zNx(1-x) \quad \textbf{(C16)}$$

Substituting:

$$U = \left(\frac{zN_A - zNx(1-x)}{2}\right) w_{AA} + \left(\frac{zN_B - zNx(1-x)}{2}\right) w_{BB} + zNx(1-x)w_{AB} \quad \textbf{(C17)}$$

Or, rearranging

$$U = \left(\frac{zw_{AA}}{2}\right) N_A + \left(\frac{zw_{BB}}{2}\right) N_B + \left(w_{AB} - \frac{w_{AA}+w_{BB}}{2}\right) \frac{N_AN_B}{N} \quad \textbf{(C18)}$$

The free energy of mixing, F = U – TS, can now be written by combining these equations:

$$\frac{F(N_A,N_B)}{kT} = N_A ln\left(\frac{N_A}{N}\right) + N_B ln\left(\frac{N_B}{N}\right) + \left(\frac{zw_{AA}}{2}\right) N_A + \left(\frac{zw_{BB}}{2}\right) N_B + \left(w_{AB} - \frac{w_{AA}+w_{BB}}{2}\right) \frac{N_AN_B}{N} \quad \textbf{(C19)}$$

What this model says is that the energy of mixing is dependent upon intermolecular interactions w_{AA} w_{AB} and w_{BB}.

Using the definition of free energy of mixing as described above, the equations for the free energy difference between the mixed states and the pure states are now:

$$\Delta F_{mix} = F(N_A, N_B) - F(N_A, 0) - F(0, N_B) \quad \textbf{(C20)}$$

Substitution into the previous equation gives Hildebrand's solution model:

$$\frac{\Delta F_{mix}}{kT} = x \ln x + (1-x)\ln(1-x) + \chi_{AB} x(1-x) \quad \textbf{(C21)}$$

Where χ_{AB}, also known as the exchange parameter, describes the energetic cost of taking one molecule of B into a medium of pure A and one A into a medium of pure B. Since according to Hildebrand's principle, for most systems, AB affinity is weaker than AA or BB affinity, this parameter is usually greater than 0. This parameter is also useful in the study of interfacial tension. This parameter is defined:

$$\chi_{AB} = \frac{z}{kT}\left(w_{AB} - \frac{w_{AA}+w_{BB}}{2}\right) \quad \textbf{(C22)}$$

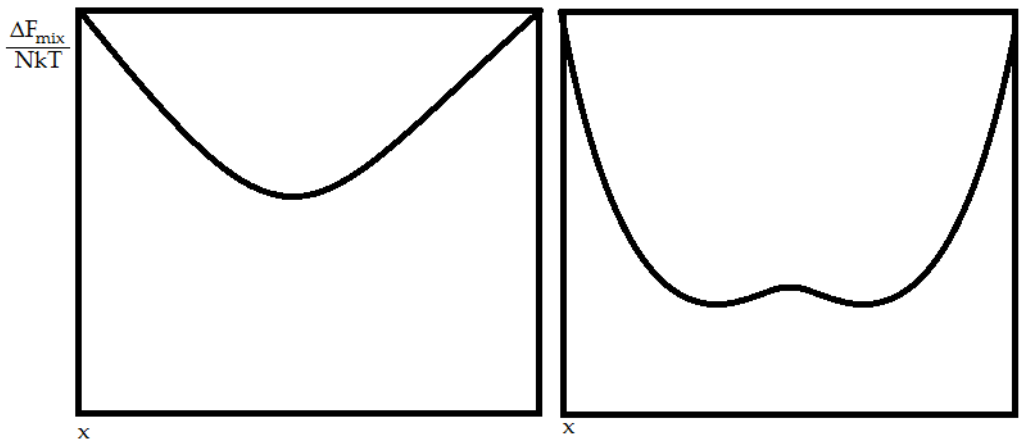

Figure 38. Example shapes of free energy plots versus mol fraction (following Dill). The plot on the left is for a miscible system, the plot on the right is for an immiscible system. The shape of the plot will change depending on temperature.

Phase separation is driven by the tendency to lower the free energy. Whether a mixture is miscible or immiscible depends on the shape of the free energy curve, as in Figure 38, which plots the free energy of mixing against the mole fraction of the system. The left curve illustrates a miscible system: there exists a free energy minimum at a certain mole fraction. The right curve illustrates an immiscible system: there are two free energy minima, corresponding to the two immiscible phases. These curves are, of course, temperature dependent (as the χ_{AB} term is temperature dependent – a system may be miscible at a higher temperature (where mixing is dominated by the entropic component), and immiscible at a lower temperature, where mixing is dominated by attractive interactions.

Thus, immiscibility is determined largely by intermolecular interactions: interactions between like molecules, and interactions between dissimilar molecules. Ideally, a parameter would allow the prediction of which systems are miscible and which are not, and so the interfacial tension of water/solvent systems versus parameters such as the dielectric constant of the solvent and the boiling point of the solvent have been plotted.

While these intermolecular forces may be roughly correlated with values like dielectric constant (which is in turn roughly correlated with the polarity of the molecule) or the boiling point of the liquid (which reflects the strength of the interactions between the molecules of the liquid), plotting the dielectric constant of a number of liquids versus

their interfacial energy with water reveals only the vaguest of trends. This is because the polarity of the molecule (and therefore by extention, the dielectric constant) is not fully reflective of all the intermolecular interactions which cause miscibility and immiscibility.

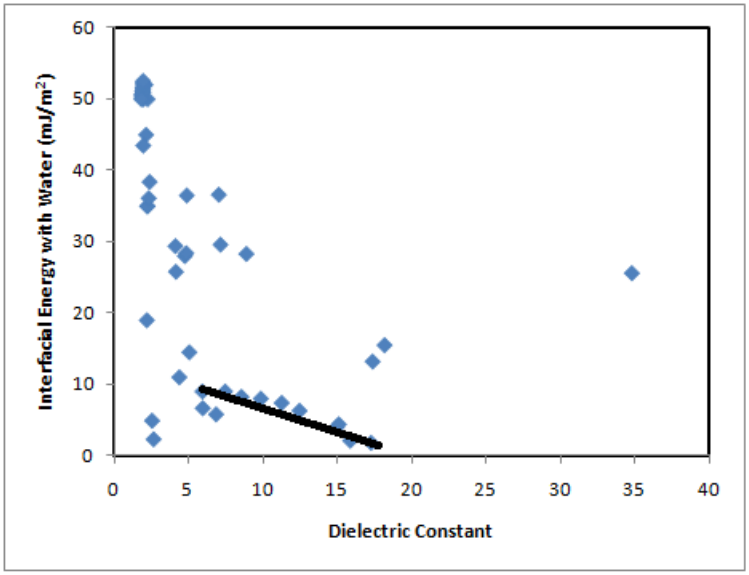

Figure 39. Interfacial energies of organic solvents with water versus the dielectric constants of the organic solvents. The dielectric constant of water is 80. The black line indicates the n-alcohols, for which there is a clear trend. However, for many of the other solvents, the trend is very general, if at all.

Plotting the interfacial energies of these solvents against their boiling points, however, reveals, again, a very vague trend. There appears to be no single property which can predict miscibility or immiscibility. Fortunately, miscibility is simple to determine experimentally.

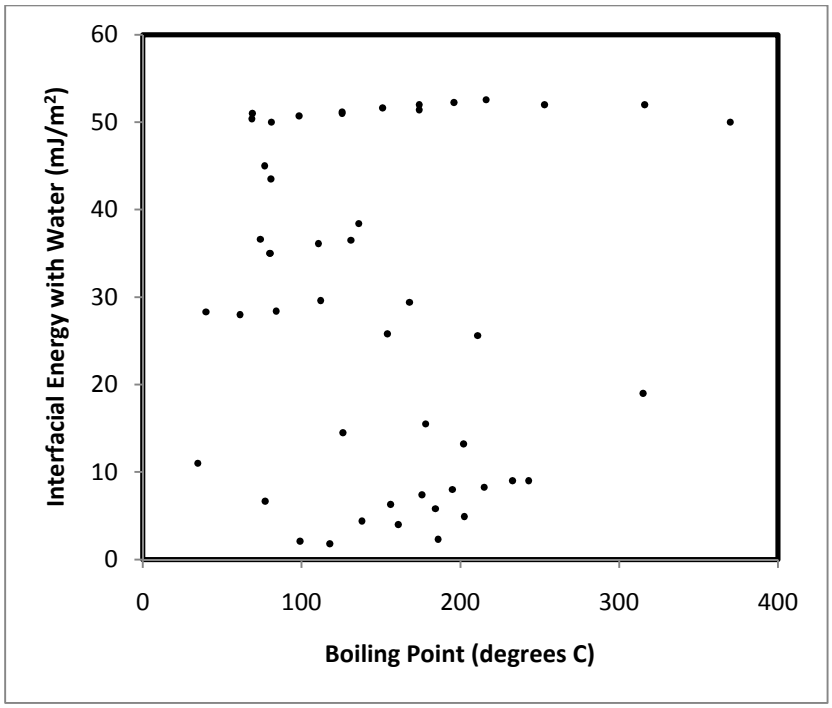

Figure 40. Interfacial Energy of organic solvents and water versus boiling point of the organic solvent.

Appendix D. Interfacial Tension

Interfacial tension is a defined as the derivative of the free energy with respect to the total area of the interface, or, in other words, the free energy cost that must be paid to increase the total area of the interface. This tension is a force that operates on an interface and tends to decrease its area, and arises from differing intermolecular interactions within two liquids which form the interface. This free energy cost to increase the interfacial area can be estimated using a lattice model.

The following derivation again follows that given in Dill's *Molecular Driving Forces.* The simplest lattice model is first considered for a liquid. A liquid consisting of N particles with z neighbors and energy per bond of w_{AA} will have a total energy U:

$$U = \frac{Nzw_{AA}}{2} \quad \textbf{(D1)}$$

If n of those N molecules are now at the surface, then N-n molecules are at the bulk, and have z nearest neighbors, as before. The n surface particles, however, will have z-1 neighbors, because of the side exposed at the surface. Thus, the total energy of the surface and the bulk can be written as:

$$U = (N-n)\left(\frac{zw_{AA}}{2}\right) + n\left(\frac{(z-1)w_{AA}}{2}\right) \quad \textbf{(D2)}$$

From the definition of a surface tension as the change in free energy with respect to area:

$$\gamma = \left(\frac{\partial F}{\partial A}\right)_{T,V,N} = \left(\frac{\partial F}{\partial n}\right)_{T,V,N}\left(\frac{dn}{dA}\right) = \left(\frac{\partial U}{\partial n}\right)_{T,V,N}\left(\frac{dn}{dA}\right) \quad \textbf{(D3)}$$

By combining this definition with the lattice model, one can obtain:

$$\left(\frac{\partial U}{\partial n}\right) = \frac{-w_{AA}}{2} \quad \textbf{(D4)}$$

Since the total area of the surface, A, can be defined as A = na, where a is the area per molecule,

$$\left(\frac{dn}{dA}\right) = \frac{1}{a} \quad \textbf{(D5)}$$

The equation for surface tension is therefore:

$$\gamma = \frac{-w_{AA}}{2a} \quad \textbf{(D6)}$$

Thus, surface tension is related to the area per molecule and the intermolecular interaction.

If two immiscible fluids, A and B are in contact, they will form an interface. Assuming that there are N_A molecules of A, of which n are at the interface, and N_B molecules of B, of which n are at the interface, it can easily be seen that N_A-n molecules are in the bulk phase of A, and N_B-n molecules are in the bulk phase of B. Further, bulk particles will have z nearest neighbors, while particles at the interface will have z-1 neighbors. The total energy of the interface, U, is the number of bonds among the particles, multiplied by the energy per bond.

$$U = (N_A - n)\left(\frac{zw_{AA}}{2}\right) + n\left(\frac{(z-1)w_{AA}}{2}\right) + nw_{AB} +$$

$$(N_B - n)\left(\frac{zw_{BB}}{2}\right) + n\left(\frac{(z-1)w_{BB}}{2}\right) \quad \textbf{(D7)}$$

Much as in the analysis of surface tension, defining interfacial tension as the change in free energy per change in interfacial area gives us:

$$\gamma_{AB} = \left(\frac{\partial F}{\partial A}\right)_{N_A,N_B,T} = \left(\frac{\partial U}{\partial A}\right) = \left(\frac{\partial U}{\partial n}\right)\left(\frac{dn}{dA}\right) \quad \textbf{(D8)}$$

The derivative of U with respect to n at constant NA, NB and temperature is

$$\left(\frac{\partial U}{\partial n}\right)_{N_A,N_B,T} = w_{AB} - \frac{w_{AA}+w_{BB}}{2} \quad \textbf{(D9)}$$

As in the surface tension equation, dn/dA = 1/a, and so:

$$\gamma_{AB} = \frac{1}{a}\left(w_{AB} - \frac{w_{AA}+w_{BB}}{2}\right) \quad \textbf{(D10)}$$

The lattice model makes certain assumptions – for example, that all the molecules are the same size – that must be kept in mind, but serves to illustrate the intermolecular origins of surface and interfacial tension.

Appendix C: C Code

```
#include <stdio.h>

main()

{

double initrad;

double initradsq;

double alpha;

double delx;

double delt;

double delxsq;

double eta, t;
```

```
int i,j,k;

double initConc;

double diffCoeff;

int counter; /* Let's write to a file only every so often */


int numTimeSteps;

double conc[51]; /* old concentration */

double newConc[51]; /* new concentration */

double holderOne; /* Broken up the big long equation to simplify bugfinding, lower

computational cost */

double holderTwo;

double holderThree;

double holderFour;

FILE *outfile;

outfile=fopen("prot.txt","a");


initrad = .005;

numTimeSteps = 300000; /* number of timesteps */

initConc = 10.0; /* Initial protein concentration */

delt = .0002; /* timestep*/
```

```
delx = .02; /* space step */

delxsq = delx * delx; /* Reduce computation */

initradsq = initrad * initrad; /* Reduce computation of radius squared */

t = 0;  /* initialize time */

counter = 0; /* initialize counter */

alpha = 0.0000000742; /* Alpha for water in octanol*/

diffCoeff = 0.000000416; /* Diffcoeff */



/* Initialize concentration of protein in droplet */


for (j = 0; j <= 50; j++){

                                        conc[j] = initConc;

}



/* Write the initial concentrations ot file */


for (j = 0; j <= 50; j++){

                                                fprintf(outfile,"%g ",conc[j]);
```

```
}

fprintf(outfile,"\n");

/* Time step loops begin */

for (i = 0; i< numTimeSteps; i++){

t = t + delt; /* Increment time */

/* Calculate the concentration at the outer boundary */

holderOne = diffCoeff / (initradsq - 2*alpha*t);

holderTwo = (conc[50]*(alpha*alpha)/diffCoeff*diffCoeff);

holderThree = conc[50]*alpha/diffCoeff;

holderFour = (-1*alpha*delx/(diffCoeff) - 2/1);

newConc[50] = conc[50] + delt * holderOne * (holderTwo - holderThree * holderFour);

/* Calculate the concentration at the origin */

holderOne = (conc[1]-conc[0])*2/(delxsq); /* holder One is the same */

holderTwo = diffCoeff/(initradsq - 2*alpha*t);
```

```
holderThree = 0;  /* dc/cn is 0 at the origin, BC */

holderFour = 0;

newConc[0] = conc[0] + holderOne*delt*(holderTwo - holderThree*holderFour);


/* loop through the rest of the droplet */


for (k = 1; k < 50; k++){

holderOne = diffCoeff/(initradsq -
2*alpha*t);

holderTwo = (conc[k+1]-2*conc[k] + conc[k-
1])/(delx*delx);

holderThree = (conc[k+1] - conc[k])/delx;

holderFour = alpha*delx/diffCoeff -
(2/(delx*k));

newConc[k] = conc[k] + holderOne * delt *
(holderTwo - holderThree * holderFour);

}

/* END OF DROPLET LOOP */

/* now make the new conc the old conc */

for (j = 0; j <= 50; j++){
```

```
                    conc[j]=newConc[j];
                }
            counter = counter + 1; /* Increment loop */
                if (counter == 2500){
                    for (j = 0; j <= 50; j++){
                        fprintf(outfile,"%g ",conc[j]);
                    }
                    fprintf(outfile,"\n");
                    counter = 0;
                }
}
/* End time loop*/
    } /* END OF MAIN */
```

References

1. **Duncan, P.B. and D. Needham,** *Test of the Epstein-Plesset model for gas microparticle dissolution in aqueous media: Effect of surface tension and gas undersaturation in solution.* **Langmuir, 2004. 20(7): p. 2567-2578.**

2. **Duncan, P.B. and D. Needham,** *Microdroplet dissolution into a second-phase solvent using a micropipet technique: Test of the Epstein-Plesset model for an aniline-water system.* **Langmuir, 2006. 22(9): p. 4190-4197.**

3. **Epstein, P.S. and M.S. Plesset,** *On the Stability of Gas Bubbles in Liquid-Gas Solutions.* **Journal of Chemical Physics, 1950. 18(11): p. 1505-1509.**

4. **Macedo, P.B. and T.A. Litovitz,** *On Relative Roles of Free Volume and Activation Energy in Viscosity of Liquids.* **Journal of Chemical Physics, 1965. 42(1): p. 245-&.**

5. **Cohen, M.H. and D. Turnbull,** *Molecular Transport in Liquids and Glasses.* **Journal of Chemical Physics, 1959. 31(5): p. 1164-1169.**

6. **Duncan, P.B.,** *Dissolution of Two-Phase Microsystems: Gas and Liquid Microparticle Dissolution and Dehydration of Biomaterials*, **in** *Mechanical Engineering and Materials Science*. **2005, Duke University: Durham, NC.**

7. **Gad, S.C.,** *Handbook of Pharmaceutical Biotechnology*. **2007, Hoboken, NJ: John Wiley & Sons.**

8. **Banting, F.G.,** *Diabetes and insulin.* **Canadian Medical Association Journal, 1926. 16: p. 221-232.**

9. **Banting, F.G.,** *Early work on insulin.* **Science, 1937. 85: p. 594-596.**

10. **Gupta, H. and A. Sharma,** *Recent trends in protein and drug delivery systems.* **Asian J Pharm, 2009. 33: p. 69-75.**

11. **Shire, S.J., Z. Shahrokh, and J. Liu,** *Challenges in the development of high protein concentration formulations.* **Journal of Pharmaceutical Sciences, 2004. 93(6): p. 1390-1402.**

12. **Barrero, A. and I.G. Loscertales,** *Micro- and nanoparticles via capillary flows.* **Annual Review of Fluid Mechanics, 2007. 39: p. 89-106.**

13. **Christopher, G.F. and S.L. Anna,** *Microfluidic methods for generating continuous droplet streams.* **Journal of Physics D-Applied Physics, 2007. 40(19): p. R319-R336.**

14. **Stone, H.A.,** *Dynamics of Drop Deformation and Breakup in Viscous Fluids.* **Annual Review of Fluid Mechanics, 1994. 26: p. 65-102.**

15. **Einstein, A.,** ***The theory of the Brownian Motion.*** **Annalen Der Physik, 1906. 19(2): p. 371-381.**

16. **Chapman, S. and C. TG,** ***The Mathematical Theory of Non-Uniform Gases*****. 1991, Cambridge, UK: Cambridge University Press.**

17. **Gray, H.,** ***Chemical Bonds: an introduction to atomic and molecular structure*****. 1994, Mill Valley, CA: University Science Books.**

18. **Gillespie, R., et al.,** ***Chemistry: Second Edition*****. 1989, Needham Heights, MA: Allyn and Bacon, Inc.**

19. **Schrodinger, E.,** ***Quantisierung als Eigenwertproblem.*** **Ann. Phys. , 1926. 79: p. 361-76.**

20. **Gray, H.B.,** ***Chemical Bonds: An Introduction to Atomic and Molecular Structure*****. 1994: University Science Books.**

21. **Israelachvili, J.N.,** ***Intermolecular and Surface Forces*****. 2003: Academic Press.**

22. **Dill, K.A. and S. Bromberg,** ***Molecular Driving Forces*****. 2003, New York, New York: Garland Science.**

23. **Pauling, L.,** ***The Nature of the Chemical Bond and the Structure of Molecules and Crystals: An Introduction to Modern Structural Chemistry*****. 1939, Ithaca, NY: Cornell University Press.**

24. **Jeffrey, G.A.,** ***An Introduction to Hydrogen Bonding*****. 1997, Oxford: Oxford University Press.**

25. **Marechal, Y.,** ***The Hydrogen Bond and the Water Molecule: The Physics and Chemistry of Water, Aqueous and Bio-Media*****. 2007, Amsterdam: Elsevier Science and Technology Books.**

26. **Cohen, E.G.D.,** ***50 Years of Kinetic-Theory.*** **Physica A, 1993. 194(1-4): p. 229-257.**

27. **Tabor, D.,** ***Gases, Liquids, and Solids and other states of matter, 3rd edition.*** **2000, Cambridge, UK: Cambridge University Press.**

28. **Israelachvili, J.N.,** ***Intermolecular and Surface Forces*****. 1992, London, UK: Academic Press.**

29. **White, F.M.,** ***Fluid Mechanics: Fourth Edition*****. 1999, Boston, MA: McGraw-Hill.**

30. **Stokes, G.,** ***On the Effect of the Internal Friction Of Fluids on the Motion of Pendulums.*** **Transactions of the Cambridge Philosophical Society, 1850. IX.**

31. **Murarka, R.K. and B. Bagchi,** ***Diffusion and viscosity in a supercooled polydisperse system.*** **Physical Review E, 2003. 67(5): p. -.**

32. **Bhattacharyya, S. and B. Bagchi, *Decoupling of tracer diffusion from viscosity in a supercooled liquid near the glass transition.* Journal of Chemical Physics, 1997. 107(15): p. 5852-5862.**

33. **Harris, K.R., *The fractional Stokes-Einstein equation: Application to Lennard-Jones, molecular, and ionic liquids.* Journal of Chemical Physics, 2009. 131(5): p. -.**

34. **Kowert, B.A., R.M. Turner, and C.V.C. Caldwell, *Diffusion of 1-alkenes and cyclohexene in alkane solvents.* Chemical Physics, 2008. 344(1-2): p. 114-120.**

35. **Kowert, B.A., et al., *Size-dependent diffusion in cycloalkanes.* Molecular Physics, 2004. 102(13): p. 1489-1497.**

36. **Kowert, B.A., et al., *Size-dependent diffusion in the n-alkanes.* Journal of Physical Chemistry A, 2003. 107(24): p. 4790-4795.**

37. **Kowert, B.A., et al., *Diffusion of dioxygen in 1-alkenes and biphenyl in perfluoro-n-alkanes.* Chemical Physics Letters, 2002. 353(1-2): p. 95-99.**

38. **Kowert, B.A., et al., *Diffusion of dioxygen in alkanes and cycloalkanes.* Journal of Physical Chemistry A, 2000. 104(38): p. 8823-8828.**

39. **Kowert, B.A. and N.C. Dang, *Diffusion of dioxygen in n-alkanes.* Journal of Physical Chemistry A, 1999. 103(7): p. 779-781.**

40. **Meier, K., A. Laesecke, and S. Kabelac, *Transport coefficients of the Lennard-Jones model fluid. II Self-diffusion.* Journal of Chemical Physics, 2004. 121(19): p. 9526-9535.**

41. **Meier, K., A. Laesecke, and S. Kabelac, *Transport coefficients of the lennard-jones model fluid. I. Viscosity.* Journal of Chemical Physics, 2004. 121(8): p. 3671-3687.**

42. **Zwanzig, R. and A.K. Harrison, *Modifications of the Stokes-Einstein Formula.* Journal of Chemical Physics, 1985. 83(11): p. 5861-5862.**

43. **Pollack, G.L. and J.J. Enyeart, *Atomic Test of the Stokes-Einstein Law .2. Diffusion of Xe through Liquid Hydrocarbons.* Physical Review A, 1985. 31(2): p. 980-984.**

44. **Eyring, H., *Viscosity, plasticity, and diffusion as examples of absolute reaction rates.* Journal of Chemical Physics, 1936. 4(4): p. 283-291.**

45. **Tyrell, H. and K. Harris, *Diffusion in Liquids: A theoretical and experimental study*. 1984, London, UK: Butterworths.**

46. **Crank, J., *Diffusion in Polymers*. 1968, London, UK: Academic Press.**

47. **March, N. and M. Tosi, *Introduction to Liquid State Physics*. 2002, New Jersey, USA: World Scientific.**

48. **Neogi, *Diffusion in Polymers*. 1996, New York, New York: Marcel Dekker.**

49. **Fick, A., *Uber Diffusion*. Poggendorff's Annalen der Physik und Chemie, 1855. 94.**

50. **Fourier, J., *Theorie analytique de la Chaleur*. 1822, Paris: Firmin-Didot pere et fils.**

51. **Suarez-Iglesias, O., et al., *Modeling of tracer diffusion in liquids when solute-solvent interactions are present*. Fluid Phase Equilibria, 2007. 253(2): p. 155-164.**

52. **Easteal, A.J. and L.A. Woolf, *Pressure and Temperature-Dependence of Tracer Diffusion-Coefficients of Methanol, Ethanol, Acetonitrile, and Formamide in Water*. Journal of Physical Chemistry, 1985. 89(7): p. 1066-1069.**

53. **Tominaga, T., S. Tenma, and F. Watanabe, *Diffusion of cyclohexane and cyclopentane derivatives in some polar and non-polar solvents - Effect of intermolecular and intramolecular hydrogen-bonding interactions*. Journal of the Chemical Society-Faraday Transactions, 1996. 92(11): p. 1863-1867.**

54. **Chen, N. and T.C. Chan, *Experimental study of hydrogen bonding by mutual diffusion*. Chemical Communications, 1997(7): p. 719-720.**

55. **Chan, T.C., N.L. Ma, and N. Chen, *The effects of molecular association on mutual diffusion in acetone*. Journal of Chemical Physics, 1997. 107(6): p. 1890-1895.**

56. **Lu, J.G., R. Kong, and T.C. Chan, *Effects of molecular association on mutual diffusion: A study of hydrogen bonding in dilute solutions*. Journal of Chemical Physics, 1999. 110(6): p. 3003-3008.**

57. **Srinivas, G., S. Bhattacharyya, and B. Bagchi, *Computer simulation and mode coupling theory study of the effects of specific solute-solvent interactions on diffusion: Crossover from a sub-slip to a super-stick limit of diffusion*. Journal of Chemical Physics, 1999. 110(9): p. 4477-4482.**

58. **Hynes, J.T., R. Kapral, and M. Weinberg, *Molecular Theory of Translational Diffusion - Microscopic Generalization of the Normal Velocity Boundary-Condition*. Journal of Chemical Physics, 1979. 70(3): p. 1456-1466.**

59. **Wakai, C. and M. Nakahara, *Attractive potential effect on the self-diffusion coefficients of a solitary water molecule in organic solvents*. Journal of Chemical Physics, 1997. 106(18): p. 7512-7518.**

60. **Cussler, E.L., *Diffusion: Mass Transfer in Fluids Systems* Second ed. 1997, Cambridge, UK: Cambridge University Press.**

61. **Bhattacharyya, S. and B. Bagchi, *Anomalous diffusion of small particles in dense liquids.* Journal of Chemical Physics, 1997. 106(5): p. 1757-1763.**

62. **Easteal, A.J., *Tracer diffusion of water in organic liquids.* Journal of Chemical and Engineering Data, 1996. 41(4): p. 741-744.**

63. **Cussler, *Diffusion: mass transfer in fluid systems*. 1997, Cambridge, UK: Cambridge University Press.**

64. **Cheremisinoff, N.P., *Industrial Solvents Handbook*. 2 ed. 2003, New York Marcel Dekker. 346.**

65. **Flick, E.W., ed. *Industrial Solvents Handbook*. 3 ed. 1985, Noyes Publications: Park Ridge. 648.**

66. **Tsonopoulos, C., *Thermodynamic analysis of the mutual solubilities of normal alkanes and water.* Fluid Phase Equilibria, 1999. 156(1-2): p. 21-33.**

67. **Maczynski, A., et al., *Mutual solubilities of water and alkanes.* Monatshefte Fur Chemie, 2003. 134(5): p. 633-653.**

68. **Polak, J. and B.C.-Y. Lu, *Mutual Solubilities of Hydrocarbons and Water at 0 and 25 °C.* Canadian Journal of Chemistry, 1973. 51(24).**

69. **Hildebrand, E.M., *Techniques for the Isolation of Single Microorganisms .2.* Botanical Review, 1950. 16(4): p. 181-207.**

70. **Terreros, D.A. and J.J. Grantham, *Barber,Marshall and the Origins of Micropipet Methods.* American Journal of Physiology, 1982. 242(3): p. F293-F296.**

71. **Johnson, H.W., *A simple micropipette holder.* Journal of Bacteriology, 1923. 8(6): p. 573-575.**

72. **Mitchinson, J. and S. MM, *The Mechanical Properties of the Cell Surface: I. The Cell Elastimer.* J. Exp Biology, 1954. 31.**

73. **Burton, A.C. and R.P. Rand, *On Mechanical Properties + Shape of Human Red Cell Membrane.* Journal of Physiology-London, 1964. 171(1): p. P16-&.**

74. **Needham, D. and E. Evans, *Structure and Mechanical-Properties of Giant Lipid (Dmpc) Vesicle Bilayers from 20-Degrees-C Below to 10-Degrees-C above the Liquid-Crystal Crystalline Phase-Transition at 24-Degrees-C.* Biochemistry, 1988. 27(21): p. 8261-8269.**

75. **Needham, D., T.J. Mcintosh, and E. Evans,** ***Thermomechanical and Transition Properties of Dimyristoylphosphatidylcholine Cholesterol Bilayers.*** **Biochemistry, 1988. 27(13): p. 4668-4673.**

76. **Needham, D., T.J. Mcintosh, and D.D. Lasic,** ***Repulsive Interactions and Mechanical Stability of Polymer-Grafted Lipid-Membranes.*** **Biochimica Et Biophysica Acta, 1992. 1108(1): p. 40-48.**

77. **Needham, D. and R.S. Nunn,** ***Elastic deformation and failure of lipid bilayer membranes containing cholesterol.*** **Biophys. J., 1990. 58: p. 997-1009.**

78. **Needham, D. and R.S. Nunn,** ***Elastic-Deformation and Failure of Lipid Bilayer-Membranes Containing Cholesterol.*** **Biophysical journal, 1990. 58(4): p. 997-1009.**

79. **Needham, D., N. Stoicheva, and D.V. Zhelev,** ***Exchange of monooleoylphosphatidylcholine as monomer and micelle with membranes containing poly(ethylene glycol)-lipid.*** **Biophysical journal, 1997. 73(5): p. 2615-2629.**

80. **Needham, D., N. Stoicheva, and D.V. Zhelev,** ***Exchange of monooleoylphosphatidylcholine as monomer and micelle with membranes containing poly(ethylene glycol)-lipid.*** **Biophysical journal, 1998. 74(2): p. A393-A393.**

81. **Needham, D. and D.V. Zhelev,** ***Lysolipid Exchange with Lipid Vesicle Membranes.*** **Annals of Biomedical Engineering, 1995. 23(3): p. 287-298.**

82. **Clift, R., J.R. Grace, and M.E. Weber,** ***Bubbles, Drops, and Particles.*** **1978, Mineola, NY: Dover Publications.**

83. **Lee, Y.L., J.R. Maa, and Y.M. Yang,** ***The effects of surfactant on the mass transfer in extraction column.*** **Journal of Chemical Engineering of Japan, 1998. 31(3): p. 340-346.**

84. **Needham, D. and R.M. Hochmuth,** ***Electro-Mechanical Permeabilization of Lipid Vesicles - Role of Membrane Tension and Compressibility.*** **Biophysical Journal, 1989. 55(5): p. 1001-1009.**

85. **Needham, D. and R.M. Hochmuth,** ***Rapid Flow of Passive Neutrophils into a 4 Mu-M Pipette and Measurement of Cytoplasmic Viscosity.*** **Journal of Biomechanical Engineering-Transactions of the Asme, 1990. 112(3): p. 269-276.**

86. **Evans, E. and A. Yueng,** ***Nanoscale Lubrication - Drag between Monolayers of Surfactant Bilayer-Membranes.*** **Abstracts of Papers of the American Chemical Society, 1993. 205: p. 334-COLL.**

87. **Chan, T.C., *Diffusion of Aromatic-Compounds - an Investigation on the Effects of Molecular Shape, Mass, and Dipole-Moment.* Journal of Chemical Physics, 1984. 80(11): p. 5862-5864.**

88. **Lusis, M.A. and G.A. Ratcliff, *Diffusion of Inert and Hydrogen-Bonding Solutes in Aliphatic Alcohols.* Aiche Journal, 1971. 17(6): p. 1492-1496.**

89. **Chan, M.L. and T.C. Chan, *Diffusion of Pseudoplanar Solutes - an Investigation on the Effects of Hydrogen-Bonding.* Journal of Physical Chemistry, 1995. 99(16): p. 5765-5768.**

90. **Chan, T.C. and M.L. Chan, *Diffusion of Pseudoplanar Molecules - an Experimental Evaluation of the Molecular Effects on Diffusion.* Journal of the Chemical Society-Faraday Transactions, 1992. 88(16): p. 2371-2374.**

91. **Smith, J.D., et al., *Response to Comment on "Energetics of hydrogen bond network: Rearrangements in liquid water".* Science, 2005. 308(5723): p. 793b-793b.**

92. **Smith, J.D., et al., *Energetics of hydrogen bond network rearrangements in liquid water.* Science, 2004. 306(5697): p. 851-853.**

93. **Skipp, C.J. and H.J.V. Tyrrell, *Diffusion in Viscous Solvents .2. Planar and Spherical Molecules in Propane-1,2-Diol at 15, 25 and 35 Degreesc.* Journal of the Chemical Society-Faraday Transactions I, 1975. 71: p. 1744-1753.**

94. **Griffith, J.H. and H.A. Scheraga, *Statistical thermodynamics of aqueous solutions. I. Water structure, solutions with non-polar solutes, and hydrophobic interactions.* Journal of Molecular Structure-Theochem, 2004. 682(1-3): p. 97-113.**

95. **Su, W.C., et al., *Diffusion coefficients and conductivities of alkylimidazolium tetrafluoroborates and hexafluorophosphates.* Fluid Phase Equilibria, 2007. 252(1-2): p. 74-78.**

96. **Su, J.T., et al., *The effect of hydrogen bonding on the diffusion of water in n-alkanes and n-alcohols measured with a novel single microdroplet method.* Journal of Chemical Physics, 2010. 132(4): p. -.**

97. **Fawcett, W., *Liquids, solutions, and interfaces: from classical macroscopic descriptions*. 2004, Oxford, UK: Oxford University Press.**

98. **Jaycock, M. and G. Parfitt, *Chemistry of Interfaces*. 1981, Chichester, UK: E. Horwood.**

99. **Lee, S., D.H. Kim, and D. Needham, *Equilibrium and dynamic interfacial tension measurements at microscopic interfaces using a micropipet technique. 1.***

A new method for determination of interfacial tension. **Langmuir, 2001. 17(18): p. 5537-5543.**

100. **Fraden, J.,** ***Handbook of Modern Sensors: Physics, Designs, and Applications, 4th Ed.*** **2010, New York, NY: Springer.**

101. **Nauman, E.B.,** ***Droplet Diffusion-Model for Micromixing.*** **Chemical Engineering Science, 1975. 30(9): p. 1135-1140.**

102. **Laby, T.,** ***The Separation of Iron from Nickel and Cobalt by Lead Oxide (Field's Method).*** **Chemical News and Journal of Industrial Science, 1904. 89-90.**

103. **ODonnell, P.B. and J.W. McGinity,** ***Preparation of microspheres by the solvent evaporation technique.*** **Advanced Drug Delivery Reviews, 1997. 28(1): p. 25-42.**

104. **Yuksel, N. and T. Baykara,** ***Preparation of polymeric microspheres by the solvent evaporation method using sucrose stearate as a droplet stabilizer.*** **Journal of Microencapsulation, 1997. 14(6): p. 725-733.**

105. **vanHamont, J.E., et al.,** ***Evaluation of solvent extraction and solvent evaporation procedures for production of tobramycin-releasing microspheres.*** **23rd International Symposium on Controlled Release of Bioactive Materials, 1996 Proceedings, 1996: p. 365-366**

940.

106. **Li, W.I., K.W. Anderson, and P.P. DeLuca,** ***Kinetic and thermodynamic modeling of the formation of polymeric microspheres using solvent extraction/evaporation method.*** **Journal of Controlled Release, 1995. 37(3): p. 187-198.**

107. **Li, W.I., et al.,** ***Prediction of solvent removal profile and effect on properties for peptide-loaded PLGA microspheres prepared by solvent extraction/evaporation method.*** **Journal of Controlled Release, 1995. 37(3): p. 199-214.**

108. **Iwata, M. and J.W. Mcginity,** ***Preparation of Multiphase Microspheres of Poly(D,L-Lactic Acid) and Poly(D,L-Lactic-Co-Glycolic Acid) Containing a W/O Emulsion by a Multiple Emulsion Solvent Evaporation Technique.*** **Journal of Microencapsulation, 1992. 9(2): p. 201-214.**

109. **Grandfils, C., et al.,** ***Preparation of Poly (D,L) Lactide Microspheres by Emulsion Solvent Evaporation, and Their Clinical-Applications as a Convenient Embolic Material.*** **Journal of Biomedical Materials Research, 1992. 26(4): p. 467-479.**

110. **Hanson, C.,** ***Recent Advances in Liquid-Liquid Extraction.*** **1971, Oxford: Pergamon Press Ltd.**

111. **Rickard, D., P.B. Duncan, and N. D;,** ***Hydration Potential of Lysozyme: Protein Dehydration Using a Single Microparticle Technique.*** **Biophysical Journal, 2010. 98(3).**

112. **Wood, B.J., H. Wise, and S.H. Inami,** ***Heterogeneous Combustion of Multicomponent Fuels.*** **Combustion and Flame, 1960. 4(3): p. 235-242.**

113. **Cheng, A.K.H., D.M. Soolaman, and H.Z. Yu,** ***Evaporation of microdroplets of ethanol-water mixtures on gold surfaces modified with self-assembled monolayers.*** **Journal of Physical Chemistry B, 2006. 110(23): p. 11267-11271.**

114. **Sefiane, K., L. Tadrist, and M. Douglas,** ***Experimental study of evaporating water-ethanol mixture sessile drop: influence of concentration.*** **International Journal of Heat and Mass Transfer, 2003. 46(23): p. 4527-4534.**

115. **Renksizbulut, M. and M. Bussmann,** ***Multicomponent Droplet Evaporation at Intermediate Reynolds-Numbers.*** **International Journal of Heat and Mass Transfer, 1993. 36(11): p. 2827-2835.**

116. **Widmann, J.F. and E.J. Davis,** ***Evaporation of multicomponent droplets.*** **Aerosol Science and Technology, 1997. 27(2): p. 243-254.**

117. **Hanson, C., ed.** ***Recent Advances in Liquid-Liquid Extraction.*** **1971, Pergamon Press Ltd.: Oxford, UK.**

118. **Thomson, J.,** ***On certain curious motions observable at the surfaces of wine and other alcoholic liquors.*** **Philisophical Magazine Series 4, 1855. 10(67): p. 330-333.**

119. **Kostarev, K.G.,** ***The study of the extraction of surface-active component of a binary liquid from model ("cylindrical") droplets.*** **Colloid Journal, 2005. 67(3): p. 318-323.**

120. **Altshuller, A.P. and H.E. Everson,** ***The Solubility of Ethyl Acetate in Water.*** **Journal of the American Chemical Society, 1953. 75(7): p. 1727-1727.**

121. **Liu, K., et al.,** ***Separation of organic compounds from water by pervaporation in the production of n-butyl acetate via esterification by reactive distillation.*** **Journal of Membrane Science, 2005. 256(1-2): p. 193-201.**

122. **Stephenson, R. and J. Stuart,** ***Mutual Binary Solubilities - Water Alcohols and Water Esters.*** **Journal of Chemical and Engineering Data, 1986. 31(1): p. 56-70.**

123. **Flick, E.W.,** ***Industrial Solvents Handbook, 3rd. Ed.*** **1985, Park Ridge, NJ, USA: Noyes Data Corporation.**

124. **Rickard, D.L., P.B. Duncan, and D. Needham,** ***Hydration Potential of Lysozyme: Protein Dehydration Using a Single Microparticle Technique.*** **Biophysical journal, 2010. 98(6): p. 1075-1084.**

125. **Meadley, C.K.,** ***Back-Diffusion in a Finite Medium with a Moving Boundary.*** **Quarterly Journal of Mechanics and Applied Mathematics, 1971. 24(Feb): p. 43-&.**

126. **Gardner,** ***Asymptotic Concentration Distribution of an Involatile Solute in an Evaporating Drop.*** **Int. J. Heat Mass Transfer, 1964. 8.**

127. **Manning, M.C., et al.,** ***Stability of Protein Pharmaceuticals: An Update.*** **Pharmaceutical Research, 2010. 27(4): p. 544-575.**

128. **Trevino, S.R., J.M. Scholtz, and C.N. Pace,** ***Measuring and increasing protein solubility.*** **Journal of Pharmaceutical Sciences, 2008. 97(10): p. 4155-4166.**

129. **McLaughlin, P., et al.,** ***Rituximab chimeric Anti-CD20 monoclonal antibody therapy for relapsed indolent lymphoma: Half of patients respond to a four-dose treatment program.*** **Journal of Clinical Oncology, 1998. 16(8): p. 2825-2833.**

130. **Miller, M.A., et al.,** ***Low Viscosity Highly Concentrated Injectable Nonaqueous Suspensions of Lysozyme Microparticles.*** **Langmuir, 2010. 26(2): p. 1067-1074.**

131. **Basu, S.K., et al.,** ***Protein crystals for the delivery of biopharmaceuticals.*** **Expert Opinion on Biological Therapy, 2004. 4(3): p. 301-317.**

132. **Yang, M., et al.,** ***Crystalline monoclonal antibodies for subuctaneous delivery.*** **Proceedings of the National Academy of Science, 2003. 100(12): p. 6934-6939.**

133. **Chick, H. and E. Lubrzynska,** ***The Viscosity of Some Protein Solutions.*** **Biochemical Journal, 1913. 8(1).**

134. **Allahham, A., et al.,** ***Flow and injection characteristics of pharmaceutical parenteral formulations using a micro-capillary rheometer.*** **International Journal of Pharmaceutics, 2004. 270(1-2): p. 139-148.**

135. **Goodwin, J.,** ***Rheology for Chemists: An Introduction.*** **2000, Cambridge, UK: The Royal Society of Chemistry.**

136. **Einstein, A.,** ***A new determination of the molecular dimensions.*** **Annalen Der Physik, 1906. 19(2): p. 289-306.**

137. **Lauffer, M.A.,** ***Motion in Viscous-Liquids - Simplified Derivations of the Stokes and Einstein Equations.*** **Journal of Chemical Education, 1981. 58(3): p. 250-256.**

138. **Krieger, I.M. and T.J. Dougherty,** ***A Mechanism for Non-Newtonian Flow in Suspensions of Rigid Spheres.*** **Transactions of the Society of Rheology, 1959. 3: p. 137-152.**

139. **Liu, J., et al.,** ***Reversible self-association increases the viscosity of a concentrated monoclonal antibody in aqueous solution.*** **Journal of Pharmaceutical Sciences, 2005. 94(9): p. 1928-1940.**

140. **Stein, H.,** ***The Preparation of Dispersions in Liquids*****. 1995, New York, NY: Marcel Dekker.**

141. **Tabeling, P.,** ***Introduction to Microfluidics*****. 2005, Oxford, UK: Oxford University Press.**

142. **Rayleigh, L.,** ***On the Instability of Jets.*** **Proceedings of the London Mathematical Society, 1878: p. 4.**

143. **Brown, K. and D. Flaming,** ***Advanced Micropipette Techniques for Cell Physiology*****. 1987, Hoboken, New Jersey: John Wiley & Sons.**

144. **Dill, K.A.,** ***Molecular Driving Forces: Statistical Thermodynamics in Chemistry & Biology*** **2002, New York, New York: Garland Science.**

Biography

Jonathan T. Su was born on April 8, 1980, in Bryan, Texas. He attended Stanford University in Stanford, California, graduating in 2001 with a Bachelor's of Science in Mechanical Engineering. Jonathan then attended Cornell University in Ithaca, New York, receiving the degree of Master of Mechanical Engineering (Bioengineering certificate) in 2002.

He published a paper, entitled *The effect of hydrogen bonding on the diffusion of water in* n-*alkanes and* n-*alcohols measured with a novel single microdroplet method* in the Journal of Chemical Physics, in 2010.

Jonathan was also an Integrative Graduate Education and Research Traineeship (IGERT) Fellow in the Center for Biologically Inspired Materials and Material Systems (CBIMMS) at Duke University during his time as a PhD student.